SANDIA REPORT

SAND2009-2194
Unlimited Release
Printed May 2009

Analysis of Cavern Stability at the West Hackberry SPR Site

Steven R. Sobolik and Brian L. Ehgartner
Energy, Resources, and Systems Analysis Center
Sandia National Laboratories
P.O. Box 5800
Albuquerque, New Mexico 87185-0751

Prepared by
Sandia National Laboratories
Albuquerque, New Mexico 87185 and Livermore, California 94550

Sandia is a multiprogram laboratory operated by Sandia Corporation,
a Lockheed Martin Company, for the United States Department of Energy's
National Nuclear Security Administration under Contract DE-AC04-94AL85000.

Issued by Sandia National Laboratories, operated for the United States Department of Energy by Sandia Corporation.

Available to DOE and DOE contractors from
U.S. Department of Energy
Office of Scientific and Technical Information
P.O. Box 62
Oak Ridge, TN 37831

Telephone: (865) 576-8401
Facsimile: (865) 576-5728
E-Mail: reports@adonis.osti.gov
Online ordering: http://www.osti.gov/bridge

Available to the public from
U.S. Department of Commerce
National Technical Information Service
5285 Port Royal Rd.
Springfield, VA 22161

Telephone: (800) 553-6847
Facsimile: (703) 605-6900
E-Mail: orders@ntis.fedworld.gov
Online order: http://www.ntis.gov/help/ordermethods.asp?loc=7-4-0#online

SAND2009-2194
Unlimited Release
Printed May 2009

Analysis of Cavern Stability at the West Hackberry SPR Site

Steven R. Sobolik and Brian L. Ehgartner
Energy, Resources, and Systems Analysis Center
Sandia National Laboratories
P.O. Box 5800
Albuquerque, New Mexico 87185-0751

ABSTRACT

This report presents computational analyses that simulate the structural response of caverns at the Strategic Petroleum Reserve (SPR) West Hackberry site. The cavern field comprises 22 caverns. Five caverns (6, 7, 8, 9, 11) were acquired from industry and have unusual shapes and a history dating back to 1946. The other 17 caverns (101-117) were leached according to SPR standards in the mid-1980s and have tall cylindrical shapes. The history of the caverns and their shapes are simulated in a three-dimensional geomechanics model of the site that predicts deformations, strains, and stresses. Future leaching scenarios corresponding to oil drawdowns using fresh water are also simulated by increasing the volume of the caverns. Cavern pressures are varied in the model to capture operational practices in the field. The results of the finite element model are interpreted to provide information on the current and future status of subsidence, well integrity, and cavern stability.

The most significant results in this report are relevant to Cavern 6. The cavern is shaped like a bowl with a large ceiling span and is in close proximity to Cavern 9. The analyses predict tensile stresses at the edge of the ceiling during repressuization of Cavern 6 following workover conditions. During a workover the cavern is at low pressure to service a well. The wellhead pressures are atmospheric. When the workover is complete, the cavern is repressurized. The resulting elastic stresses are sufficient to cause tension around the edge of the large ceiling span. With time, these stresses relax to a compressive state because of salt creep. However, the potential for salt fracture and propagation exists, particularly towards Cavern 9. With only 200 ft of salt between the caverns, the operational consequences must be examined if the two caverns become connected. A critical time may be during a workover of Cavern 9 in part because of the operational vulnerabilities, but also because dilatant damage is predicted under the ledge that forms the lower lobe in the cavern.

The remaining caverns have no significant issues regarding cavern stability and may be safely enlarged during subsequent oil drawdowns. Predicted well strains and subsidence are significant and consequently future remedial actions may be necessary. These predicted well strains certainly suggest appropriate monitoring through a well-logging program. Subsidence is currently being monitored.

ACKNOWLEDGEMENTS

The authors would like to thank Darrell Munson, Lupe Arguello, Allan Sattler, Tom Pfeifle, and David Borns for their review and support of this work.

TABLE OF CONTENTS

LIST OF FIGURES

LIST OF TABLES

This page has been intentionally left blank.

1. INTRODUCTION

1.1 OBJECTIVE

The U.S. Strategic Petroleum Reserve (SPR) stores crude oil in solution-mined caverns in the salt dome formations of the Gulf Coast. There are a total of 62 caverns located at four different sites in Texas (Bryan Mound and Big Hill) and Louisiana (Bayou Choctaw and West Hackberry), as shown in Figure 1. Each cavern is constructed and then operated using casings inserted through a well bore or well bores that are lined with steel casings cemented in place from the surface to near the top of the cavern.

The SPR sites, as well as most other oil and natural gas storage sites in salt domes along the Gulf Coast, are varied in terms of cavern structure and layout. At West Hackberry, the SPR purchased five existing caverns in the early 1980s. These five caverns, Caverns 6, 7, 8, 9, and 11, known as Phase 1 Caverns, were created as early as 1946 and were used for brine storage before the SPR took ownership of them in 1981. After purchase of the site, additional caverns were leached using standards that resulted in tall cylindrical shaped caverns; these caverns, numbered 101 through 117, are referred to in this report as Phase 2 or post-1981 caverns. This analysis evaluates the stress and deformation history of the Phase 1 and SPR leached caverns to the present day, and predicts the effects on cavern stability and well strain of subsequently enlarging the caverns.

When the SPR took ownership of the Phase 1 caverns in 1981, finite element analyses were performed to assess the long-term performance and stability of the caverns (Preece and Foley, 1984). The analyses were two-dimensional axisymmetric idealizations and each cavern was simulated independently of the others. The failure function was based on accumulated strain as a function of pressure. While the analyses at that time predicted stability, cavern workover conditions were not simulated. Today's capabilities extend far beyond those original analyses. The current analyses simulate the entire cavern field in three dimensions and thus capture cavern interactions. The model presented herein also includes the drop in cavern pressures during workovers, an obvious adverse condition for the caverns from a closure and stability point of view. In addition, the rock mechanics community has migrated away from accumulated strain based failure criteria for salt in favor of a stress criterion, and a large data base now exists to support the merits of that criterion. The technology has dramatically improved since the 1980's and since that time, SPR has collected cavern and subsidence data that enable comparison of model predictions to actual cavern and surface deformations. This information enables a calibration of the model to field data and results in a much more accurate assessment of the stress state. The necessity to update the analyses of West Hackberry is undeniable. The following analyses will provide the best prediction to date of the current and future state of the SPR caverns at West Hackberry.

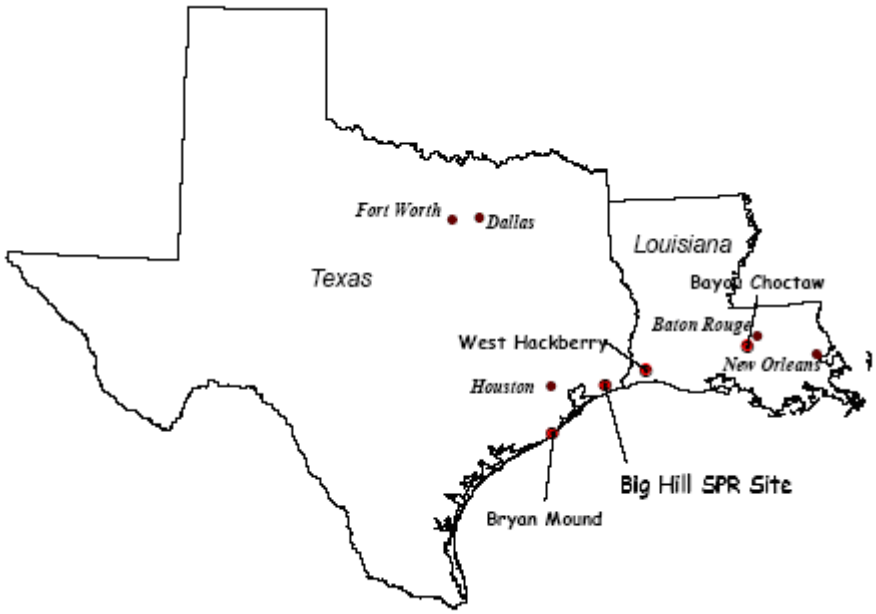

Figure 1: Location of SPR sites.

The analysis of the West Hackberry site differs significantly from previous analyses. The computational domain for this analysis includes specific caverns – the Phase 1 caverns plus Caverns 101, 103, 105, 108, 109, 110, and 117 – and half of the salt dome, as opposed to the previous two-dimensional calculations, or three-dimensional calculations that used a 30-degree wedge to a simulate symmetric 19-cavern field geometry of West Hackberry (Ehgartner and Sobolik, 2002). Many of the caverns in this analysis are meshed with geometries based on sonar data measurements. The entire lives of the caverns (construction, brine or oil storage, operating and workover pressures) are modeled individually for each cavern. Finally, the sandstone that surrounds the salt dome is included in this analysis, providing a realistic far-field stress boundary condition.

For these analyses, each of the caverns (except 103) experiences five leaching operations to grow the cavern, with a volume growth of approximately 15% for each leach. The leaching operations are simulated to begin in September 2008. Caverns 6, 8, and 9 have significant potential interference issues which must be addressed in operational planning; this analysis has made assumptions about how those caverns will be enlarged.

Four measures of cavern performance are evaluated in this study. The first measure uses dilatant damage factors as identified by a damage criterion, a linear function of the hydrostatic pressure (Van Sambeek et al., 1993). An additional damage criterion developed in recent literature (DeVries et al, 2002) will also be used to evaluate potential dilatant damage to the salt. The second performance measure looks at cavern volume closure for each cavern. The third measure evaluates the axial well strain in the caprock above the cavern, and the fourth measure looks at the maximum subsidence at the surface for each cavern. First, the long-term stability of the Phase 1 caverns, particularly for possible cavern volume expansion by leaching during oil

drawdowns, will be evaluated using these criteria. Then, the other caverns in the analysis simulation (except for 103) are also evaluated for volume closure potential. Cavern 103 is kept at its current shape to allow for a detailed examination of the effects of its non-conic section shape on salt stability.

1.2 REPORT ORGANIZATION

This report is organized in the following fashion: Section 2 gives a brief description of the West Hackberry cavern site to show the diversity of cavern geometries. Section 3 describes the analytis model, including the cavern designs, stratigraphy, material models, material properties, and damage criteria used for the analyses. Section 4 shows the results of the calculations, and identifies failure modes for the salt and the casings. Section 5 discusses the relationship between Caverns 6 and 9, and provides recommendations for site operations activities regarding them. Section 6 summarizes the results, and provides concluding remarks. The report concludes with a list of cited reference in Section 7.

2. SITE DESCRIPTION

West Hackberry is located in the extreme southwestern corner of Louisiana, some 15 miles from the Louisiana/Texas border to the west and the Gulf of Mexico to the south (Munson, 2006). The geological characteristics related to the West Hackberry site were first described by Whiting (1980). Magorian et al. (1991) utilized the earlier work, together with additional information on dome geology, surrounding stratigraphy, and relevant environmental information, to update the dome characterization. Conversion of the two-dimensional databases from these earlier characterization reports formed the basis for the most recent reexamination by Rautman et al. (2004) using modern three-dimensional methods for representation of the dome and its surroundings. While major aspects of the dome, caprock and surrounding strata defined by the earlier characterizations remain unchanged, the updated three-dimensional models of Rautman et al. (2004) used more refined analysis of the data and produced models of the dome that differed slightly from the earlier models. The three-dimensional models also achieve a level of visualization clarity and graphical manipulation previously impossible.

The West Hackberry dome consists of the more-or-less typical geologic sequence of rocks. With increasing depth below the ground surface, initially there is roughly 1500 ft of soil and unconsolidated gravel, sand, and mud, followed by approximately 400 ft of caprock, consisting of anhydrite and carbonate (a conversion product of anhydrite). Generally, the upper portions of the caprock consist of the anhydrite conversion products of gypsum and dolomite, while the lower portion of the caprock is the initial anhydrite residue from the solution of the original domal material. The caprock is generally lens shaped with the thickest part of the lens over the central portion of the dome, tapering to thin edges toward the periphery of the dome; however, some portions of the caprock, even at the dome edge, are quite thick. In the updated model, the caprock even laps over the dome edge in several locations. The caprock is in contact with the top of the domal salt body. Beneath the caprock, the domal salt body extends to considerable depth, potentially to the original Louann bedded salt source.

Figure 2 shows a plan view of the West Hackberry site (Magorian et al., 1991) with contour lines defining the approximate location of the salt dome's interface with the caprock and surrounding sandstone. The approximate cavern locations are shown in the plan view. An updated geologic perspective of the salt dome and caprock is provided in Figure 3 (Rautman et al., 2004).

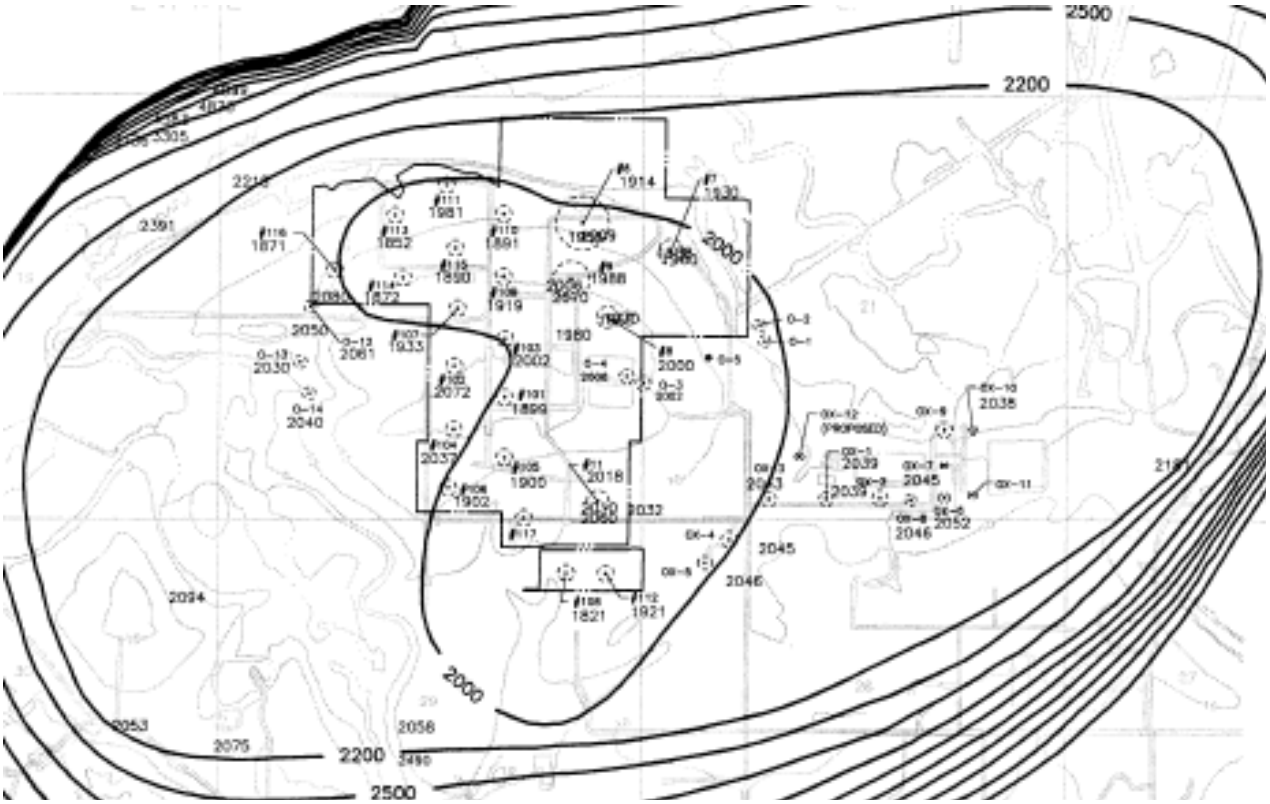

Figure 2: Plan view of the West Hackberry SPR site (Magorian et al., 1991).

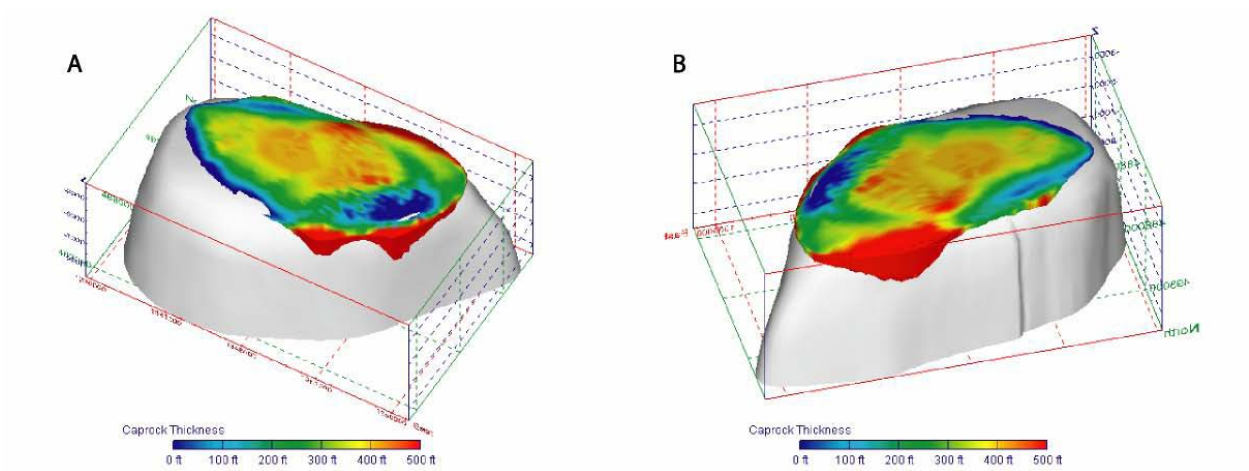

Figure 3: Perspective views of salt dome and caprock (Rautman et al., 2004)

Figure 4 shows the cavern layout at the West Hackberry site (Munson, 2006). Two major shear sections have been identified near the caverns; these extend along the entire distance of the caprock, and for an unknown distance into the salt. These shear zones are not included in the computational model presented in this report. Figure 5 shows cavern geometries based on sonar measurements obtained through 2007 (Rautman and Snider, 2007). Note the enlarged tops and asymmetries of the cavern shapes. In general, caverns in the SPR are intentionally shaped with

larger tops to accommodate future oil drawdowns where the bottom portions of the caverns are preferentially leached, and hence the overall cavern shape becomes more cylindrical, because of raw water injections to remove the oil. Salt properties also result in unpredictable cavern shapes as the insoluble content or dissolution rates of salt can vary spatially. This explains some of the asymmetries found in the cavern shapes. The Phase 1 caverns were acquired through purchase; these caverns have unusual shapes as they were not intentionally leached for product storage, but were used to produce brine. Clearly a variety of shapes are currently found in the SPR and this variety of cavern shapes will continue through future drawdowns.

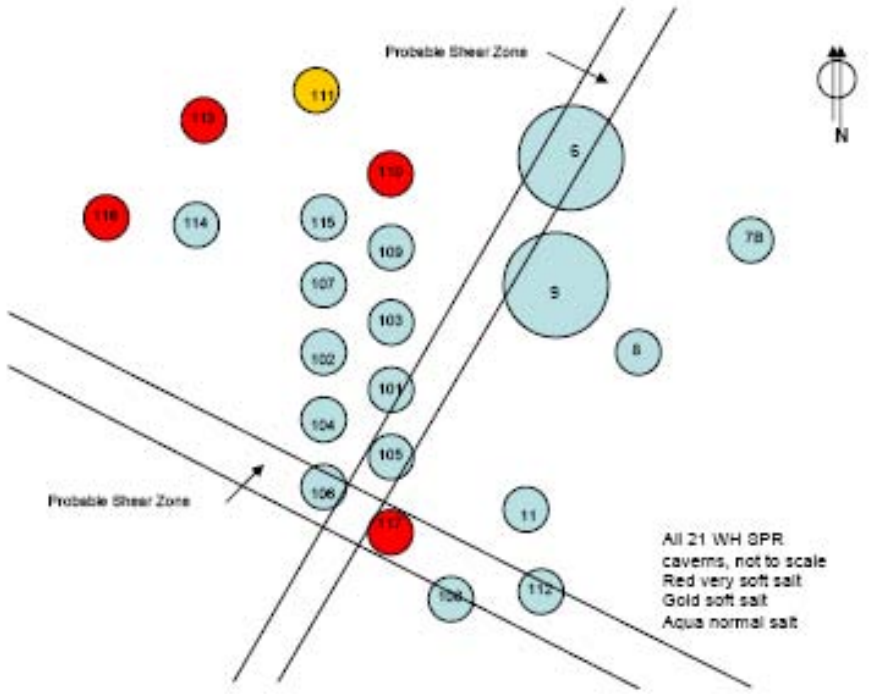

Figure 4. Schematic of the Location of the SPR Caverns at West Hackberry (Munson, 2006)

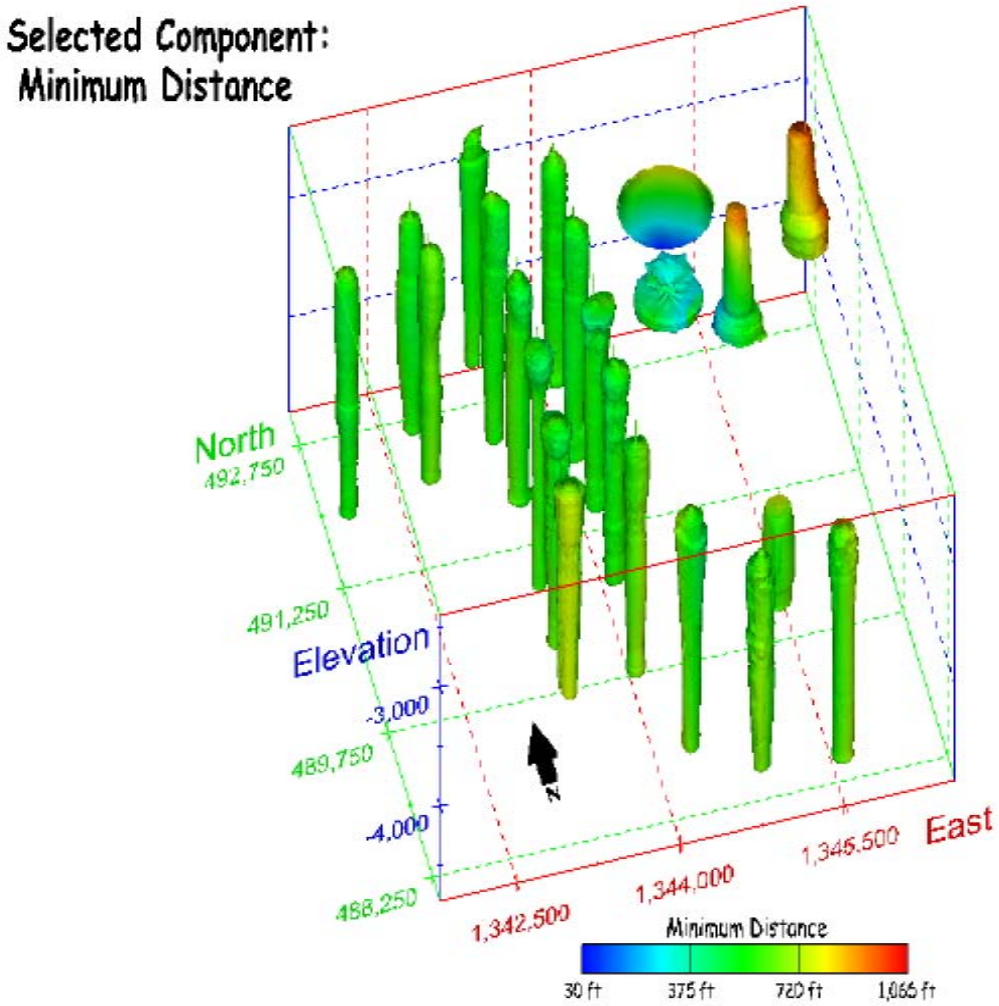

Figure 5. Visualization of the 22 oil-storage caverns at West Hackberry SPR site viewed from the south (Rautman and Snider, 2007).

3. ANALYSIS MODEL

3.1 MODEL DESCRIPTION

In several previous analyses, SPR sites have been modeled using a 30-degree wedge section cut out of a 19-cavern field (Ehgartner and Sobolik, 2002). Such a mesh has been used to apply three-dimensional geometric and geomechanical effects to an SPR cavern field with a minimum of mesh elements (usually under 100,000 elements). Several recent advances now permit a more comprehensive analysis of a salt dome cavern field. First, the computational code JAS3D has been parallelized, allowing for the use of up to 64 CPU nodes for calculations. Second, recent advances in cavern and salt dome geometric visualization based on sonar data allow a realistic representation of cavern geometry. Third, recent advances in meshing capabilities such as mesh cutting allow for converting cavern visualization geometries to computational meshes. Because of these advances, a new computational domain has been developed for the West Hackberry cavern field which encompasses half of the salt dome, with a vertical symmetry plane through six WH caverns (110, 109, 103, 101, 105, and 117).

At the West Hackberry site, the five caverns known as Phase 1 – Caverns 6, 7, 8, 9, and 11 – were created as early as 1946 and were used for brining and brine storage before the SPR took ownership of them in 1981. After that time, seventeen other storage caverns were created over an eight-year period. Six of these post-1981 caverns (110, 109, 103, 101, 105, and 117) are arranged in a nearly linear fashion, allowing for the use of a vertical symmetry plane through them. A seventh cavern, 108, is also included in the computational field, for a total of five Phase 1 and seven post-1981 caverns. The analysis simulates the Phase 1 caverns that were leached to full size over some period of time and filled with brine until 1981 and then filled with oil. The analysis also simulates the leaching of the post-1981 caverns and subsequent filling with oil. In general, these caverns have been maintained at constant operating pressures except during workovers. The standard pressure condition applied to the cavern is based on an average wellhead pressure ranging between 900 and 975 psi. Beginning in 1984, a series of five-year cycles of cavern workovers was initiated. During the five year cycle, every cavern is scheduled for a workover. During the workover, the affected cavern is held at 0 psi wellhead pressure for three months. The pressures for all caverns are then at normal operating pressure for the fourth month (so that the workover rig can be moved to a new well) and then the workover of the next scheduled well begins. Previous analyses have shown that the abrupt pressure drop during the workover will induce the greatest potential for damage. The duration of the simulated workover may be slightly longer than is typically encountered in the field, but is chosen to provide an adverse condition and closely simulate actual subsidence measurements, which reflect periods of low to intermediate operating pressures associated with fluid transfers. After 2008, the simulation incorporates an additional feature. Each of the caverns (except 103) are expected to experience five leaching operations to grow the cavern, with a volume growth of approximately 15% for each leach. The leaching operations are simulated to begin in September 2008, which is the final four-month window in that particular five-year workover cycle. This is repeated in 2013, 2018, 2023, and 2028, and the calculation then performs one more workover for each cavern through 2033. Caverns 6, 8, and 9 have significant potential interference issues which

must be addressed in operational planning; this analysis has made assumptions about how those caverns will be enlarged.

In order to perform a cavern stability analysis that investigates damage in salt, the analytical tools ideally need to be able to perform the following functions: 1) calculate the changes in the in situ stress field and deformations surrounding the well and cavern over a long period of time resulting from the creep deformation of the salt; 2) include criteria by which tensile failure or shear damage of the salt can be determined and located; 3) have the ability to reduce the time step of the analysis to discretize short-time events such as changes in cavern pressure because of workovers; and 4) allow post-processing to be able to identify high strain and failure regions and compute cavern volume changes. The computational models utilized the finite element code JAS3D (ideal for simulations of processes occurring over many years), the power law creep model for salt, and the half-dome computational mesh.

3.2 STRATIGRAPHY AND COMPUTATIONAL MESH

The mesh for the computational model is illustrated in Figures 6 and 7. Figure 6 shows the entire mesh used for these calculations, and Figure 7 shows the same view with the overburden and caprock removed to expose the salt formation. Four material blocks are used in the model to describe the stratigraphic layers: the overburden, caprock, salt dome and sandstone surrounding the salt dome. The overburden is made of sand, and the caprock layer is made of gypsum or limestone. This stratigraphic material closely matches that used for Big Hill (Park et al., 2005), and it is thought to be reasonably accurate for the other SPR sites. The overburden layer is 1600 feet thick, and the caprock is 400 feet thick. The post-1981 caverns were typically constructed on 750-feet center-to-center spacings. Table 1 lists the cavern coordinates, top-of-cavern depths, and initial heights and volumes used in the analysis. The coordinates are based on Louisiana field coordinates, and converted to mesh coordinates with Cavern 103 at the origin, and coordinate axes aligned with compass directions (X-axis for W-E, Y-axis for N-S).

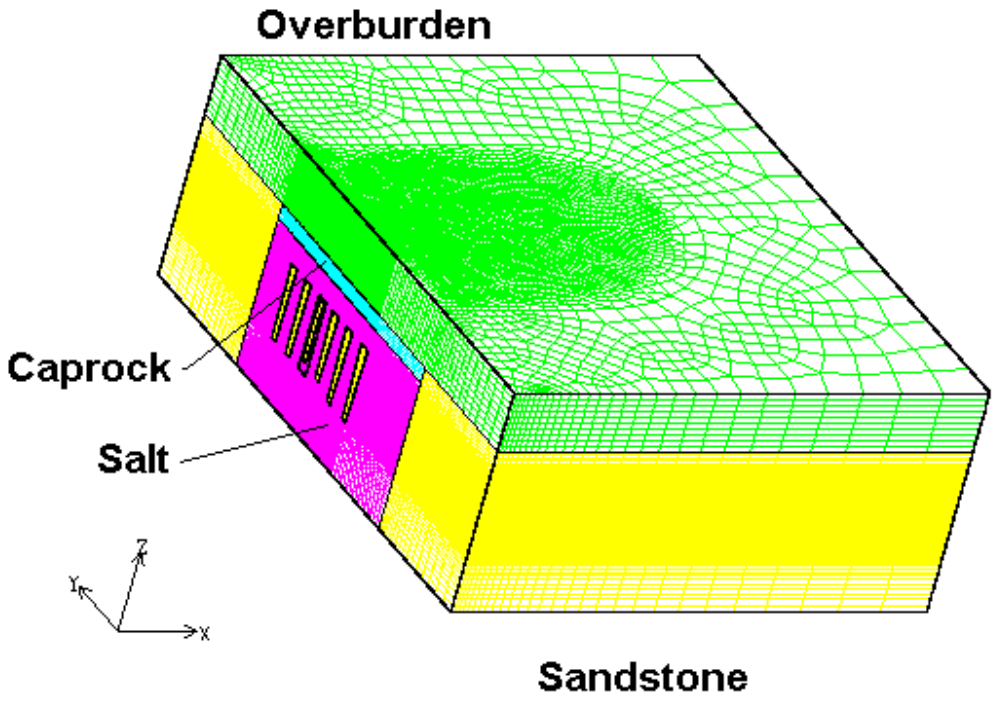

Figure 6. Computational mesh used for the West Hackberry calculations.

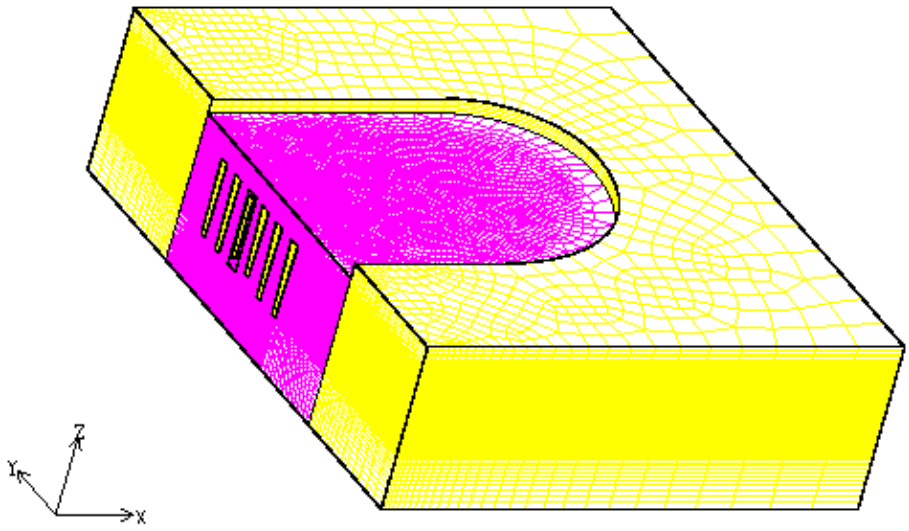

Figure 7. Computational mesh showing the salt formation and surrounding sandstone.

Table 1: Cavern coordinates, depths, heights, and construction dates.

Cavern	Coordinates* X, feet	Coordinates* Y, feet	Depth to Ceiling, feet	Init. Height, feet	Init. Volume, MMB	Begin Construct	End Construct	Begin Oil Storage
Post-1981 caverns along the vertical plane of symmetry								
110	23.11	1499.328	2600	2000	11.0	2/1/1982	3/1/1985	3/1/1985
109	8.878	750.074	2600	2000	11.9	3/1/1984	11/1/1985	11/1/1985
103	0	0	2674	1676	12.0	5/1/1981	1/1/1984	1/1/1984
101	-12.665	-748.739	2600	1800	11.5	5/1/1981	12/1/1983	12/1/1983
105	-22.083	-1499.731	2600	2000	11.8	1/1/1981	1/1/1984	1/1/1984
117	257.024	-2314.750	2600	2000	13.1	6/1/1985	9/1/1988	9/1/1988
Other post-1981 cavern in analysis								
108	756.382	-2890.575	2600	1800	11.5	2/1/1982	12/1/1984	12/1/1984
Phase 1 caverns								
6	1021.734	1401.375	3240	160	8.7	1/1/1946	1/1/1947	1/1/1981
7	2140.457	1054.855	2520	1000	12.9	1/1/1946	1/1/1947	1/1/1981
8	1330.002	275.576	2420	1020	11.1	1/1/1946	1/1/1947	1/1/1981
9	877.573	697.521	3180	440	9.0	1/1/1947	1/1/1948	1/1/1981
11	1113.49	-2110.067	2940	820	9.1	1/1/1962	1/1/1963	1/1/1981

* Based on Louisiana field coordinates and converted to mesh coordinates with Cavern 103 at the origin (X-axis aligned along W-E, Y-axis aligned along N-S)

Figure 8 shows three views of the layout of the meshed caverns used for these calculations, which includes the six half caverns listed above, plus full cavern representations for 108 and the Phase 1 caverns (6, 7, 8, 9, and 11). The figures show the caverns at their current volumes plus five additional extraction layers. The salt extraction layers, or onion skins, represent the proposed additional salt leaching operations to grow the existing West Hackberry caverns. For this analysis, the first leaching operation was scheduled for September 2008, with each subsequent leaching at five-year intervals afterward. Three types of cavern realizations are included in this computational domain. Five of the caverns on the vertical plane of symmetry (110, 109, 101, 105, and 117) are represented as frustums with approximate dimensions to the actual caverns, with five surrounding layers representing the five additional leaches to grow the caverns in the future. Current meshing technology does not allow for the building of “onion skin” layers around irregular geometry, so frustum shapes are used for these caverns to allow them to be grown and produce the 3-D volumetric creep effects on the entire salt dome. Cavern 103 is created from rounded, off-center cylinders and frustums to simulate the irregular shape of the cavern. This allows for a more realistic analysis of the salt fall potential in that cavern. (The original intent was to use mesh cutting with the sonar geometry; however, a double cut was required for the half-cavern on the vertical plane of symmetry, which is not yet functional in the meshing program. For future analyses, the entire salt dome will be modeled, allowing for very precise modeling of the cavern geometry.) Cavern 108 and the Phase 1 caverns were created by developing an average cavern radius as a function of elevation, and rotating the curve to create the irregularly-shaped caverns and the additional onion skin layers. Each onion skin, when deleted, adds about 15% to the volume of the cavern (Caverns 6 and 9 being the exceptions).

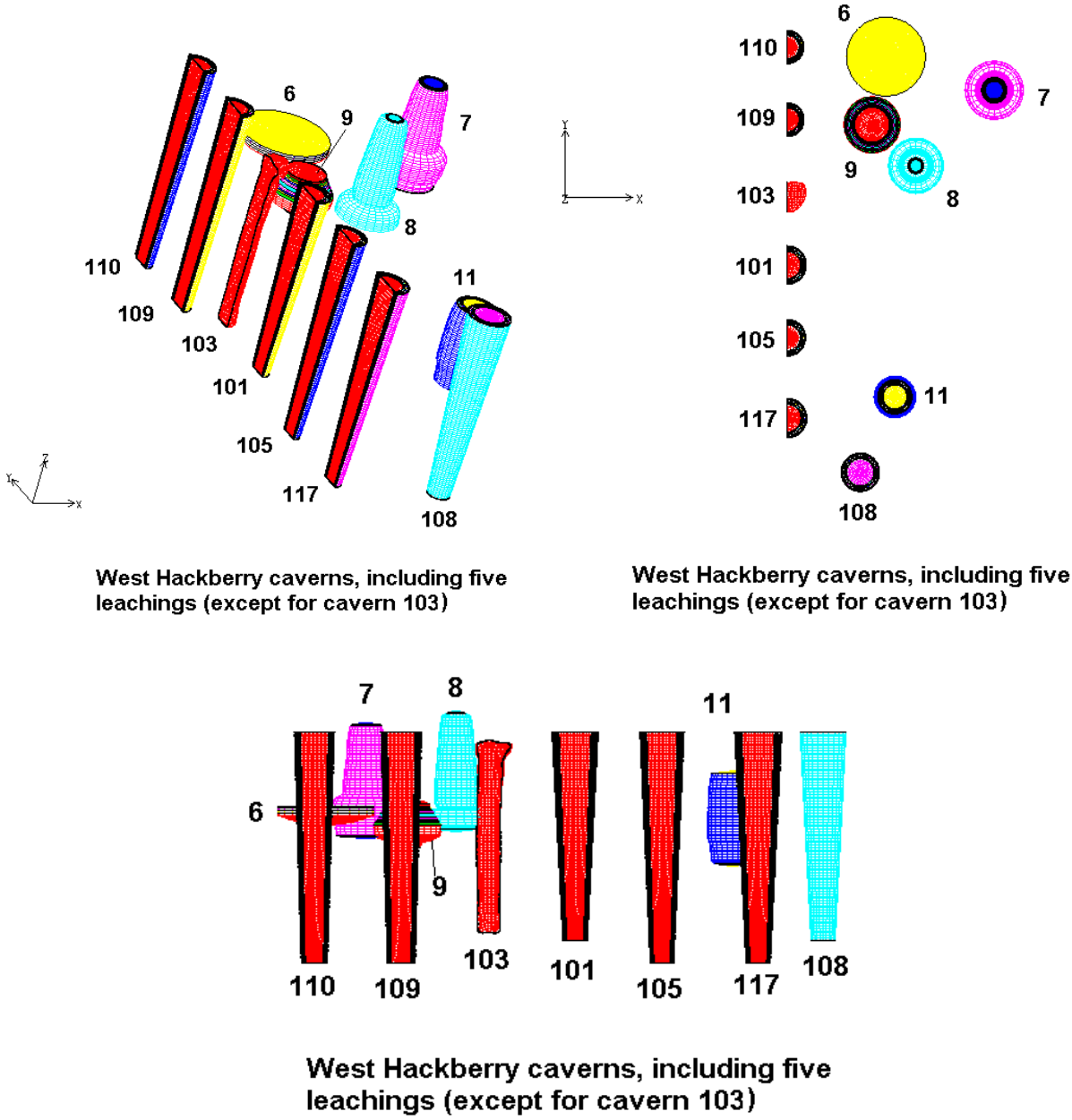

Figure 8. West Hackberry caverns included in the computational mesh (3 views).

Caverns 6 and 9 represent a significant challenge, both from a modeling standpoint and perhaps from an actual operational aspect in the future as the cavern sizes increase along with the potential for adverse interactions. The meshes for these caverns are shown in Figure 9; the dimensions and relative locations of the caverns are shown to scale. If one were to take cylinders surrounding the outmost diameter of each cavern, the pillar thickness between those cylinders is only about 15 ft. Because of the location of these two caverns to each other, and their unusual shapes, the pillar between these caverns was thought to be a prime location for potential dilatant or salt tensile damage. Furthermore, in both actual solution mining and computational meshing

of these caverns, it is important to avoid possible interference between the "arms" of Cavern 9 with the long dish-like Cavern 6. When the onion skin layers were designed for these caverns, it was decided to maintain Cavern 6 at the same maximum radius, and to gradually remove material until it looked like a short, wide cylinder. The final shape is consistent with that predicted by Sansmic (Preece and Foley, 1984) and does not increase the large ceiling span of the cavern (in some SPR literature, the cavern ceiling is also called the roof). Also, the onion skins on Cavern 9 were designed to gradually remove the large mid-cavern ledge, resulting in a final bell shape. While this can be accomplished numerically and would be desired from an operational perspective, the actual shape achieved in the field may be significantly different than simulated. Therefore, all conclusions in this report regarding Caverns 6 and 9, must be understood within the context of the idealizations and modeling procedures used here. In practice, these geomechanics simulations should be updated following any large scale drawdown of the site utilizing sonar data of actual post-drawdown shapes and changes in cavern closure and subsidence rates to verify that our models are capturing the mechanics and assure continued use and integrity of the caverns.

Because of the close proximity of Cavern 8 to Caverns 9 and 6, there exists the potential for pillar interference with five leachings of salt. Therefore, Cavern 8 is provided with only four onion skin layers, maintaining a pillar between it and Cavern 6. Operating the caverns as a gallery would likely be considered at that time.

Cavern 6 poses an additional technical challenge. The sonar data used to create the dish-like shape of Cavern 6 in the original mesh as illustrated in Figure 8 was based on a set of measurements performed in 1982. It was later learned that additional data sets existed for Cavern 6. Three wells enter into West Hackberry Cavern 6, and these wells were deviated. Deviations in the three wells in Cavern 6, in addition to strapping data not originally included in the original sonar data sets, provide a more accurate picture of the true geometry of Cavern 6 in 1982. Unfortunately, no sonar or strapping data have been obtained for Cavern 6 since 1982. The original results of the calculations using the mesh illustrated in Figure 8 are described in Section 4 of this report. The results of those calculations indicated the need to more closely examine the relationship between Caverns 6 and 9, and the full complement of 1982 cavern geometry data were used for Cavern 6. These updated calculations are described in Section 5 of this report.

The other stratigraphic layers represented in the computational mesh include a 1600'-thick layer of overburden modeled as a loose sandstone and a 400'-thick layer of caprock. The caprock and salt dome are surrounded by sandstone. These units are modeled with an elastic model much like previous SPR analyses. The addition of the surrounding sandstone allows for a better representation of the evolution of stress in the salt dome than had been performed in Ehgartner and Sobolik (2002), for which the 30-degree wedge included an infinite salt dome. The salt dome geometry was modeled after the results presented in Rautman et al., (2004), and is to date the most realistic representation of an actual salt dome geometry used in a finite element analysis for SPR.

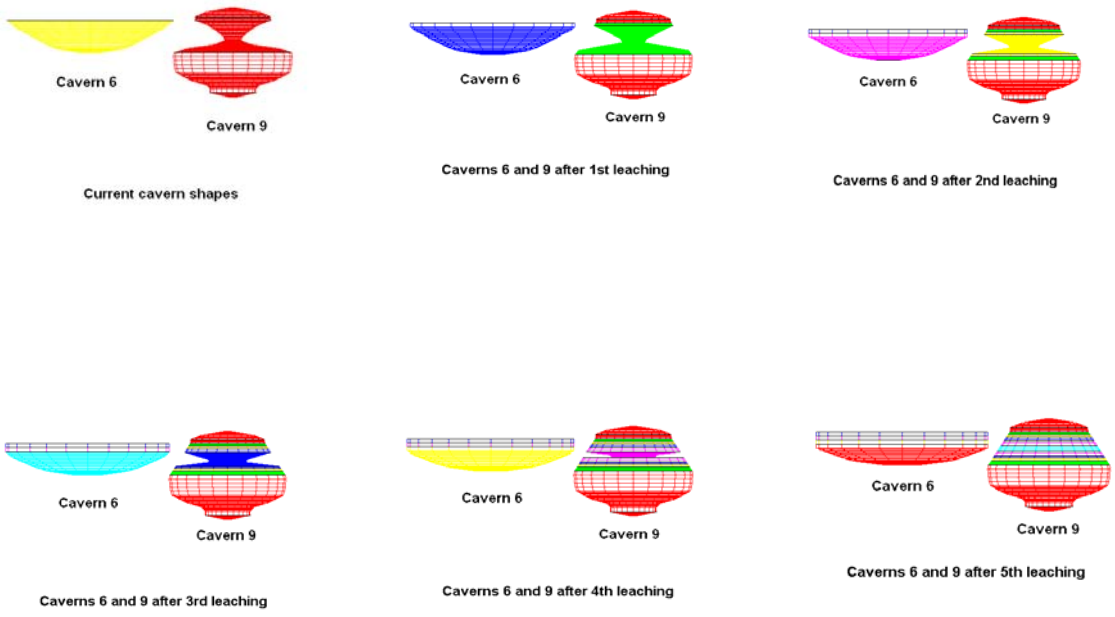

Figure 9. Evolution of Caverns 6 and 9 through five leaching operations.

3.3 NUMERICAL AND MATERIAL MODELS

This analysis utilized JAS3D, Version 2.0.F (Blanford et al., 2001); a three-dimensional finite element program developed by Sandia National Laboratories, and designed to solve large quasi-static nonlinear mechanics problems. Several constitutive material models are incorporated into the program, including models that account for elasticity, viscoelasticity, several types of hardening plasticity, strain rate dependent behavior, damage, internal state variables, deviatoric creep, and incompressibility. The continuum mechanics modeled by JAS3D are based on two fundamental governing equations. The kinematics are based on the conservation of momentum equation, which can be solved either for quasi-static or dynamic conditions (a quasi-static procedure was used for these analyses). The stress-strain relationships are posed in terms of the conventional Cauchy stress.

The power law creep model has been used for Waste Isolation Pilot Plan (WIPP) and Strategic Petroleum Reserve (SPR) simulations for many years. This creep constitutive model considered only secondary or steady-state creep. The creep steady state strain rate is determined from the effective stress as follows:

$$\dot{\varepsilon}_s = A(\sigma)^n \exp\left(-\frac{Q}{RT}\right), \tag{1}$$

where, $\dot{\varepsilon}_s$ = creep strain rate,

σ = effective or von Mises stress,

T = absolute temperature,

A, n = constants determined from fitting the model to creep data,

Q = effective activation energy, determined from fitting the model to creep data, and

R = universal gas constant.

The salt creep properties assume a homogeneous material, and are generally obtained from laboratory measurements. Values for the creep constant, the stress exponent, and the thermal activation energy constant for the power law creep model have been obtained for hard and soft salts through mechanical property testing of salt cores collected from boreholes (Munson, 1998). The West Hackberry and Big Hill salts are identified in Munson (1998) as "soft" salts, as opposed to "hard" salts at Bayou Choctaw and Bryan Mound. For the West Hackberry site, these properties were further calibrated by numerical analysis to match the measured cavern closure and surface subsidence rates at the site (Ehgartner and Sobolik, 2002). Those calculations used a three-dimensional, 30° wedge slice computational domain, which used symmetry conditions to simulate a 19-cavern field. The resulting properties from the 2002 analysis indicated that the in situ creep rates of the West Hackberry salt were up to eight times greater than were predicted using the Munson soft salt properties. Because this current analysis models half of the West Hackberry salt dome and specific caverns, a more comprehensive comparison between measured cavern closure and surface subsidence data can be performed.

3.4 MATERIAL PROPERTIES

Three sets of salt creep properties were used in calculations to compare with West Hackberry historical data: the Munson (1998) soft salt properties, the Ehgartner and Sobolik (2002) properties, and a set identical to Munson's except that the creep constant A has been increased by a factor of 4 (the reasons for this set will soon become apparent). These properties are listed in Table 2. A comparison of the calculated creep rates for expected in situ stress levels at West Hackberry is shown in Figure 10.

Additionally, an elastic modulus reduction factor (RF) was used to simulate the immediate primary creep response that is not captured in the power law creep (i.e. secondary creep) model. In order to obtain agreement with the measured closure of underground drifts at the WIPP, a reduced modulus was used to simulate the transient response of salt (Morgan and Krieg, 1990). The RF is known to vary for salts (Munson, 1998). Limited creep testing of SPR salts (Wawersik and Zeuch, 1984) showed considerable variability in creep rates (up to an order of magnitude difference). For the West Hackberry site (Ehgartner and Sobolik, 2002), a value for RF of 12.5 was determined by calibrating to match the measured closure and subsidence rates at those sites through back-fitting analysis. For these analyses, the modulus values in Table 2 are obtained from the standard modulus values in Munson (1998) divided by a reduction factor of 12.5.

Table 2. Power Law Creep Mechanical Properties Used for West Hackberry Salt

Property	Ehgartner and Sobolik (2002)	Munson (1998)	Modified Munson, where A is multiplied by factor of 4
Density, lb/ft^3	143.6	143.6	143.6
Elastic modulus, lb/ft^2	51.8×10^6	51.8×10^6	51.8×10^6
Bulk modulus, lb/ft^2	34.5×10^6	34.5×10^6	34.5×10^6
Poisson's ratio	0.25	0.25	0.25
Creep Constant A, $1/(psf^n\text{-sec})$	7.42×10^{-27}	9.72×10^{-30}	3.89×10^{-29}
Exponent n	4.9	5.0	5.0
Q, cal/mol	12000	10000	10000
Thermal constant Q/R, °R	10871	9059	9059

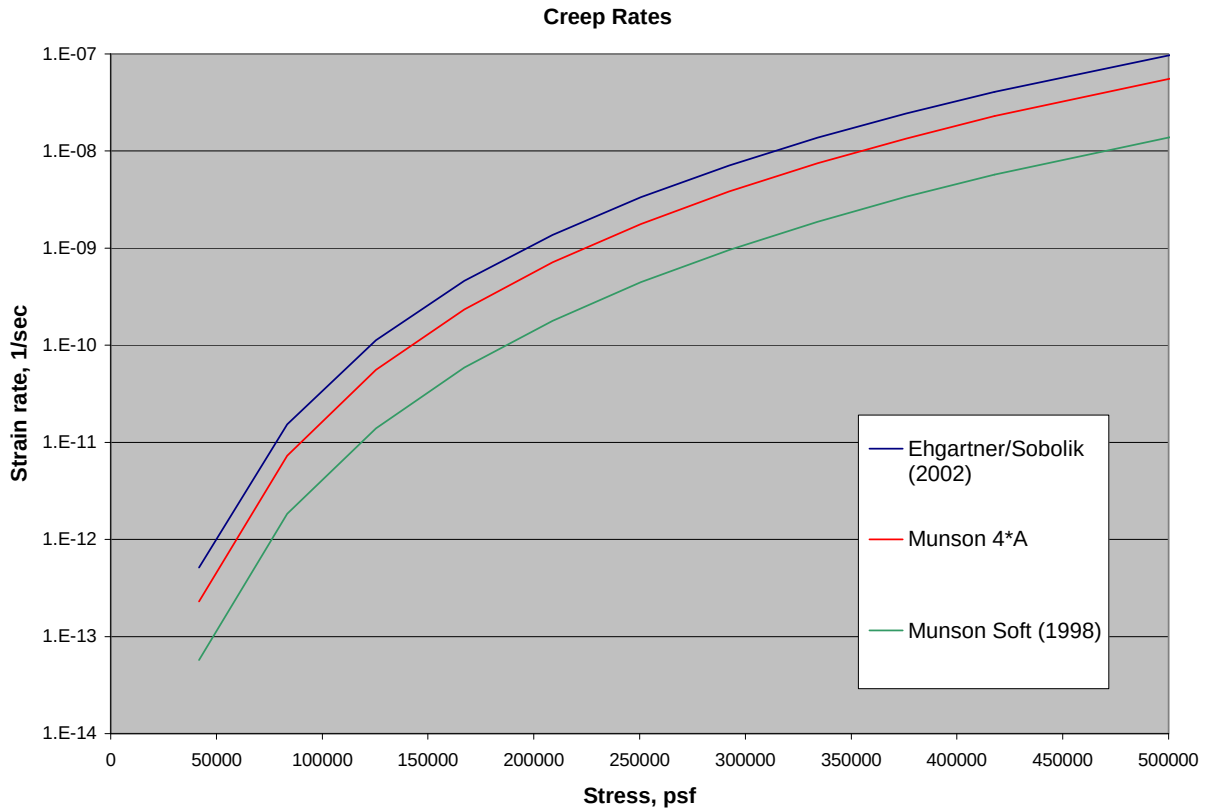

Figure 10. Creep Rates Calculated Using Different Property Sets

Measured surface elevation data over West Hackberry Caverns 6 through 11 and 101 through 117 were obtained from January 1983 through September 2006. These data are easily converted to surface subsidence distances over the same period. Figures 11 through 13 show the measured subsidence data in comparison with the Ehgartner/Sobolik 2002, Munson 1998, and modified Munson (4*A) data, respectively. The Ehgartner/Sobolik properties match the data fairly well until around 1991, when the mean daily wellhead pressures were increased at the West Hackberry site (Woodrum, 2001). Other factors aside from pressure dependent cavern closure have historically contributed to subsidence at West Hackberry including oil extraction at Black Lake and regional subsidence (Magorian et al., 1991), thus making exact comparisons with the data unlikely.

The calculations use constant operating head pressures for the entire period of analysis, after which they overpredict the subsidence. The original Munson properties significantly underpredict the subsidence; this result agrees with the earlier Ehgartner and Sobolik (2002) analysis that the in situ West Hackberry salt is more conducive to creep than the laboratory data indicate. The modified Munson properties moderately underpredict the total subsidence, but the subsidence rates over the period after 1991 are remarkably similar. Table 3 compares the average subsidence rates for the period after 1991, and the rates obtained with the modified Munson properties match the measured rates very well for Caverns 101-117, and reasonably well for Caverns 6-11. Figure 14 shows a modified prediction for subsidence for Caverns 101-117, for which the predicted subsidence rates are added to the measured subsidence on 5/1/1991, for

which a more correct pressure history is applied to each cavern. This modified prediction compares extremely well to the data. The measured and predicted values for subsidence for Caverns 6-11, using the predicted subsidence rates from the modified Munson properties and indexed to the measured subsidence on 5/1/1991, are shown in Figure 15. While the match between predicted and measured subsidence for the Phase 1 caverns is not as good as for Caverns 101-117, it is still reasonably good given the standard range of variability of the salt properties throughout the salt dome.

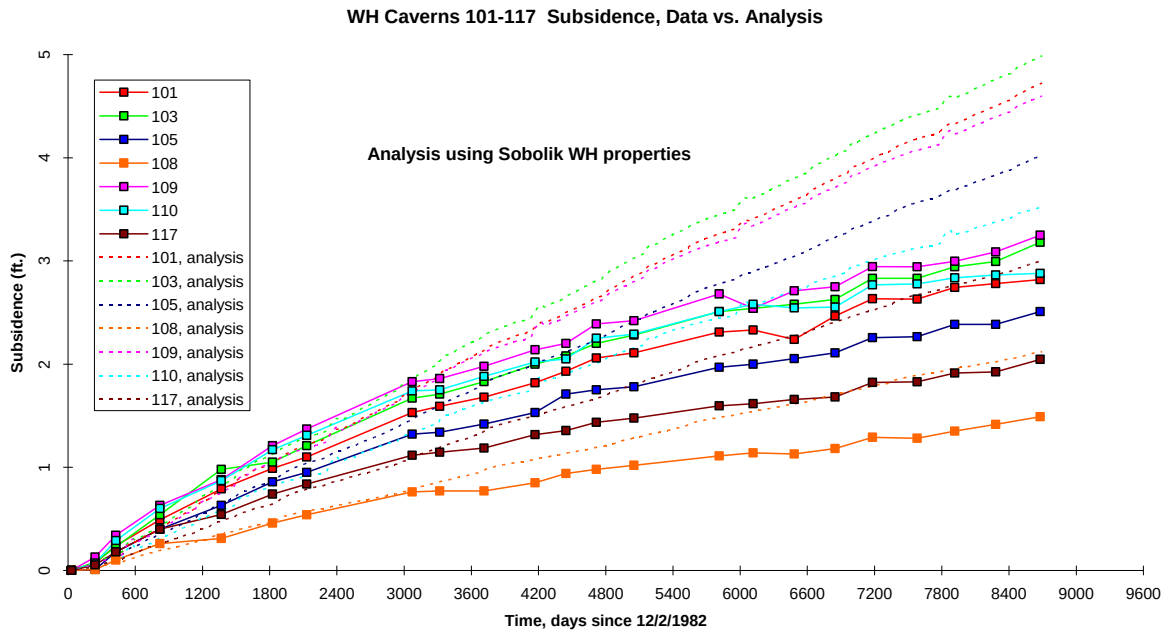

Figure 11. WH Surface Subsidence Data, Caverns 101-117, Compared to Predictions Using Ehgartner/Sobolik (2002) WH Salt Properties

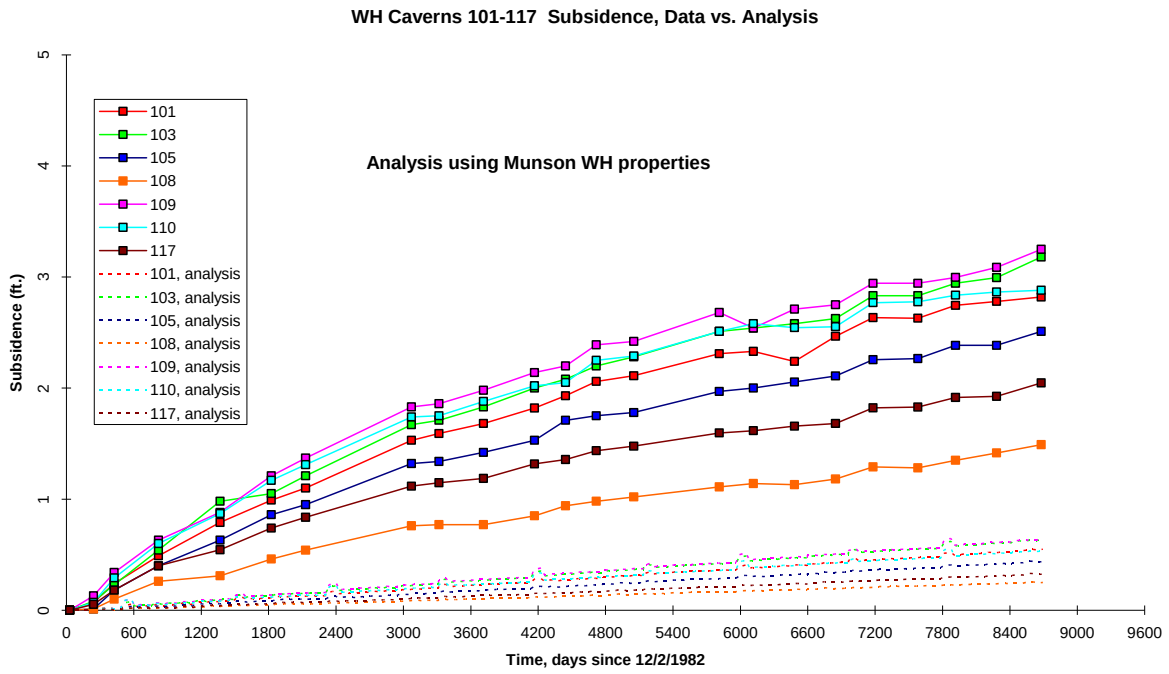

Figure 12. WH Surface Subsidence Data, Caverns 101-117, Compared to Predictions Using Munson (1998) WH Salt Properties

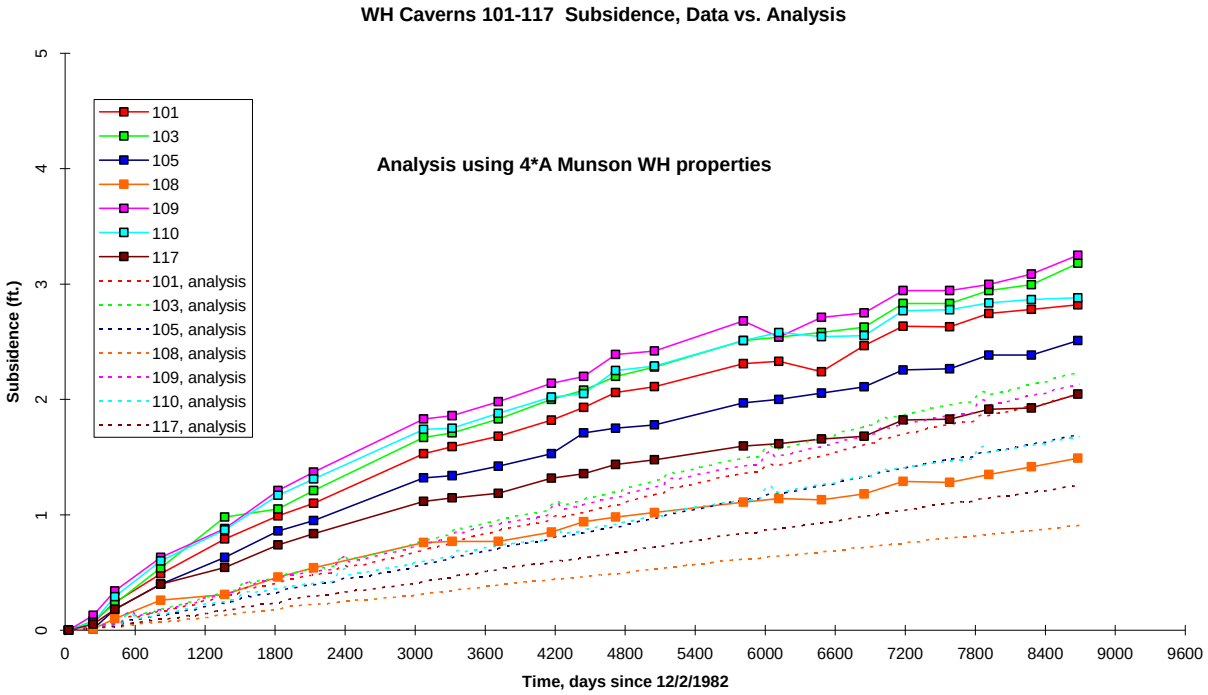

Figure 13. WH Surface Subsidence Data, Caverns 101-117, Compared to Predictions Using Modified Munson (4*A) WH Salt Properties

Table 3. Average Subsidence Rate, 1991-2006, Data and Property Sets

	West Hackberry Caverns Subsidence rates (ft/yr)											
	101	103	105	108	109	110	117	6	7	8	9	11
Data	0.084	0.098	0.078	0.048	0.093	0.074	0.061	0.074	0.060	0.123	0.093	0.086
Modified Munson	0.088	0.095	0.073	0.039	0.090	0.070	0.054	0.063	0.043	0.074	0.081	0.050
Munson (1998)	0.023	0.026	0.019	0.011	0.026	0.022	0.014	0.020	0.014	0.022	0.024	0.014
Ehgartner/ Sobolik	0.194	0.204	0.167	0.087	0.187	0.143	0.125	0.130	0.090	0.159	0.171	0.114

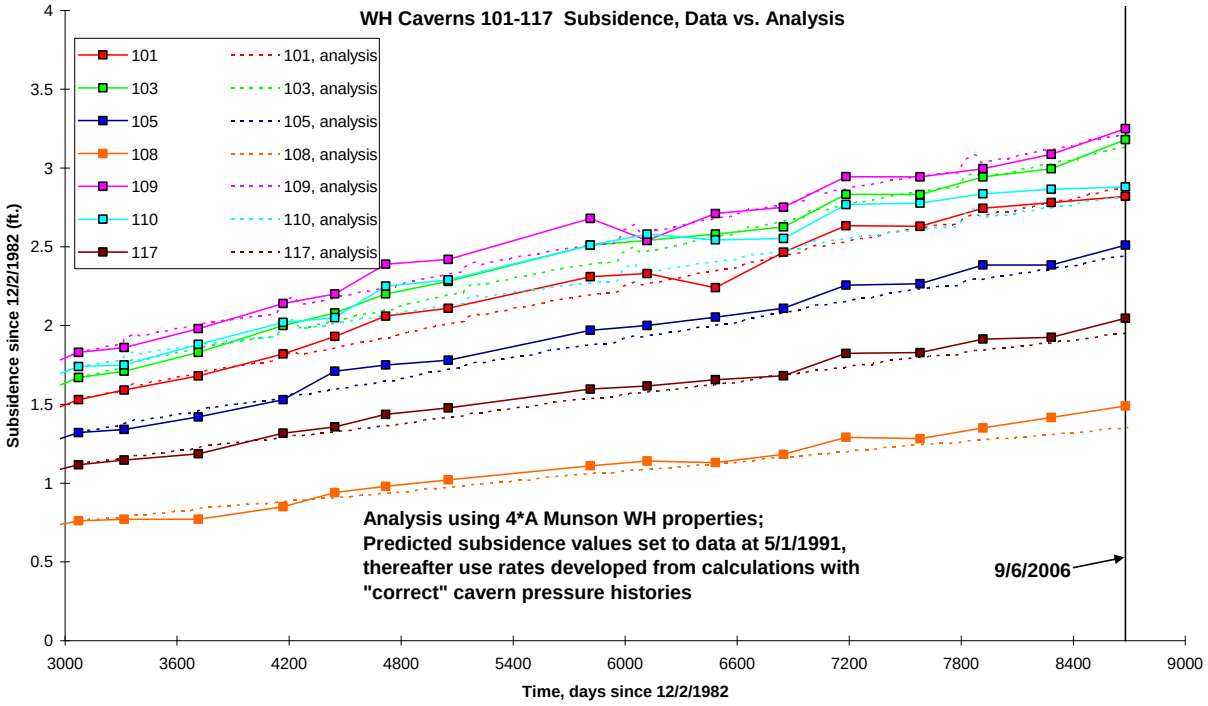

Figure 14. WH Surface Subsidence Data, Caverns 101-117, Compared to Modified Predictions Beginning 5/1/1991

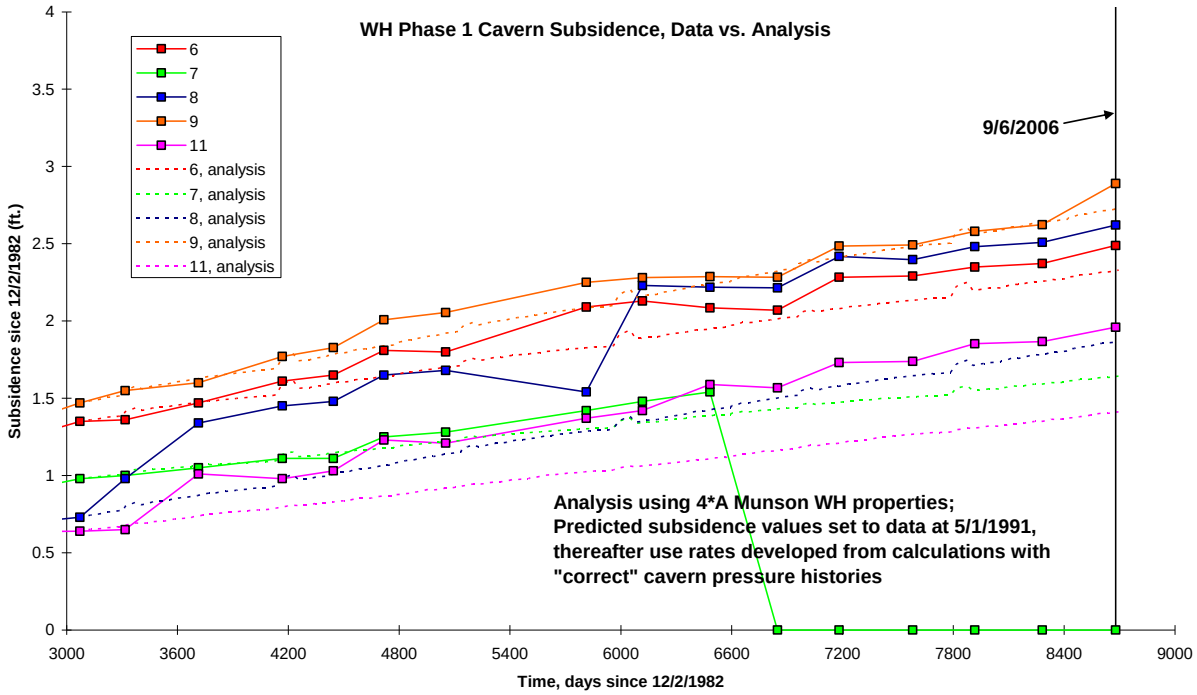

Figure 15. WH Surface Subsidence Data, Caverns 6-11, Compared to Modified Predictions Beginning 5/1/1991

Cavern volume closure information was obtained between 1990 and 1995 for WH Caverns 101-117. The cavern closures as calculated from pressure data (Ehgartner, 2006) are compared to analyses in Figures 16 through 18 using the three property sets. For the Ehgartner/Sobolik (2002) properties in Figure 16, the cumulative closure was overpredicted by a factor between 2 and 3. The Munson (1998) property predictions shown in Figure 17 are underpredicted by a factor of about 3. The modified Munson properties in Figure 18 result in predicted behavior in the same range as the data, with predictions for specific caverns ranging from a great match for Cavern 108 to a 50% overprediction for Cavern 103. The properties of salt are believed to vary spatially in this and other domes. While more effort could be placed into formulating a property set that perhaps better matches the measured surface subsidence and cavern closure data (including the use of a variable operation pressure history for each cavern), of the three sets of properties presented here, the modified Munson clearly provide a reasonable comparison to measured phenomena. The remainder of the report will present results using the modified Munson properties.

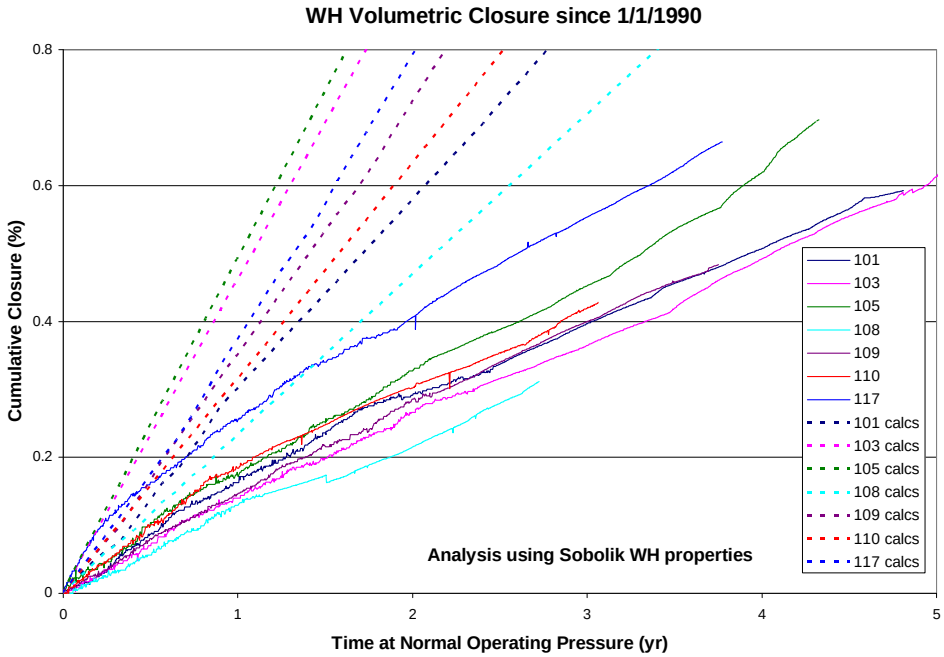

Figure 16. Cavern Volume Closure Data, Caverns 101-117, Compared to Predictions Using Ehgartner/Sobolik (2002) WH Salt Properties

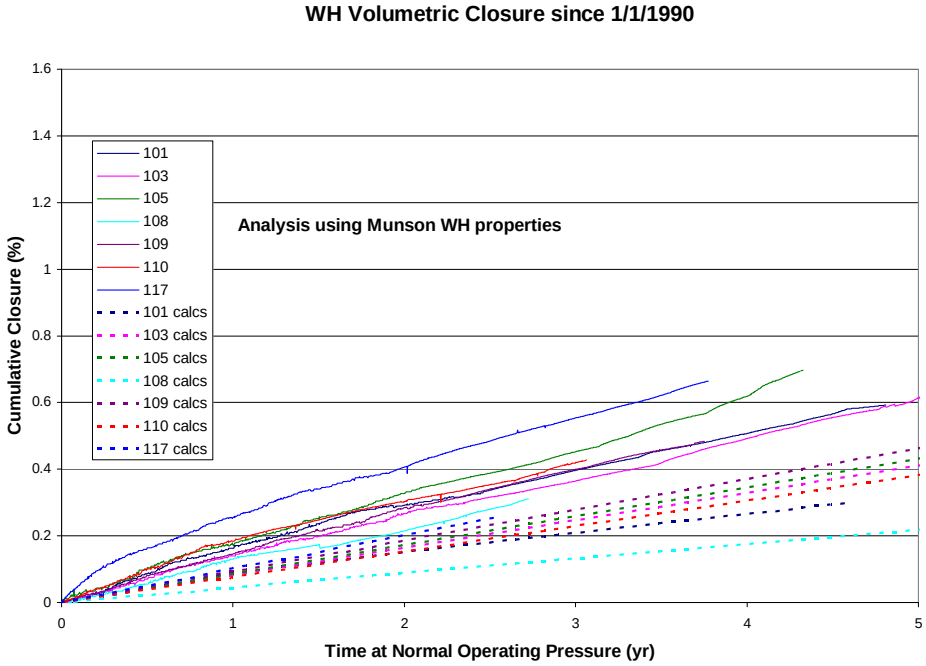

Figure 17. Cavern Volume Closure Data, Caverns 101-117, Compared to Predictions Using Munson (1998) WH Salt Properties

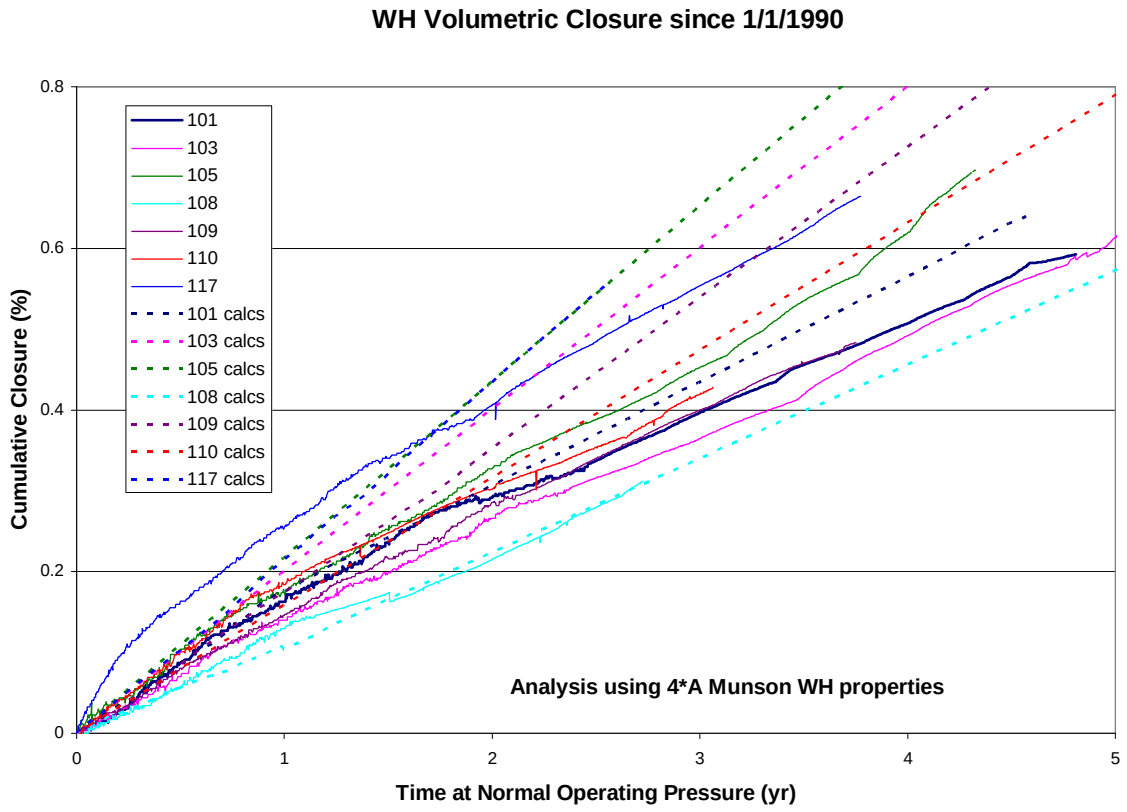

Figure 18. Cavern Volume Closure Data, Caverns 101-117, Compared to Predictions Using Modified Munson WH Salt Properties

The surface overburden layer, which is mostly comprised of sand and sandstone, is considered isotropic and elastic, and has no assumed failure criteria. The caprock layer, consisting of gypsum and limestone, is also assumed to be elastic. Its properties are assumed to be the same as those used for the West Hackberry analyses (Ehgartner and Sobolik, 2002). The sandstone surrounding the salt dome is assumed to be elastic (Lama and Vutukuri, 1978). Mechanical properties of each of these geologic materials used in the present analysis are listed in Table 4.

Table 4: Material properties of other geologic materials.

Parameters	Units	Overburden	Caprock	Sandstone
Density	lbm/ft^3	117.	156.	133.6
Young's Modulus	lb/ft^2	2.09×10^6	146×10^6	153×10^6
Poisson's Ratio		0.33	0.29	0.33

3.5 SALT DAMAGE CRITERIA

The salt damage factor (analogous to a safety factor) has been developed from a dilatant damage criterion based on a linear function of the hydrostatic pressure (Van Sambeek et al., 1993). Dilatancy is considered as the onset of damage to rock resulting in significant increases in permeability. Dilatant damage in salt typically occurs at a stress state where a rock reaches its minimum volume, or dilation limit, at which point microfracturing increases the volume. Dilatant criteria typically relate two stress invariants: the mean stress invariant I_1 (equal to three times the average normal stress) and the square root of the stress deviator invariant J_2, or $\sqrt{J_2}$ (a measure of the overall deviatoric or dilatant shear stress). (By convention, tensile normal stresses are positive, and compressive normal stresses are negative, hence the sign nomenclature in the following equations.) The dilatant criterion chosen here is the equation typically used from Van Sambeek et al. (1993),

$$\sqrt{J_2} = -0.27 I_1 . \tag{2}$$

The Van Sambeek damage criterion defines a linear relationship between I_1 and $\sqrt{J_2}$, and such linear relationships have been established from many suites of laboratory tests on WIPP, SPR, and other salt samples. This criterion was applied during post-processing of the analyses. A damage factor (safety factor) index was created (SF_{VS}) by normalizing I_1 by the given criterion:

$$SF_{VS} = \frac{-0.27 I_1}{\sqrt{J_2}} \tag{3}$$

Several earlier publications define that the Van Sambeek damage factor SF_{VS} indicates damage when $SF_{VS}<1$, and failure when $SF_{VS}<0.6$. In previous studies, values of $SF_{VS}<1.5$ have been categorized as cautionary because of unknown localized heterogeneities in the salt that cannot be captured in these finite element calculations. This report will use these damage thresholds.

Recent developments in laboratory testing of salt from several underground storage sites indicate that the Van Sambeek linear dilatant damage criterion may not adequately define the damage envelope for all salt formations. Triaxial compression (TXC) tests performed on samples of salt from the Big Hill SPR site at several values of confining pressure (Lee et al., 2004) indicate a nonlinear relationship between I_1 and $\sqrt{J_2}$. The Big Hill salt is characterized in Munson (1998) as a soft salt comparable to the salt at West Hackberry. A dilatant criterion equation based on laboratory tests performed on samples of salt from the Big Hill site is given in Lee et al. (2004) as:

$$\sqrt{J_2}(MPa) = 12.04 - 9.104 e^{-0.04931 I_1(MPa)} \tag{4}$$

RESPEC of Rapid City, South Dakota recently performed laboratory testing of Cayuta salt recovered from the Bale No. 1 Well, located approximately 1 mile southwest of Cayuta in

Schuyler County, New York (DeVries et al., 2005). These laboratory tests were used to characterize the strength and deformation behavior of bedded salt formations. Both constant mean stress triaxial compression (CMC) and constant mean stress triaxial extension (CMX) test suites were performed. The data indicated that the dilation limit in extension was around 30% less than in compression. This dependence on compression or extension correlates to a dependence on the Lode angle ψ, which is defined using the principal stresses σ_1, σ_2, and σ_3 by:

$$\psi = \tan^{-1}\left(\frac{1}{\sqrt{3}}\frac{2\sigma_2 - \sigma_1 - \sigma_3}{\sigma_1 - \sigma_3}\right) \tag{5}$$

From these tests, DeVries et al. developed a new dilation criterion based on the Mohr-Coulomb criterion written in its invariant form. This RESPEC Dilation criterion, or RD, was developed to address the shortcomings of the Van Sambeek linear criterion when compared to laboratory data: namely, a nonzero intercept, a nonlinear relationship between I_1 and $\sqrt{J_2}$, and the effects of the Lode angle. This RD criterion is defined by:

$$\sqrt{J_2} = \frac{D_1\left(\frac{I_1}{\sigma_0}\right)^n + T_0}{\left(\sqrt{3}\cos\psi - D_2\sin\psi\right)}, \tag{6}$$

where σ_0 is a dimensional constant equal to –1 MPa; T_0 is the unconfined tensile strength; ψ is the Lode angle; and n, D_1, and D_2 are parameter estimates that must be determined for each salt formation. DeVries et al. developed values for the fitting parameters for Cayuta salt; the parameters are listed in Table 5, both in their original SI and converted to English units. Figure 19 compares the laboratory data to the RD criterion curves obtained with Equation 6 and the values in Table 5. These are also compared to the Van Sambeek criterion, and to the in situ values of I_1 at the top and bottom of the Phase 2 caverns (Caverns 101-117). Note that the RD damage envelope in the region of in situ stress is significantly smaller than that using the Van Sambeek criterion.

Table 5. RD Criterion Parameter Values for Cayuta Salt (DeVries et al., 2005)

Criterion Parameters	Fitted Value (SI)	Fitted Value (English)
σ_0	-1 MPa	-20885 psf
n	0.693	0.693
D_1	0.773 MPa	16100 psf
D_2	0.524	0.524
T_0	1.95 MPa	40700 psf

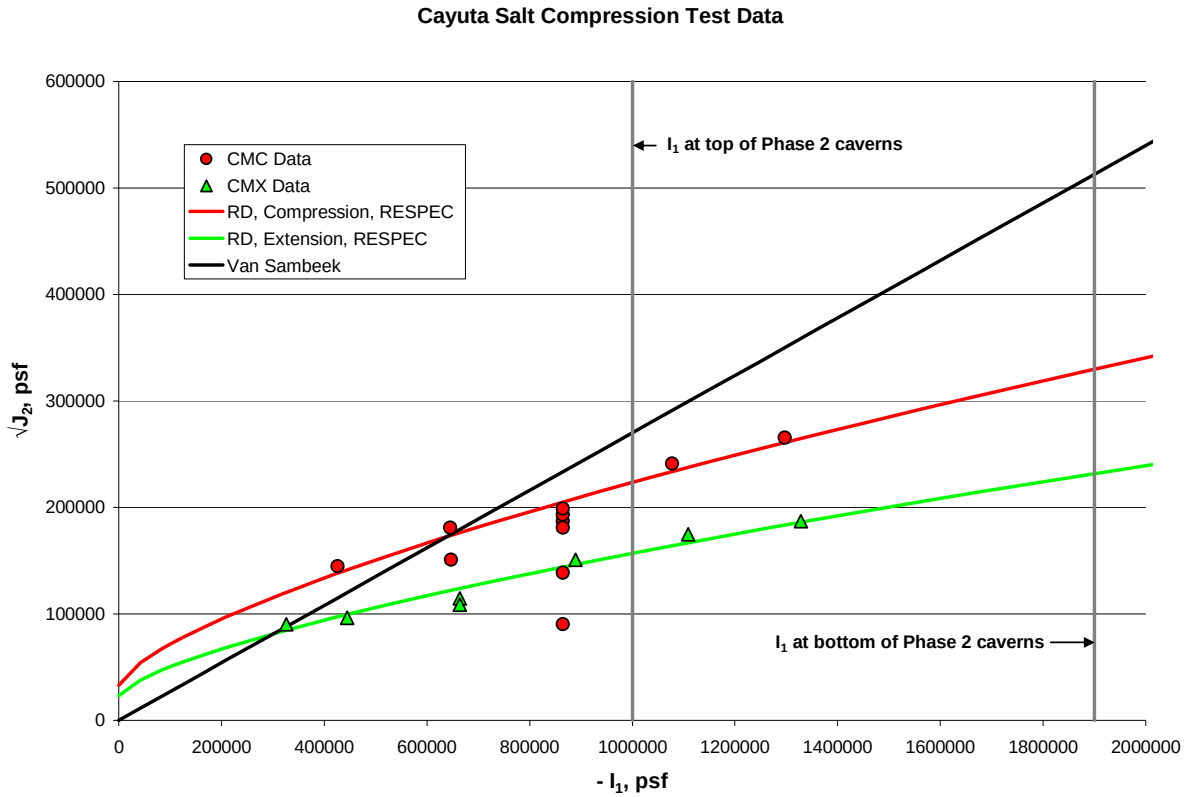

Figure 19. Comparison between test data and RD criterion, Cayuta salt (DeVries et al., 2005).

A similar Lode angle-based criterion would be desired for the Big Hill data, but no data exists for triaxial extension tests for that salt. Using the triaxial compression data from Lee et al. (2004), and estimated behavior of similar triaxial extension tests based on those observed in the Cayuta tests, an estimated set of parameters for Equation 6 was developed for the Big Hill salt. These parameters have been developed only for the sake of exploration, and should not be considered as a laboratory-based set. The estimated Big Hill parameters are listed in Table 6, both in SI and English units. Figure 20 compares the laboratory and estimated data to the RD criterion curves obtained with Equation 6 and the values in Table 6. These are also compared to the Van Sambeek criterion, to the in situ values of I_1 at the top and bottom of the Phase 2 caverns (Caverns 101-117), and to the curve from Lee et al. defined by Equation 4. Finally, Figure 21 compares the three criteria to the in situ stress values at the top and bottom of the caverns. The two Lode angle-based criteria will predict damage at significantly lower deviatoric stresses than the Van Sambeek criterion.

Table 6. Estimated RD Criterion Parameter Values for Big Hill Salt

Criterion Parameters	Fitted Value (SI)	Fitted Value (English)
σ_0	-1 MPa	-20885 psf
n	0.3668	0.3668
D_1	2.164 MPa	45200 psf
D_2	0.5632	0.5632
T_0	4.0 MPa	83540 psf

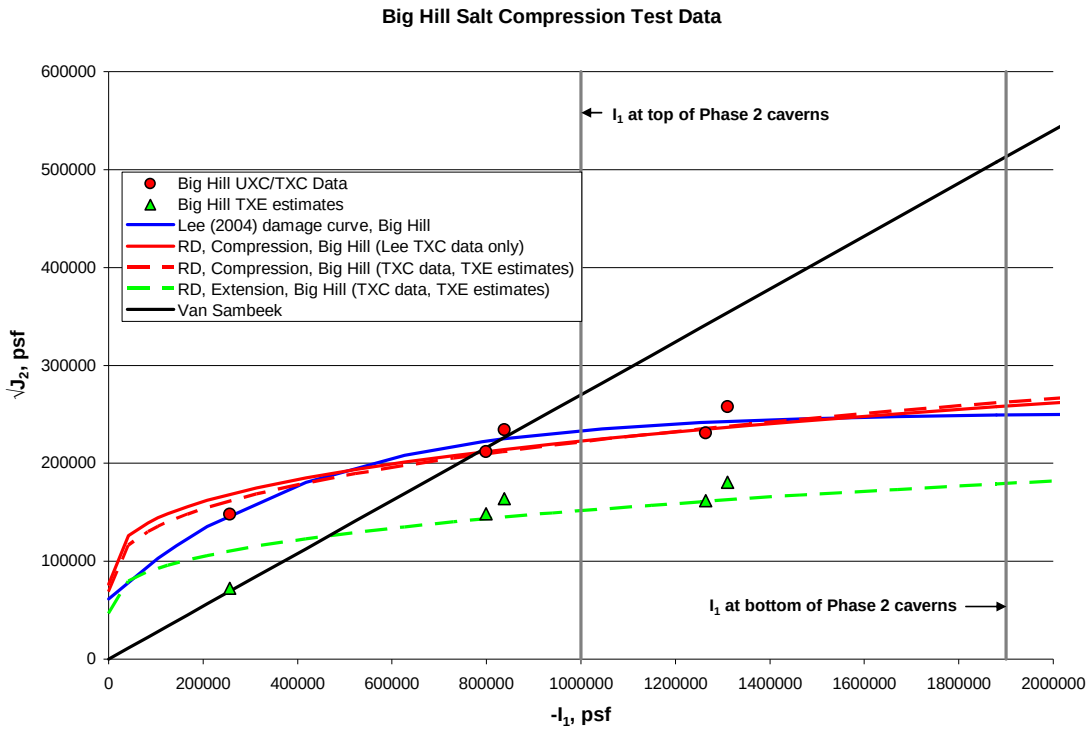

Figure 20. Comparison between data and RD criterion, Big Hill salt (based on Lee et al., 2004).

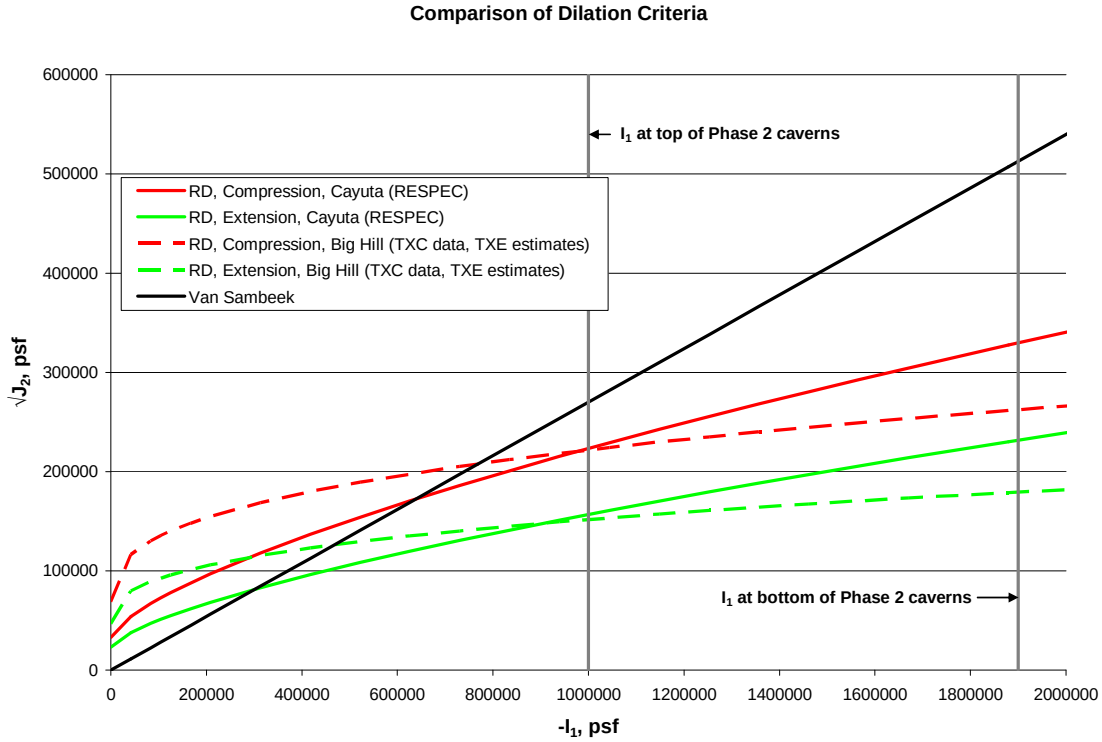

Figure 21. Comparison between the three dilatant damage criteria.

These three criteria were applied during post-processing of the analyses. A damage factor index was created for the RD criterion (SF_{RD}) by normalizing or $\sqrt{J_2}$ by the given criterion; as for the Van Sambeek damage factor, values less than 1 indicate damage:

$$SF_{RD} = \frac{\sqrt{J_2}}{\left[\frac{D_1\left(\frac{I_1}{\sigma_0}\right)^n + T_0}{\left(\sqrt{3}\cos\psi - D_2\sin\psi\right)}\right]} \tag{7}$$

The damage factor using the Cayuta salt properties is designated SF_C, and for the Big Hill salt properties SF_{BH}. Because there are no laboratory data sets available containing both triaxial compression and extension test using West Hackberry salt, the use of the Cayuta and Big Hill criteria here is for illustrative purposes to show where problems of dilatant damage may be occurring. As will be explained, one of the conclusions of this report is that these laboratory data should be developed for all the SPR sites to ascertain the linearity of the damage curve and its dependence on Lode angle.

4. RESULTS

The historical performance of the West Hackberry caverns, and their predicted future performance, will be evaluated on the basis of several design factors: dilatant and tensile stress damage to the salt surrounding the caverns, cavern volume closure, axial well strain in the caprock, and surface subsidence. These performance factors will provide metrics to determine the feasibility of expanding the storage capacity of the caverns. The performance of the Phase 1 caverns will be emphasized in Sections 4.1 through 4.4 (particularly relating to expansion); the performance of the Phase 1 caverns and Caverns 101 and 103 will be further evaluated in Section 4.5 using the RESPEC Lode angle-based damage criteria.

4.1 DILATANT AND TENSILE STRESS DAMAGE NEAR THE PHASE 1 CAVERNS

There are two ways in which the salt surrounding the caverns can be damaged: by dilatant damage resulting from microfracturing that increases permeability and the potential for crack propagation, and by tensile stresses which cause salt fracture and crack propagation. A quick way to evaluate the potential for damage is by the use of history plots of the extreme values of damage factor and maximum principal stress in the salt surrounding the cavern through each of the five leaching operations. Figure 22 shows the minimum value of the Van Sambeek damage factor (Equation 3) surrounding each of the five Phase 1 caverns as a function of time. Note that the lowest values of damage factor occur during workover operation periods. The first leaching operation occurs at 9395 days on the plot (see arrow on plot); the first workover operation for Cavern 6 after this leaching (days 9660-9730) results in a damage factor well below 1 and nearly to the value of 0.6 used as a failure threshold. This damage occurs around the perimeter of Cavern 6. Figure 23 shows a vertical cross-section of Caverns 6 and 9 on day 9730; note how the top layer of Cavern 6 is red, indicating a damage factor less than 1. Figure 24 is a close-up of the edge of Cavern 6, showing the location of the high deviatoric stress region around the perimeter. Note also in Figure 22 that for Caverns 6 and 9, there are usually two areas of low values in safety factor bounding the 90-day workover period. Because of the unusual shapes of these two caverns, the pressure changes during the drawdown to zero wellhead pressure, and the re-pressurization back to normal operating pressure causes transient deviatoric stresses in specific regions around the caverns. For Cavern 6, this region is always the perimeter of the dish-shaped cavern. At the start of the workover, the lower pressure in the cavern causes a temporarily larger compressive stress around the perimeter, creating the first low spike in the damage factor. The stresses improve with time during the workover, until the cavern pressure in Cavern 6 is increased again. Upon repressurization of the cavern to normal pressures, the same perimeter locations experience a temporary tensile loading, creating the potential for both tensile and dilatant fracturing. These damaging conditions are decreased as Cavern 6 is further enlarged during subsequent leaches to a more cylindrical shape, but it is not until the fourth leaching that the damage factor is once again above the damage threshold during workovers. Cavern 9 displays a similar “double-minimum” during workovers. Figures 25 and 26 show contour plots of the damage factor around Cavern 9 for the beginning and end of its workover cycle prior to the first leaching. The primary location of deviatoric stress on the cavern walls directly beneath the circular shelf within Cavern 9, about two/thirds of the height from the bottom of the cavern. There is also some high deviatoric stress on the top surface of the shelf during the drawdown phase. Note from Figure 22 how the conditions in Cavern 9 improve if solution mining is

designed to remove the shelf in Cavern 9, resulting in a bell-shaped final cavern. For a final observation from Figure 22, note how the minimum damage factor for Cavern 6 decreases during a workover for Cavern 9, and vice versa. The influence of these two caverns on each other is an important design criterion for future operations.

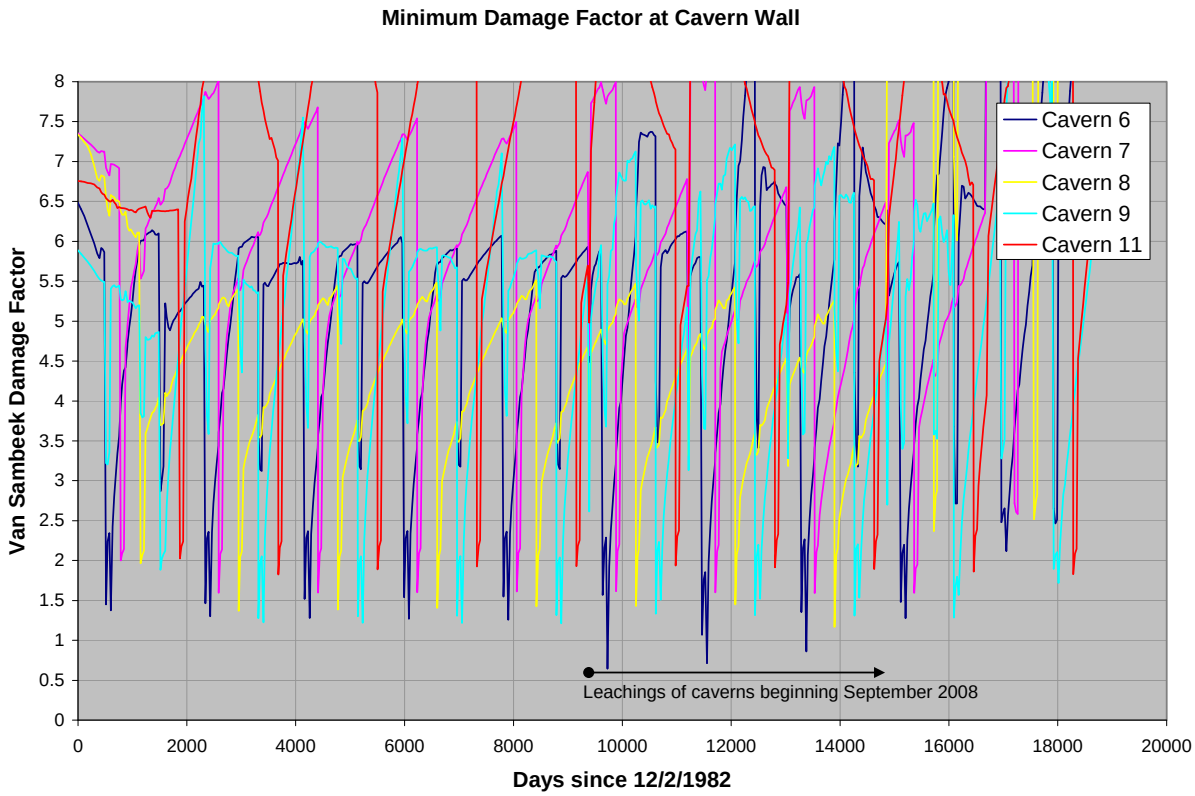

Figure 22. Minimum value of the Van Sambeek damage factor surrounding each Phase 1 cavern.

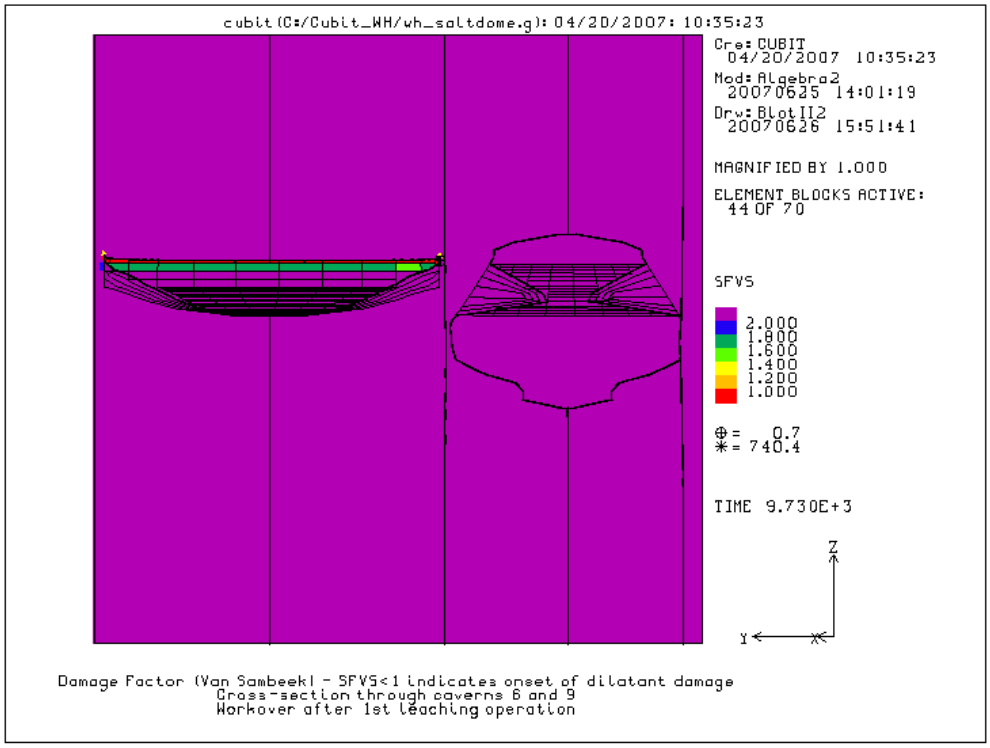

Figure 23. Contour plot of Van Sambeek damage factor, cross-section of Caverns 6 and 9, 1st workover period after 1st leaching.

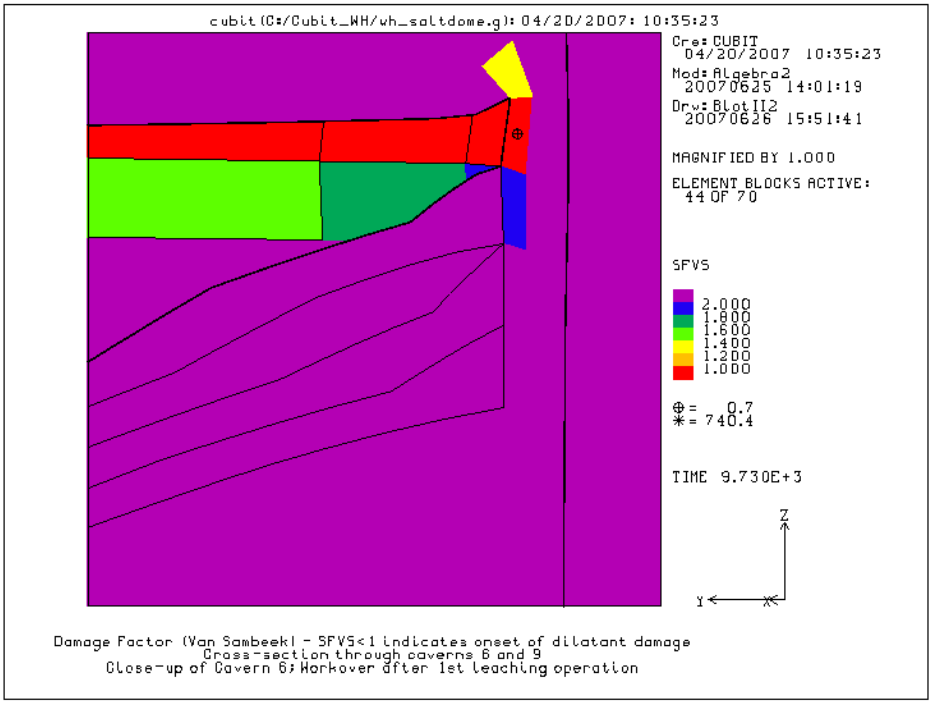

Figure 24. Close-up of Cavern 6 from Figure 23.

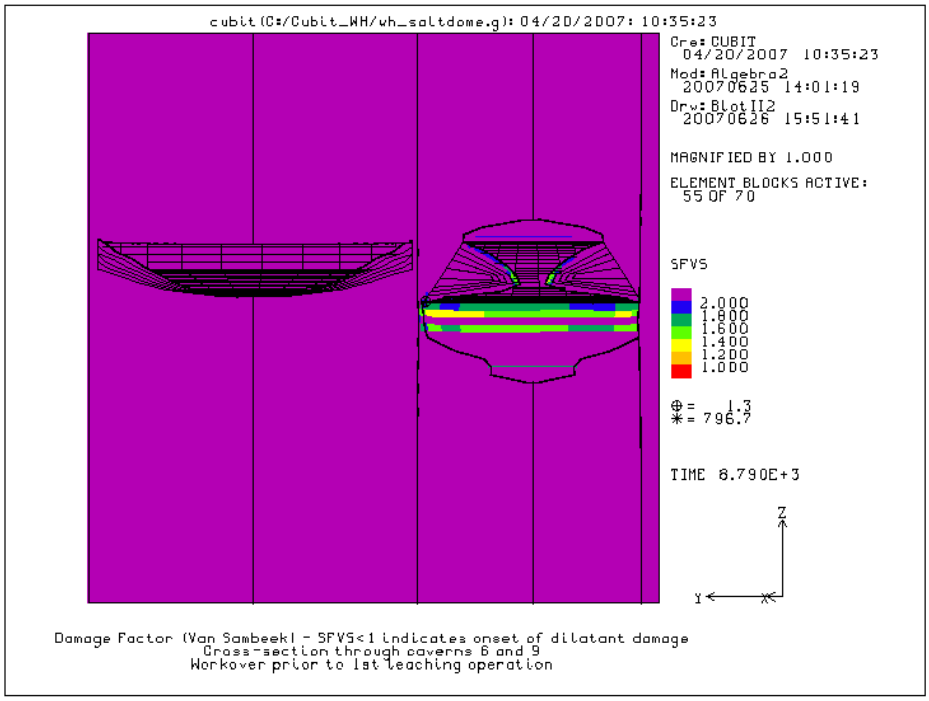

Figure 25. Contour plot of Van Sambeek damage factor, cross-section of Caverns 6 and 9, beginning of workover period prior to 1st leaching.

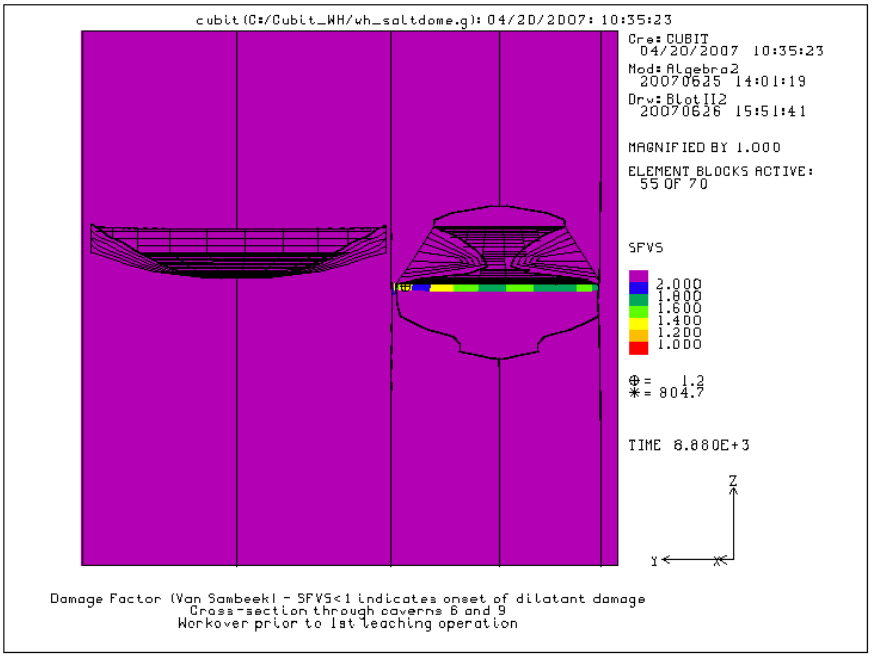

Figure 26. Contour plot of Van Sambeek damage factor, cross-section of Caverns 6 and 9, end of workover period prior to 1st leaching.

Figure 27 shows the maximum value of the maximum principal stress around the Phase 1 caverns as a function of time. The perimeter of Cavern 6 experiences spikes in tensile stress during the repressurization at the end of workovers after the cavern has been leached because of drawdown. Cavern 9 is the only other cavern that experiences stresses that approach tension, but remain compressive, and its conditions improve as leaching removes the circular shelf in the cavern. Note the length of time required for the maximum principal stress at the wall to recover from the workover operation and return to a near-hydrostatic value.

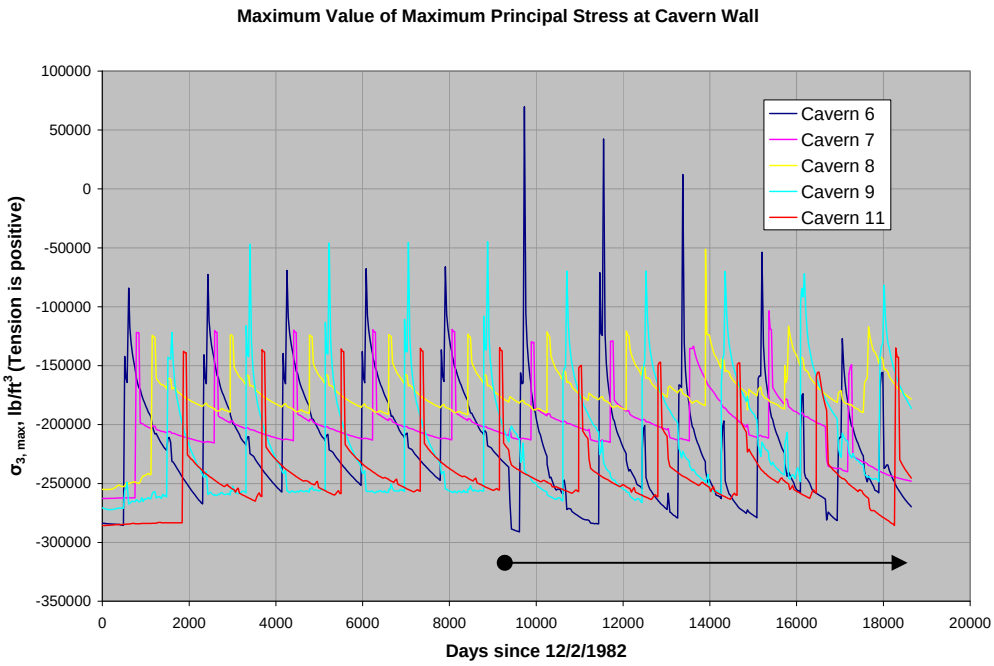

Figure 27. Maximum value of the maximum principal stress surrounding each Phase 1 cavern.

Because the perimeter of Cavern 6 is predicted to have both dilatant damage and tensile fracture conditions after repressurization at the end of a workover period, it is important to know whether that condition is affected by the rate of repressurization. The primary calculations in this report model the close of the workover with an instantaneous wellhead pressure increase from 0 to 975 psi. A portion of the calculations were re-run with linear repressurization periods of 12, 16, and 36 hours, and with small time increments during repressurization. A comparison of the minimum damage factors for the different rates is shown in Figure 28; in general, there is no significant difference. Figure 29 expands the time scale around the repressurization period, and the indication is that the rate of repressurization has no effect on this phenomenon. Figure 30 presents a similar plot of the maximum principal stress; again, the repressurization rate has no effect on the results. The primary conclusion is that the times of highest potential of salt damage/salt falls are during large cavern pressure changes, such as depressurization or repressurization in workovers. Even at low cavern pressures, over time the stresses in the cavern walls will adjust to near isotropic conditions; there will be increased creep and cavern closure, but the potential for damage will dissipate as the cavern pressure remains constant.

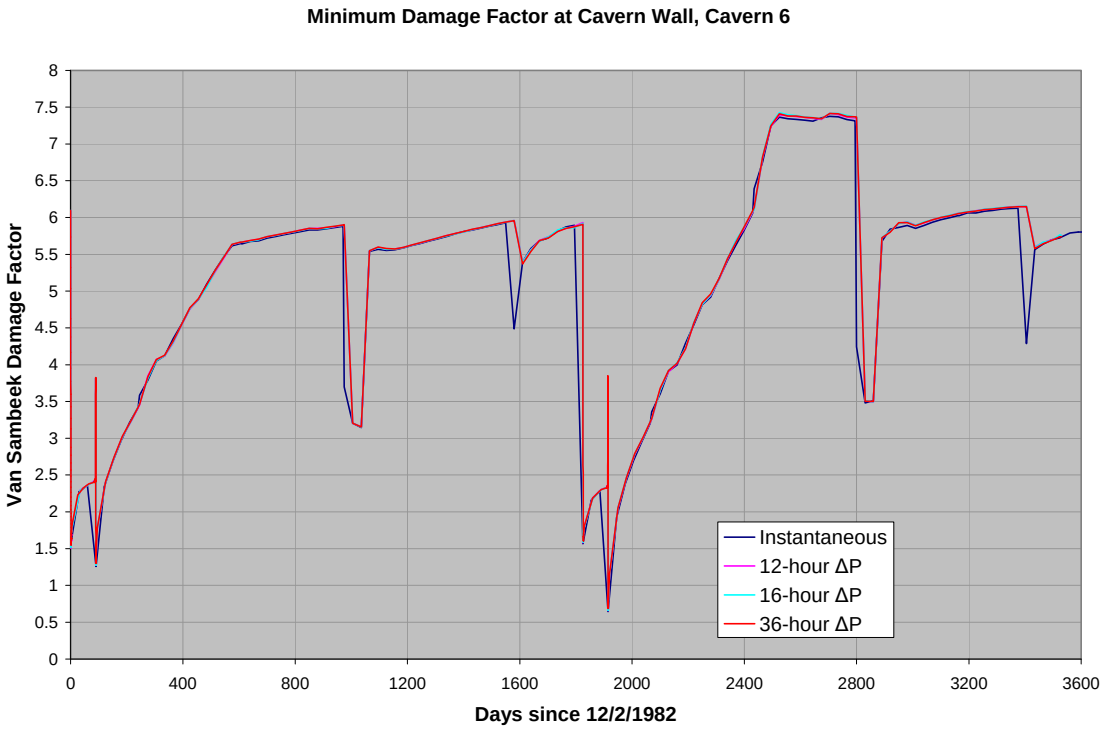

Figure 28. Minimum damage factor in Cavern 6 as a function of repressurization rate

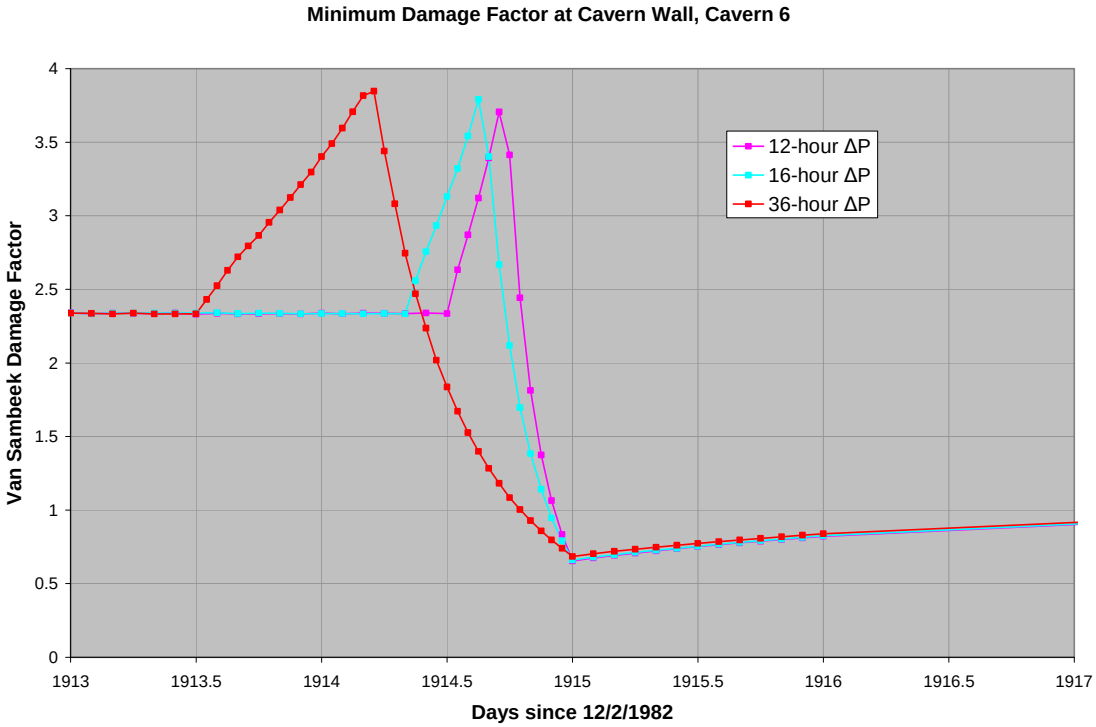

Figure 29. Minimum damage factor near Cavern 6 for different repressurization rates at the end of a workover period.

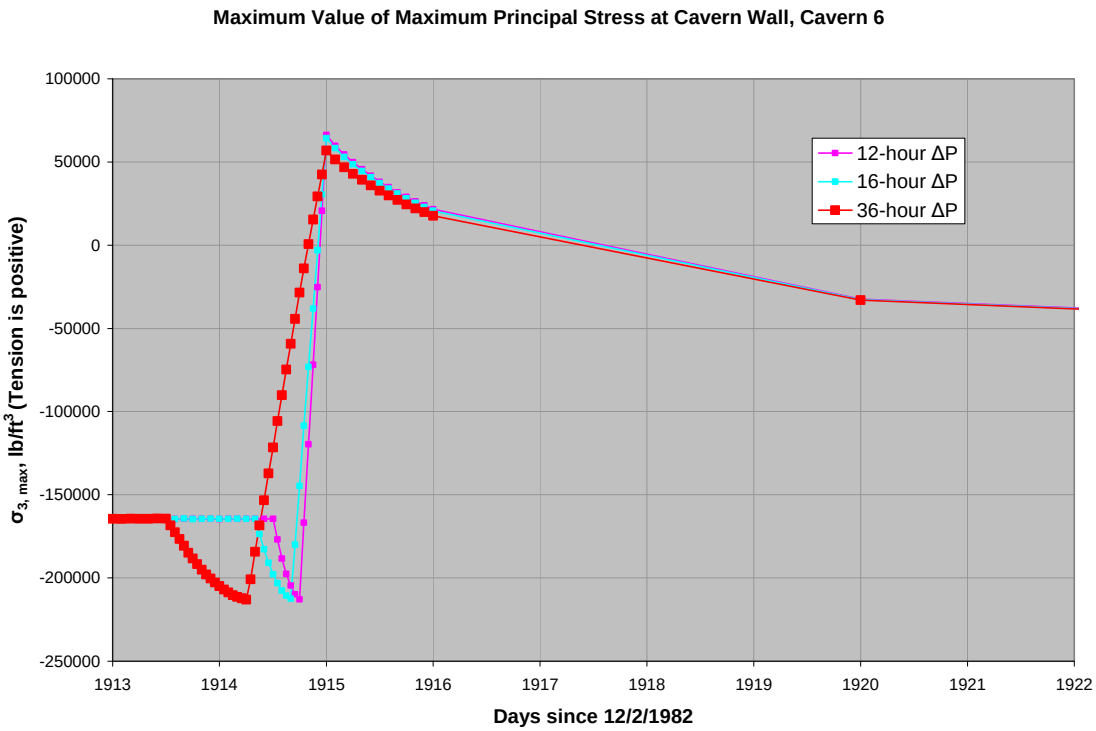

Figure 30. Maximum principal stress near Cavern 6 for different repressurization rates at the end of a workover period.

The preceding calculations indicate that West Hackberry Cavern 6 is predicted to experience tensile cracking during repressurization of the cavern following workover conditions. The cracking is predicted around the edge of the cavern ceiling and was insensitive to the range of cavern repressurization durations (12 to 36 hrs) studied. The cracking was not predicted for the current cavern geometry, but occurred after the first leaching resulting from oil drawdown and was present following workovers for the first three subsequent cavern geometries changed by leaching. To determine if the predicted cracking was mesh dependent, the finite element mesh was refined in the cracked area to further delineate and verify the predictions. The results indicated that the middle of the cavern walls around the perimeter of Cavern 6 would experience tensile stresses, even somewhat higher than the original predictions. Because the situation is geometry dependent and the exact geometry of Cavern 6 near the edge of the ceiling is not well known (sonar limitations), it is possible that the fracturing could be occurring with the current cavern geometry. The close proximity of Cavern 9 poses a risk of cavern communications. The caverns are located 120 feet at their closest point in the model. A more refined estimate using detailed sonar data of the caverns calculates a minimum separation of only 100 ft (Rautman and Snider, 2007). The risk is further increased by a zone of potentially anomalous salt that connects the two caverns (the potential shear zone in Figure 4), as the salt may well be weaker than normal. The tensile stresses are only predicted during and immediately following repressurization of the cavern and last for several months. Pressure applied to the large ceiling span apparently induces an elastic, tensile response at the edges of the ceiling. The tensile stresses are relaxed with time resulting from creep into a normal compressive state. If a crack

were to propagate and intersect Cavern 9, cavern pressures would equilibrate. The maximum equilibrated pressures are not problematic to the wellhead or production casings in either caverns, but an operational scenario of having Cavern 9 in workover mode during the breach would pose a serious risk to operational safety and containment of oil. A breach when Cavern 6 is fully repressurized (the most likely condition) would result in approximately 55,000 bbl of oil entering into Cavern 9. With the wellhead removed during workover mode, the oil would eject onto the surface. This would pose a serious safety risk to the workover crew and potential environmental damage. More details of this type of scenario are discussed by Ehgartner (2004). The obvious reaction would be to operationally prohibit sequential workovers of Caverns 6 then 9, allowing for an adequate time between repressurization of Cavern 6 and the workover of Cavern 9. These analyses suggest a three-month period, but a reasonable safety factor must be applied given the analysis uncertainties and severe consequences. Additional analysis of the interactions between Caverns 6 and 9 are discussed in Section 5.

Caverns 7, 8, and 11 are not predicted to experience any stress conditions indicative of dilatant or tensile damage, either through their current history or through the planned cavern expansions. Cavern 8 does experience some instances where the minimum safety factor is less than 1.5, with one instance with a value of 1.17 after the third leaching. The highest dilatant and maximum principal stresses tend to be at three locations: along the top surface of the cavern, along the bottom surface near the outer edge, and near the large change in diameter near the bottom of the cavern. The influence of nearby Caverns 6 and 9 also affects the stress history around Cavern 8. Figures 31-36 are contour plots of damage factor for cross sections of Caverns 9 and 8, 6 and 8, 6 and 7, and 11. These are at the times of highest deviatoric stress (lowest damage factor) for Caverns 8, 7, and 11. As these are the most severe conditions predicted in the calculations, it can be seen that Caverns 7 and 11 have no major stability concerns, and Cavern 8 has minimal concerns.

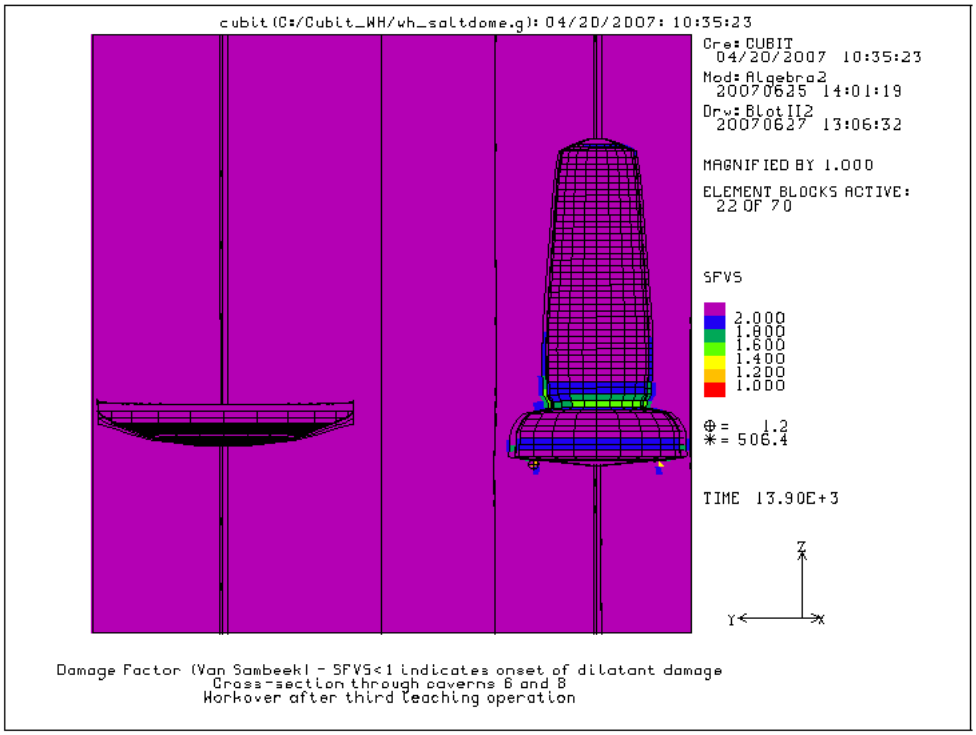

Figure 31. Contour plot of Van Sambeek damage factor, cross-section of Caverns 6 (left) and 8 (right), beginning of workover period after 3rd leaching.

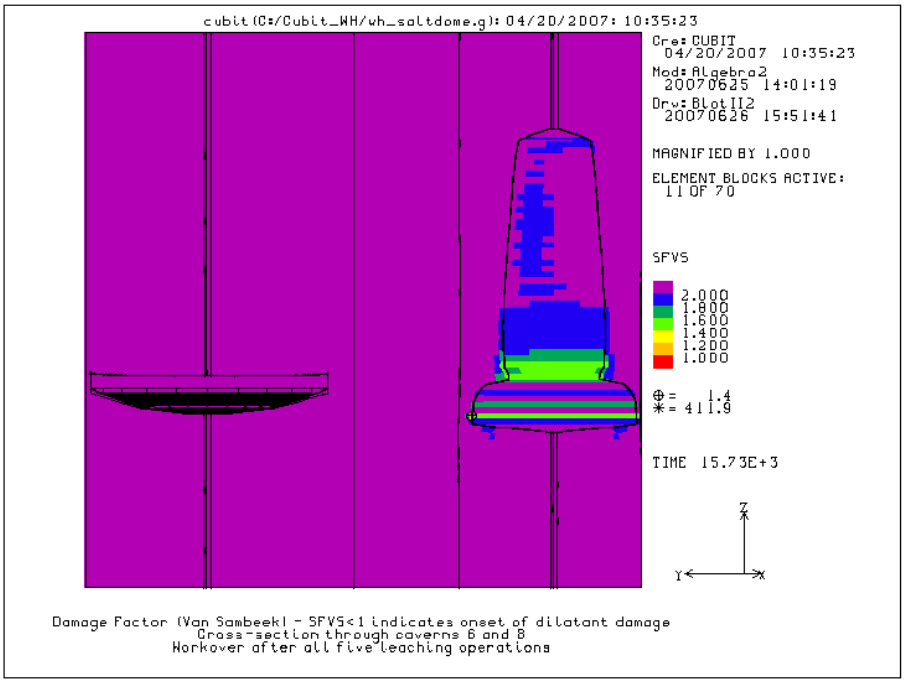

Figure 32. Contour plot of Van Sambeek damage factor, cross-section of Caverns 6 (left) and 8 (right), beginning of workover period after 5th leaching.

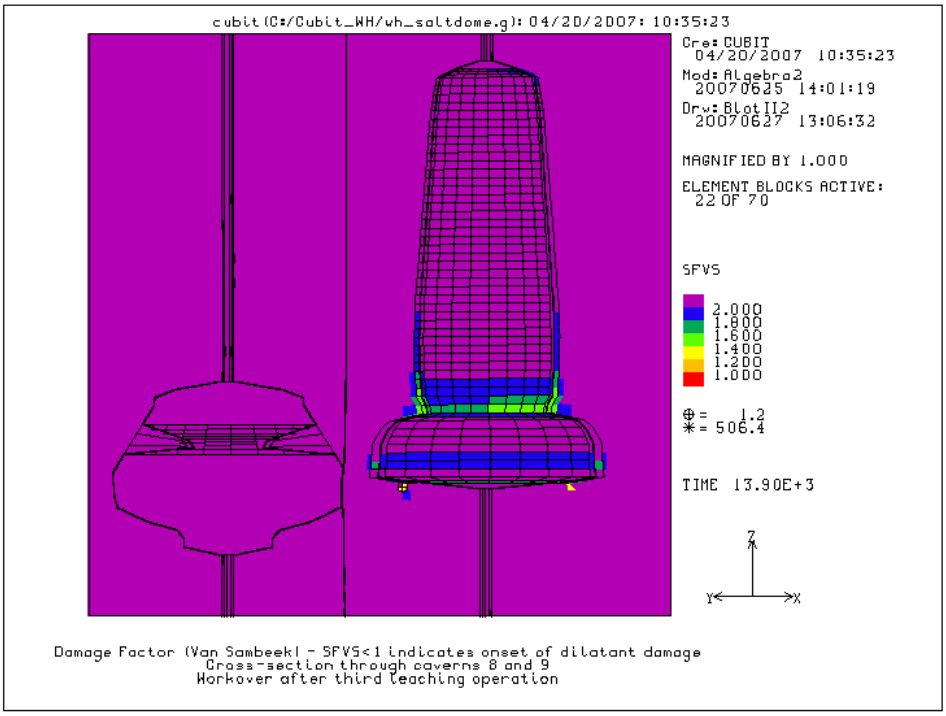

Figure 33. Contour plot of Van Sambeek damage factor, cross-section of Caverns 9 (left) and 8 (right), beginning of workover period after 3rd leaching.

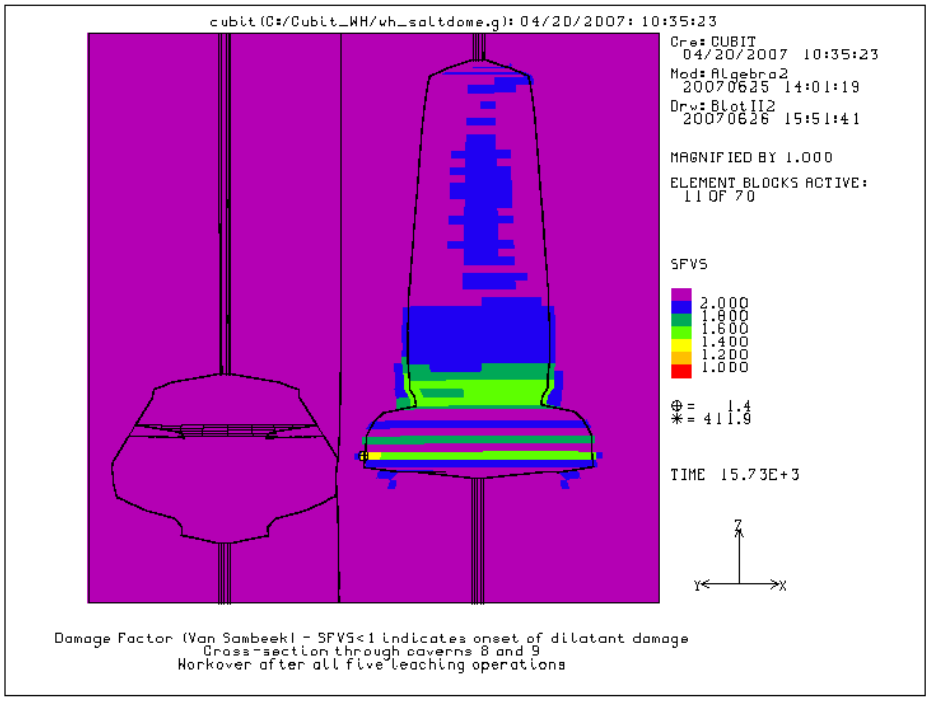

Figure 34. Contour plot of Van Sambeek damage factor, cross-section of Caverns 9 (left) and 8 (right), beginning of workover period after 5th leaching.

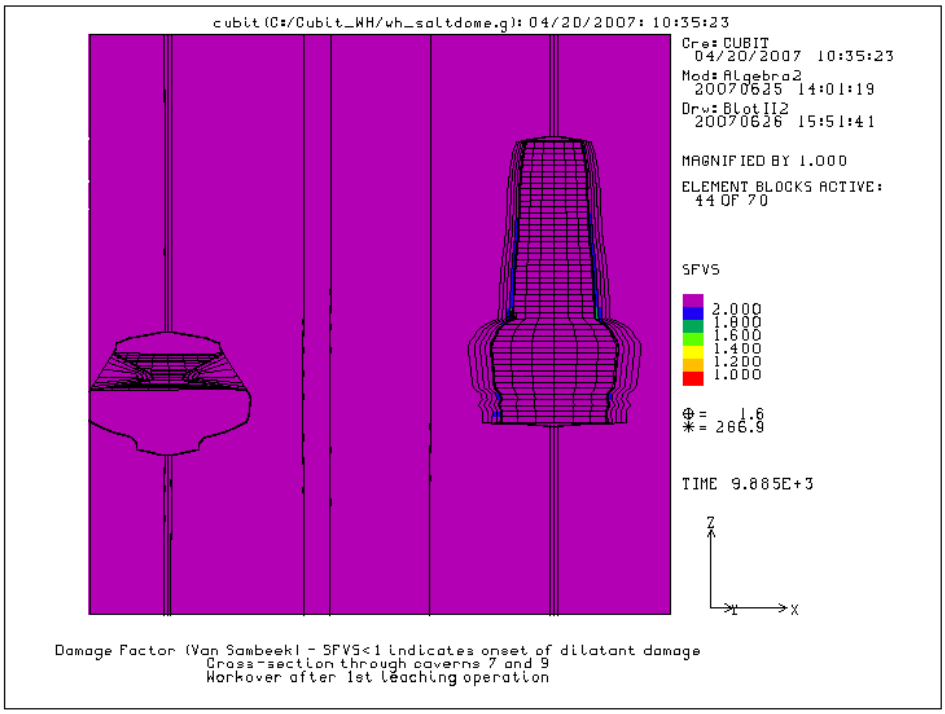

Figure 35. Contour plot of Van Sambeek damage factor, cross-section of Caverns 9 (left) and 7 (right), beginning of workover period after 1st leaching.

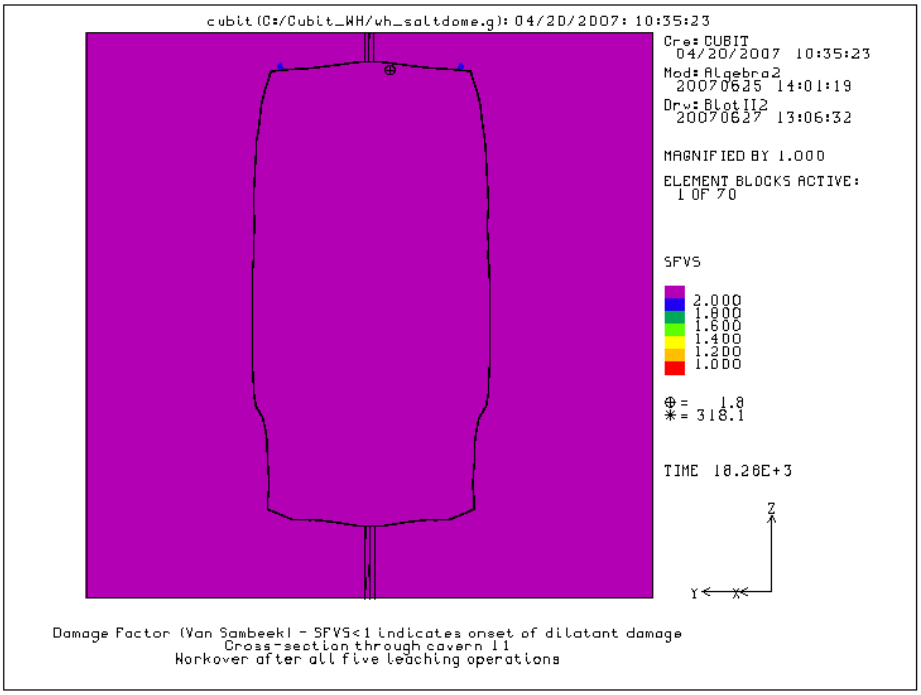

Figure 36. Contour plot of Van Sambeek damage factor, cross-section of Cavern 11, beginning of workover period after 5th leaching.

4.2 CAVERN VOLUME CLOSURE

The volume of the caverns decreases as the salts creeps. Figure 18 showed a good agreement between the predicted cavern closure and that measured for a five-year period starting in 1990. Predicted cavern closure up to the present, and into the future, depends upon the timing of workover operations, during which the caverns undergo their greatest deformation, and of future cavern expansion (leaching) operations. Figure 37 shows the predicted cumulative cavern closure for the Phase 1 caverns based on a normalized volume. The normalized volume is the volume at a given time divided by the initial volume of each cavern for its given leaching cycle. For example, cavern expansion activities are forecast to begin in late 2008; when each cavern is expanded, a new initial volume is defined equal to the initial volume after leaching. Cavern 6 experiences the greatest cavern closure, because of its dish-like shape. Cavern 6 also experiences the largest volume change during workovers, and the largest recovery upon repressurization. These results correlate with the large swings in deviatoric and maximum principal stresses described in Section 4.1. Figure 38 shows the same values for cumulative cavern closure for the post-1981 caverns. The predicted closure for these caverns is nearly the same as that for Cavern 6, and significantly greater than the other Phase 1 caverns. The post-1981 caverns extend much deeper than the other caverns, and at these depths the differential between in situ stress and oil pressure is much greater. Because of the greater stress differential, the majority of the volume loss occurs near the bottom of these caverns.

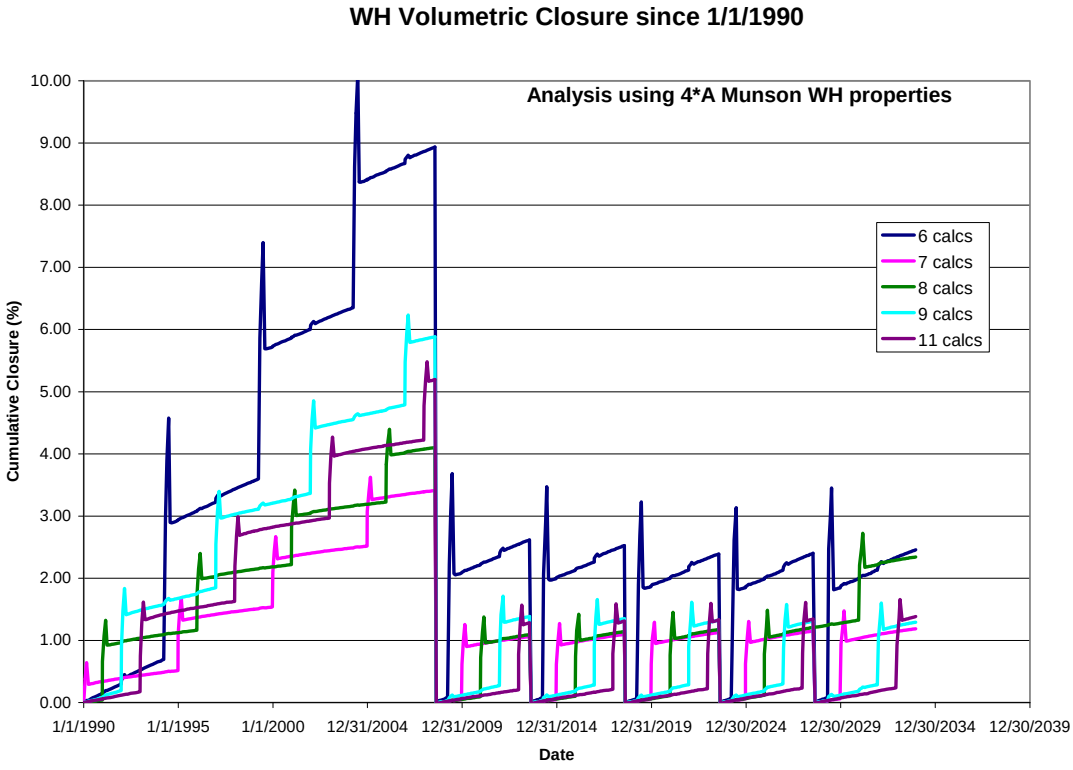

Figure 37. Cumulative cavern closure for the Phase 1 caverns.

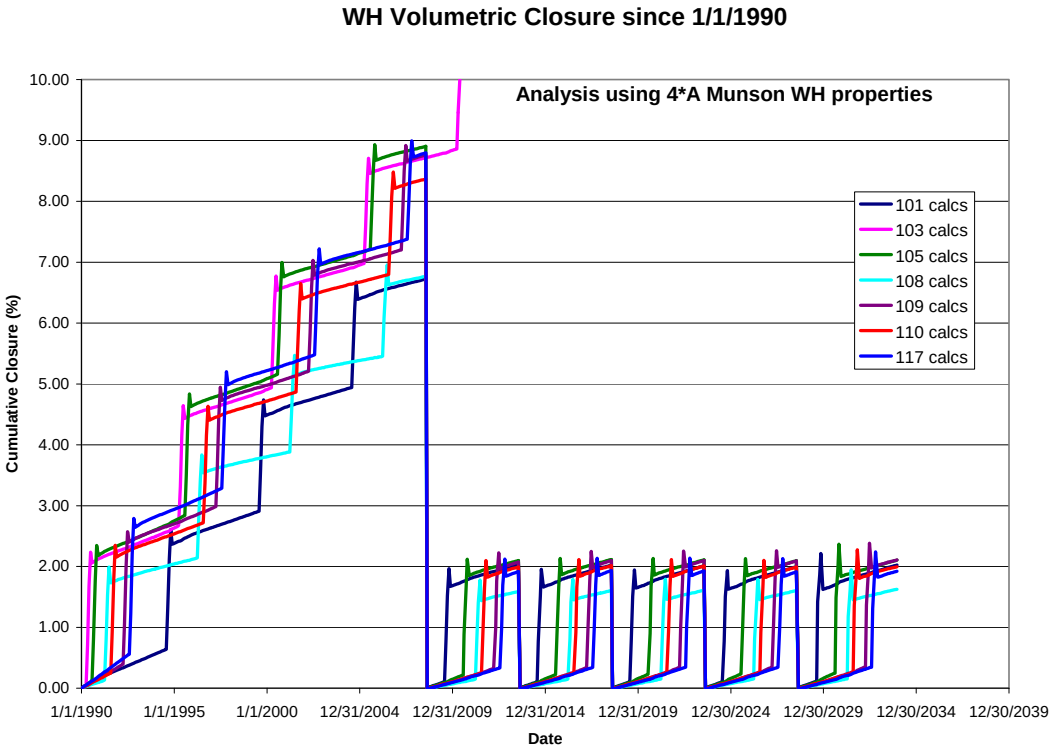

Figure 38. Cumulative cavern closure for the post-1981 caverns.

Another interesting phenomenon can be observed in Figure 37, in the cavern closure histories for Caverns 6 and 9. The simulated workovers for these caverns were placed 2.5 years apart, making the workover for one cavern happen at the middle of the period between workovers for the other cavern. Note the slight jump in cavern closure for Caverns 6 and 9 when the other cavern is in workover mode. These slight jumps in closure rate represent an increase in that rate by factors ranging from 2 to 3. Cavern closure can also be measured by the change in wellhead pressure over a period of time. The wellhead pressure naturally increases as a result of the decrease of volume by salt creep into the cavern; the wellhead pressure is then adjusted periodically at the surface facilities to maintain a reasonably uniform pressure over time. Wellhead pressure data are collected daily for all SPR wells. Pressure data from Caverns 6 and 9, plotted at times before and after the onset of workovers at the other cavern, show an increase in the pressure change rate; these pressure change rates correspond to changes in the cavern closure rate by factors of 2 to 4. Examples of pressure data for Cavern 6 at the onset of a workover in Cavern 9, and for Cavern 6 at the onset of a workover in Cavern 9, are shown in Figure 39. This measured change in closure rates verifies the predictions that significant cavern interactions occur between Caverns 6 and 9 during workovers. This verification further strengthens the position that workover activities in Caverns 6 and 9 must be planned very carefully to prevent undesired communication between them.

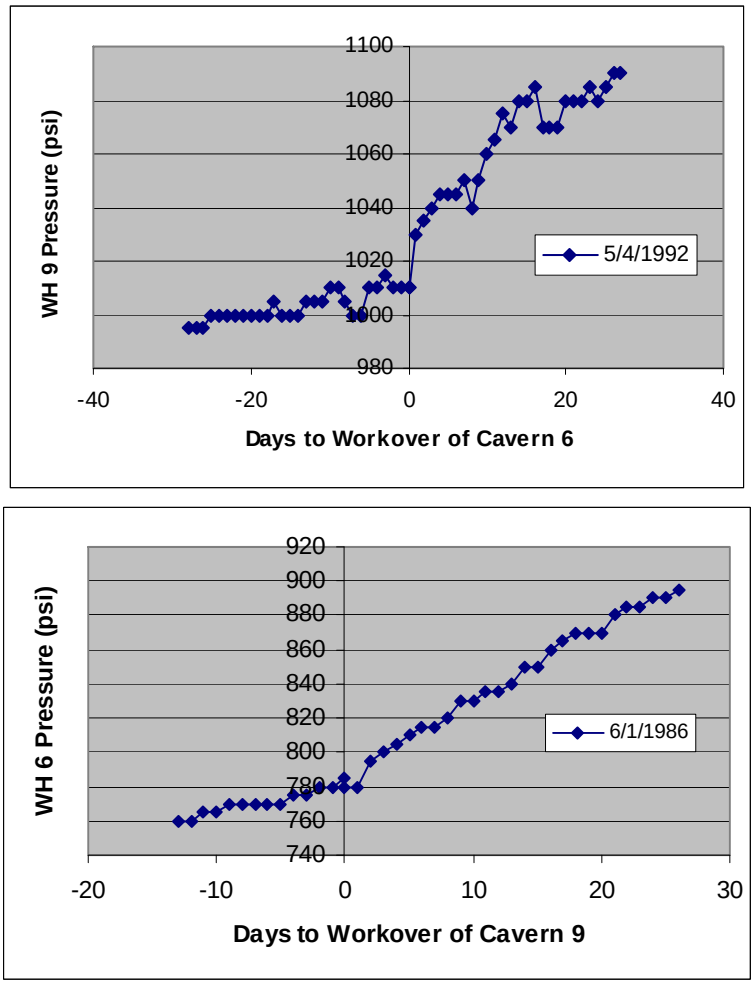

Figure 39. Evidence of Cavern interaction Between Caverns 6 and 9 Based on Pressure Data

4.3 AXIAL WELL STRAIN

The physical presence of wells and surface structures are not included in the finite element model, but the potential for ground deformation to damage these structures can be conservatively estimated by assuming that they will deform according to the predicted ground strains. At well locations, subsidence will primarily induce elongation of the axis of the well. Under these conditions, the cemented annulus of the wells may crack forming a horizontal tensile fracture that may extend around the wellbore. This fracture may not result in vertical fluid migration along the casing, but could permit horizontal infiltration into ground waters. This condition may be a well vulnerability, especially in the caprock, where acidic ground waters may gain access to the steel casing and corrode it. More extensive damage could heavily fracture the cement which could result in a loss of well integrity in that leakage could occur from the cavern along the outside of the casing. Such leakage could result in flow to the surrounding environment, resulting in loss of product. The allowable axial strain for purposes of this report is assumed to be 0.2 millistrains in tension. This would be typical of cement with a compressive strength in the range from 2500 to 5000 psi (Thorton and Lew, 1983). It should also be noted that vertical well strain reduces the collapse resistance of the steel casings. For a typical SPR well located in the caprock, negligible resistance to casing collapse is predicted at 1.6 millistrains.

The Phase 1 caverns were built in 1946-1947, except for Cavern 11, which was built in 1962. The original wells used to mine these caverns are still in place and accessible (except for the original well for Cavern 7, which has no well head and has been abandoned). The original wells are designated with the number of its cavern. No well or cavern pressure history for the Phase 1 caverns during the period before 1981 was available, so a cavern pressure equal to hydrostatic brine with zero wellhead pressure was assumed. When the Phase 1 caverns were transferred to SPR control, liners were emplaced in some of the old wells and new wells were drilled into the caverns. These wells are designated 6A, 6B, etc. The dates of the construction of these newer wells were not immediately available, so for this report the vertical strain in these well locations will be evaluated for the period after 1/1/1981.

Figure 40 shows a history of the total vertical strain from the surface to the ceiling of the cavern for the original well holes used to create the Phase 1. The cement liner and steel casing thresholds are also shown on the plot. All of the original cavern wells are predicted to have exceeded the 0.2-millistrain threshold for the cement liners within a few years after their construction. The 1.6-millistrain steel casing threshold is predicted to be exceeded in Well 6 in the mid-1960s, and in Well 9 around 1987. Figure 41 shows the total vertical strain from surface to ceiling for all the Phase 1 well head locations. Note that nearly all the cavern wells exceeded the 0.2-millistrain threshold for the cement liners by the year 2000, and that the wells for Cavern 6 are predicted to be currently approaching the 1.6-millistrain steel casing threshold. Caverns 9 and 11 might experience the 1.6-millistrain threshold before completion of the fifth leaching.

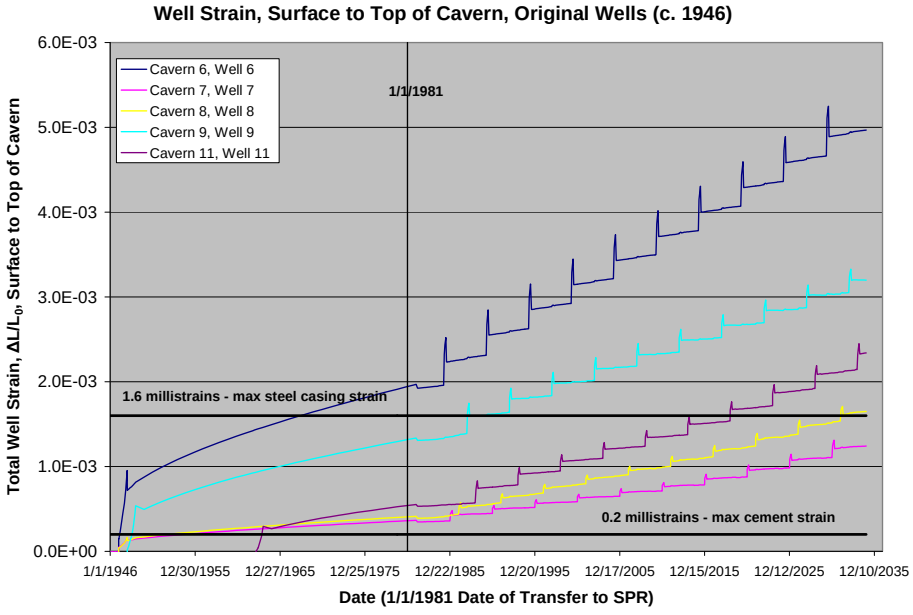

Figure 40. Total vertical strain, surface to cavern ceiling, for original Phase 1 wells since 1946

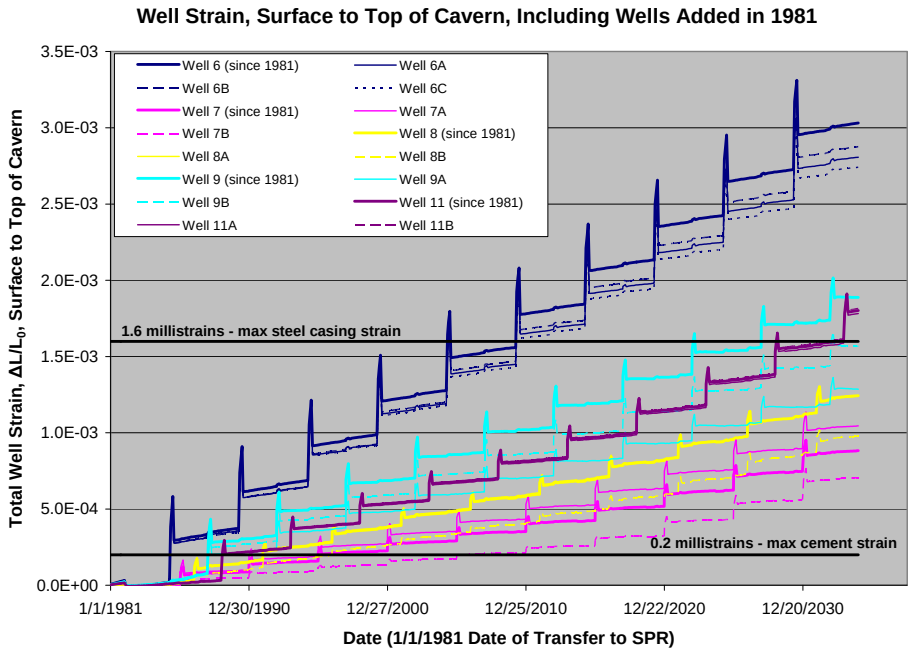

Figure 41. Total vertical strain, surface to cavern ceiling, for all Phase 1 wells since 1981

The numbers presented in Figures 40 and 41 represent the entire length of the wells; a more detailed analysis requires examining the total strain from the top of the caprock to the cavern ceilings. Figures 42 and 43 show the total vertical strain for the original wells and for all wells since 1981, respectively, from the top of the caprock to the cavern ceilings. The strains here are calculated for a shorter segment of well casing, so much higher strains would be expected. These figures present a more severe prediction of the potential for well casing damage over the Phase 1 caverns. Wells 6, 9, and 11 have already exceeded the steel casing strain threshold, and wells 7 and 8 are predicted to be nearing that threshold now. Even the newer wells in Cavern 6 exceeded the steel casing threshold sometime between 2000 and 2002, and the wells in Caverns 9 and 11 are currently approaching that limit. Indeed, in 2001 the cavern integrity test failed for Well 6B, requiring a liner that was added in 2002 to a depth of 2547 ft. The casing leaked at two locations in the salt. Well casing concerns can also be expected as the caverns are enlarged. These calculations would indicate that the potential for cement liner and steel casing failure in the Phase 1 cavern wells is significant, and cement bond and casing inspection logs should be performed as part of operations and potential mitigating measures should be considered especially as the caverns are leached. The vertical strain predictions presented here should be correlated with known well casing problems to determine field-appropriate strain threshold values. Events that would indicate a possible casing/liner failure include loss of pressure during cavern integrity testing, measurable loss of oil during normal operating procedures, obstruction of the borehole resulting from the displacement of fractured casing and liner material. Also, fiber optic cameras and other types of logs sent down the boreholes might identify failure or corrosion areas. To date, there have been no indications that a steel casing or cement liner has failed in any West Hackberry cavern, but the wells are not being logged. It is also possible that casing failures or yielding has occurred, but have yet to be detected. Because of the high strain values predicted for the current borehole liners, it is important to ascertain the current status of

the liners and determine field-appropriate strain threshold values and possible mitigation procedures (Sattler, 2004).

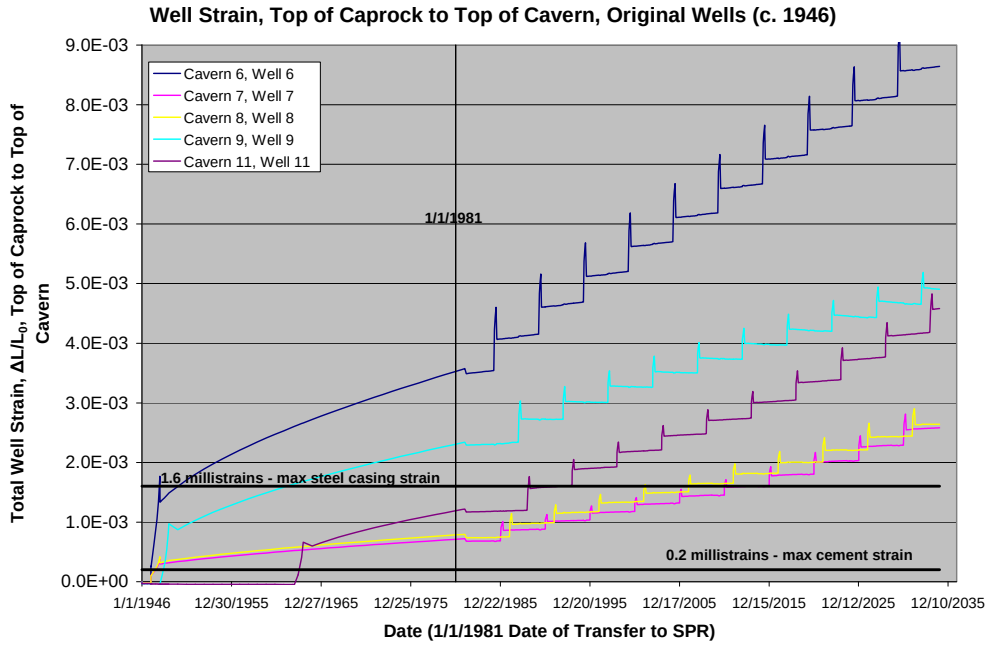

Figure 42. Total vertical strain, top of caprock to cavern ceiling, for original Phase 1 wells since 1946

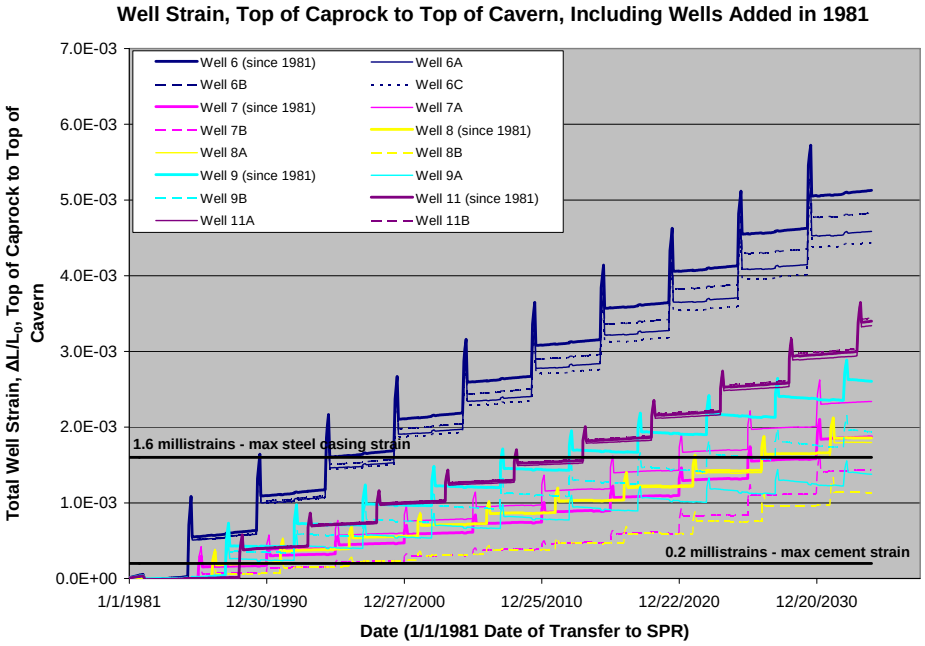

Figure 43. Total vertical strain, top of caprock to cavern ceiling, for all Phase 1 wells since 1981

4.4 SURFACE SUBSIDENCE

The issue of surface subsidence is an important design and operations factor for surface facilities, especially for those located in flood prone areas, but subsidence also results in horizontal ground strains that can damage buildings, pipelines, and other infrastrusture. The SPR is currently over 25 years old and the life of the SPR may extend well into this century depending upon a number of factors, including oil consumption, import dependency, and geopolitical instability. Expected subsidence during a 100-year life of an SPR site on the order of up to ten feet is possible. Therefore, a reliable prediction of surface subsidence can be very valuable for site management. The plots in Figures 14 and 15 that compared surface subsidences measured since 5/1/1991 to predicted values showed very good agreement, particularly for the post-1981 caverns. Figures 44 and 45 show the predicted surface displacement with the assumed workover and cavern expansion cycles out to the year 2034 (when the facility is approximately 50 years old). The predictions indicate surface subsidence of an additional four feet between 2006 and 2034, to a total of 7 feet since 1991. If extended over a potential 100-year life of the facility, the potential displacement could reach a total of approximately 12 feet between 2006 and 2084 (15 feet since 1991). Because the surface structures at the wellhead are at elevations between 4 and 18 feet above sea level, the predicted subsidence may cause some of the wellheads to sink below sea level by the 2030's.

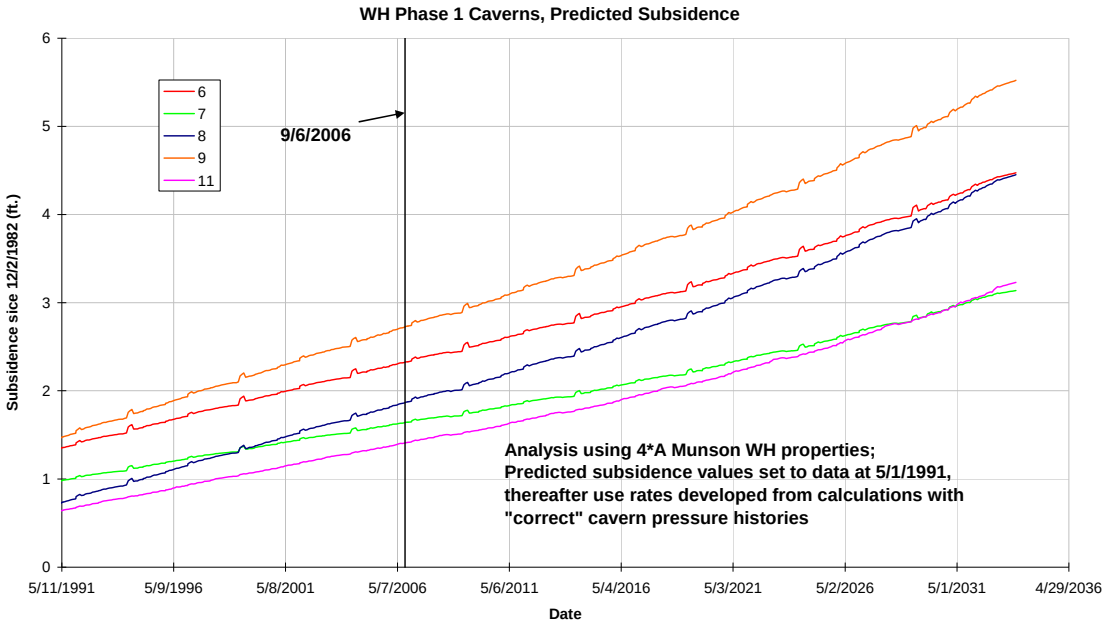

Figure 44. Predicted WH Surface Subsidence Data, Caverns 6-11, to the year 2034.

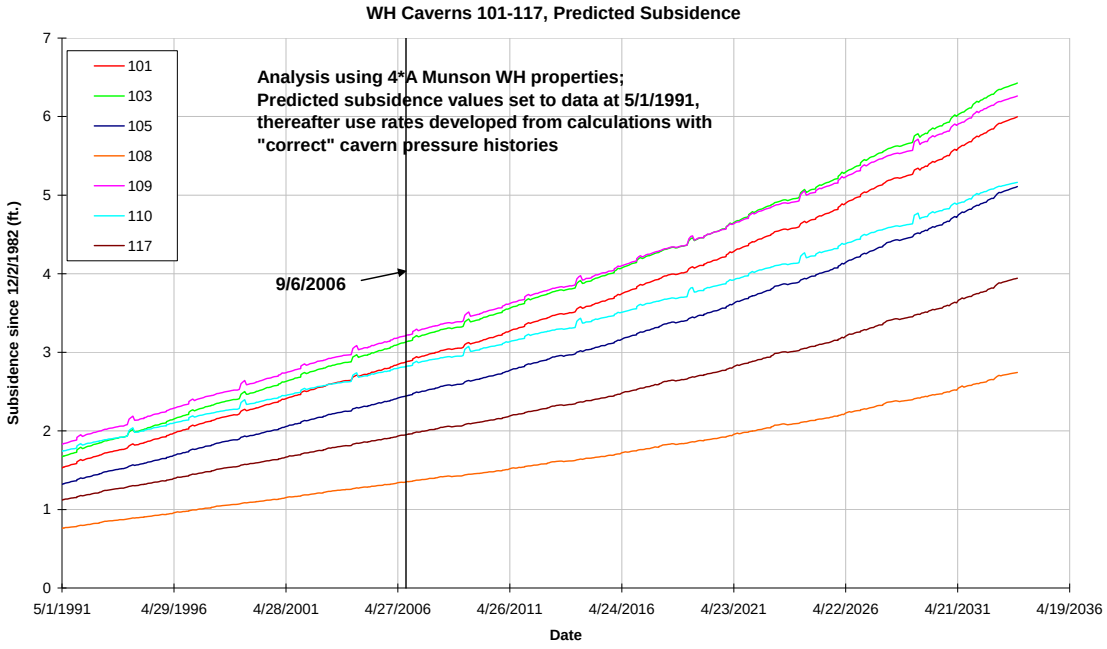

Figure 45. Predicted WH Surface Subsidence Data, Caverns 101-117, to the year 2034.

Structural damage on the surface is typically caused by large accumulated surface strains caused by surface subsidence. These strains can cause distortion, damage, and failure of buildings, pipelines, roads, bridges, and other infrastructure. Surface strains will accumulate in structures over time, which increases the possibility of damage in older facilities. Typically, subsidence strains tend to be compressive in the central portion of the subsided area and become tensile in nature for areas farther removed. Some guidance and solutions are available to evaluate the predicted surface strains. These criteria vary from country to country, possibly because of different building codes and structural materials. Some examples of allowable strains are presented by Peng (1985). The criteria vary in some countries depending on application. For purposes of this report, the allowable strain is taken to be 1 millistrain for both compression and tension. Criteria for shear strains have not been found, perhaps because they are less important. In practice, allowable strain limits for a structure are design specific and should be examined on a case-by-case basis.

The horizontal surface strains are related to the subsidence above the caverns. Typically, the region above the caverns undergo compressive horizontal stresses at the surface as the geologic units sag, but at some distance away from the cavern field the horizontal strains become tensile as the surface rises up to its original elevation. Figure 46 shows the maximum compressive and tensile strains at the surface as a function of time. This figure shows that the 1-millistrain threshold for compressive strains could be exceeded by the year 2023. The tensile strains do not exceed the threshold, but are also significant. A better understanding of the effects of these strains can be gained by looking at contour plots of strain at the surface over the salt dome. Figure 47 shows the predicted minimum horizontal principal strains at the surface at four times: October 1980 (just prior to SPR ownership), September 2007 (approximately the current time), September 2012, and December 2034. By convention, negative strains are compressive, and positive strains are tensile. The minimum principal strains (i.e., maximum compressive strains)

are centered above Cavern 103, and become steadily less compressive radially from that point. A similar plot of the west-east directional strain, shown in Figure 48, indicates that the maximum compressive strains tend to be in the east-west direction. Similarly, Figure 49 shows the predicted maximum horizontal strains at the surface, and Figure 50 shows the north-south directional strains. Several important observations can be made from these figures. First, the largest tensile strains, aligned primarily in the north-south direction, are generated on the surface above the edge of the dome, north and south of the group of caverns along the vertical symmetry plane. Second, the maximum principal strains in the center of the cavern field, above Cavern 103, also exceed the compressive strain threshold, meaning the surface facilities/infrastructure in the vicinity of Cavern 103 are experiencing highly compressive strains from all directions. Third, significant tensile strains are generated east of Caverns 6, 8, and 9 on the surface even though east-west and north-south strains there are close to zero. This indicates the principal strains are aligned along NE-SW and NW-SE directions in that location.

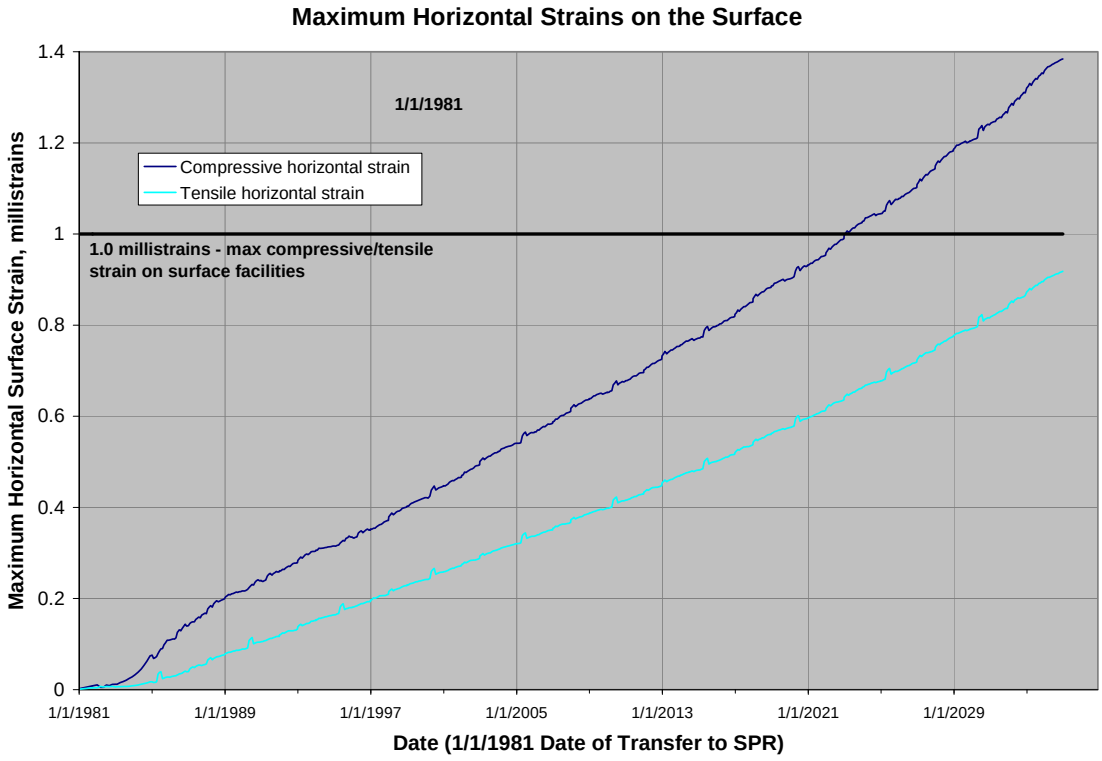

Figure 46. Maximum horizontal compressive and tensile strains as a function of time.

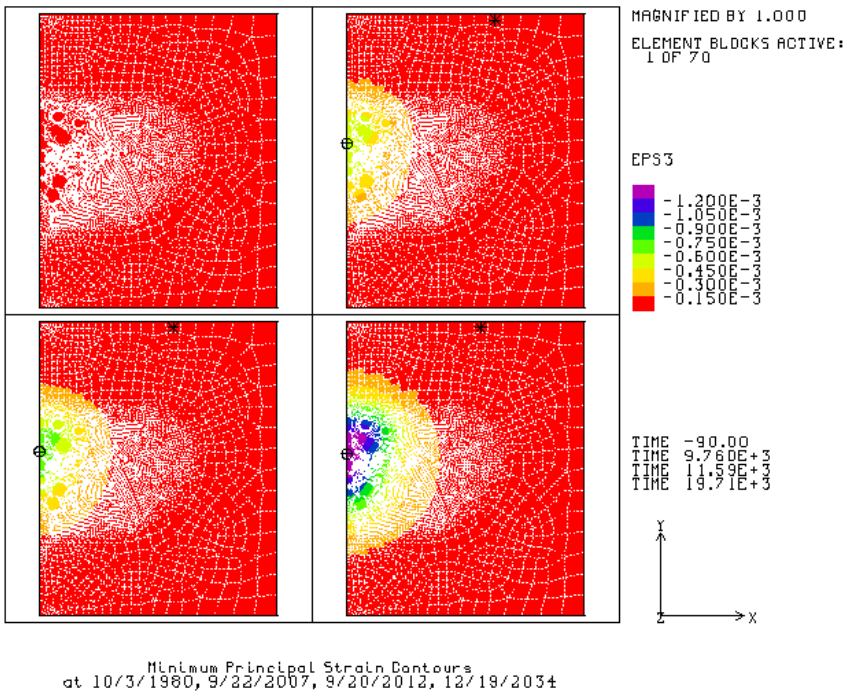

Figure 47. Minimum horizontal principal strains at the surface (negative strains in compression).

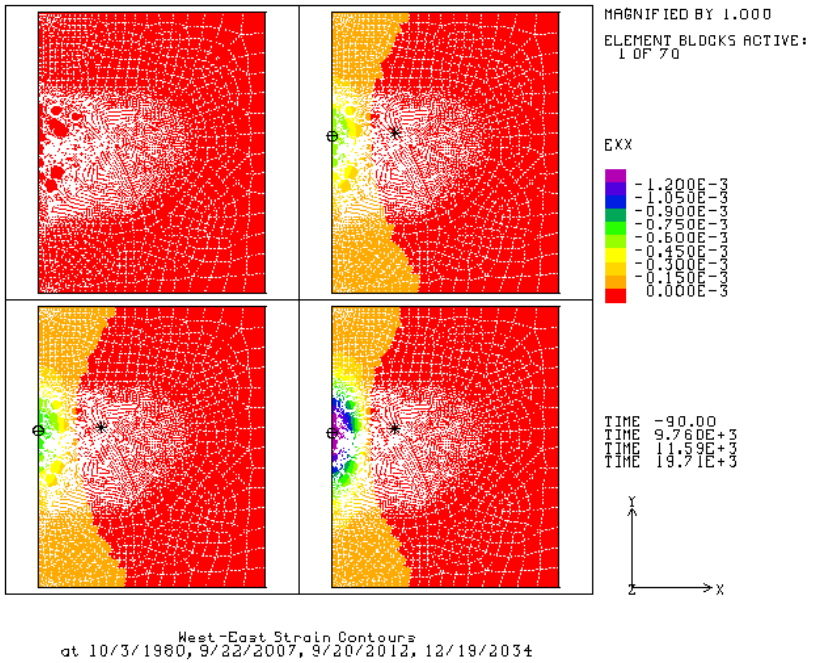

Figure 48. West-east directional strains at the surface (negative strains in compression).

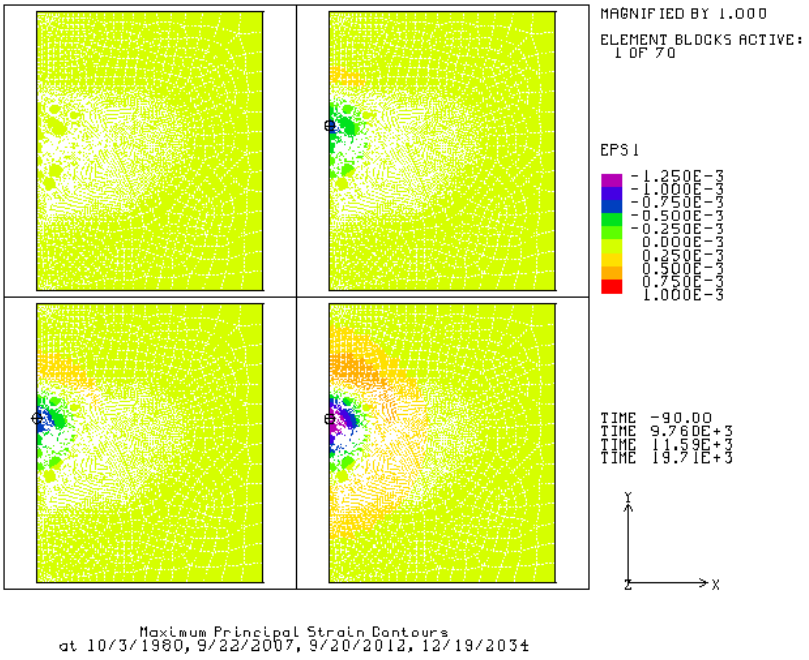

Figure 49. Maximum horizontal principal strains at the surface (positive strains in tension).

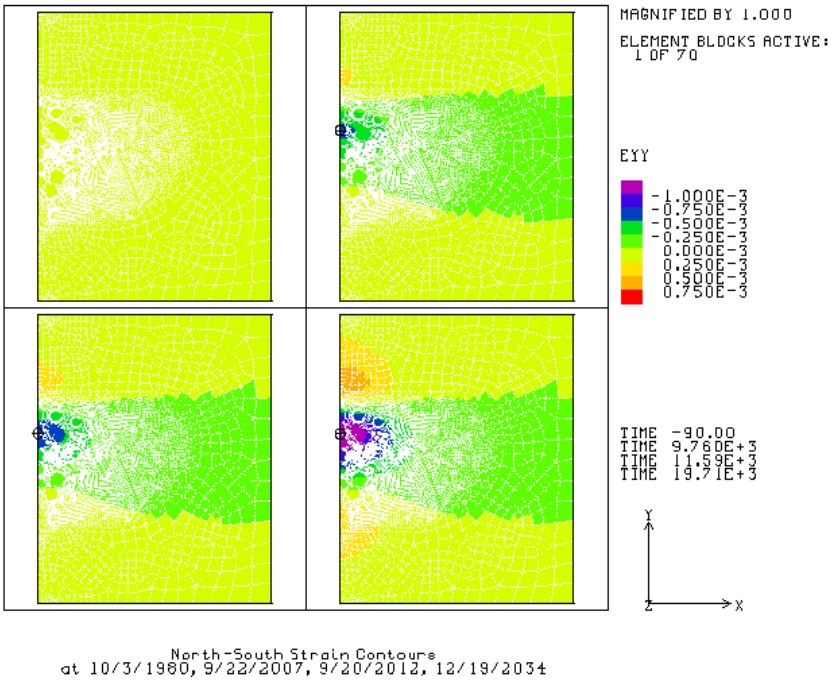

Figure 50. North-south direction strains (positive strains in tension).

4.5 EVALUATION OF LODE ANGLE-BASED DILATANT DAMAGE

An extensive discussion of the potential for dilatant damage of salt around the Phase 1 caverns was desribed in Section 4.1. That discussion relied on a damage criterion (Equation 3) based on the Van Sambeek (1993) linear relationship between stress invariants I_1 and $\sqrt{J_2}$. The discussion concluded that only Caverns 6 and 9 had significant potential for salt damage or failure, primarily at the beginning and end of the workover cycles. The other Phase 1 caverns (and the post-1981 caverns as well) were predicted to experience acceptable values of the damage criterion and thus no dilatant damage. However, documentation of hanging string failure in several of the West Hackberry caverns (Munson, 2006) would seem to indicate that salt falls of significant magnitude to damage hanging strings are occurring in the caverns. In addition, recent laboratory data from SPR (Lee et al. 2004) and non-SPR (DeVries et al., 2005) salts indicate that the onset of dilatant damage in salt is nonlinear between I_1 and $\sqrt{J_2}$, and that there may be an additional dependence on the Lode angle ψ, which relates to the relative compression or extension among the principal stresses. RESPEC (DeVries et al., 2002) has developed a new dilatant damage criterion that includes dependence on the Lode angle. Additionally, a damage factor (Equation 7) and set of damage constants from the Cayuta and Big Hill salts (Tables 5 and 6) have been developed from these works. This section will evaluate potential dilatant damage scenarios for Caverns 6, 9, 101, and 103, using the RESPEC damage criterion, hanging string damage histories, and sonar measurements of Cavern 101.

Figure 51 compares the values for the three damage factors (Van Sambeek, SF_{VS}; RESPEC criterion using the Cayuta salt properties, SF_C; and the RESPEC criterion using the Big Hill salt properties, SF_{BH}.) immediately after Cavern 6 has been depressurized at the beginning of a workover cycle. Whereas the Van Sambeek criterion does not predict salt damage at this time (damage was predicted after repressurization at the end of the workover; see Section 4.1), the RESPEC criteria indicate a significant potential for dilatant damage at the perimeter of the cavern. Figure 52 shows the same comparison for Cavern 9; in this case, salt damage is predicted for significant portions of the cavern wall beneath the circular ledge. Results like these would indicate that salt falls should have occurred in these caverns during workovers. Both caverns have had multiple, documented workover periods; however, no hanging string failures have been reported in these caverns, and the log data indicating floor elevation do not correlate with cavern pressure change events. Therefore, no conclusions can be drawn about the condition of Caverns 6 and 9 from this information.

Cavern 103, however, has had seven instances of hanging string failures between July 1982 and November 2006. Figure 53 shows the same comparison between the three damage factors. Note how the Big Hill salt properties indicate salt damage for nearly the entire bottom half of the cavern. This damage results in part from the larger differential between cavern pressure and in situ stress at the deeper elevations of the Phase 2 caverns. Sufficient log data exist to possibly identify events and conditions which might lead to salt falls in the caverns. Figure 54 presents much of that data for Cavern 103. Log data of the rise of the cavern floor, wellhead pressures, and cavern and oil volume are plotted along with predicted floor rise from the calculations and

the hanging string failure events. The hanging string failures nearly always occurred after a large change in pressure, either from a workover cycle (wellhead pressure drops to zero) or a cavern integrity test (maximum cavern pressure). Also, the actual rise in the cavern floor is significantly higher than that predicted by the analysis suggesting salt fall debris has accumulated on the floor.

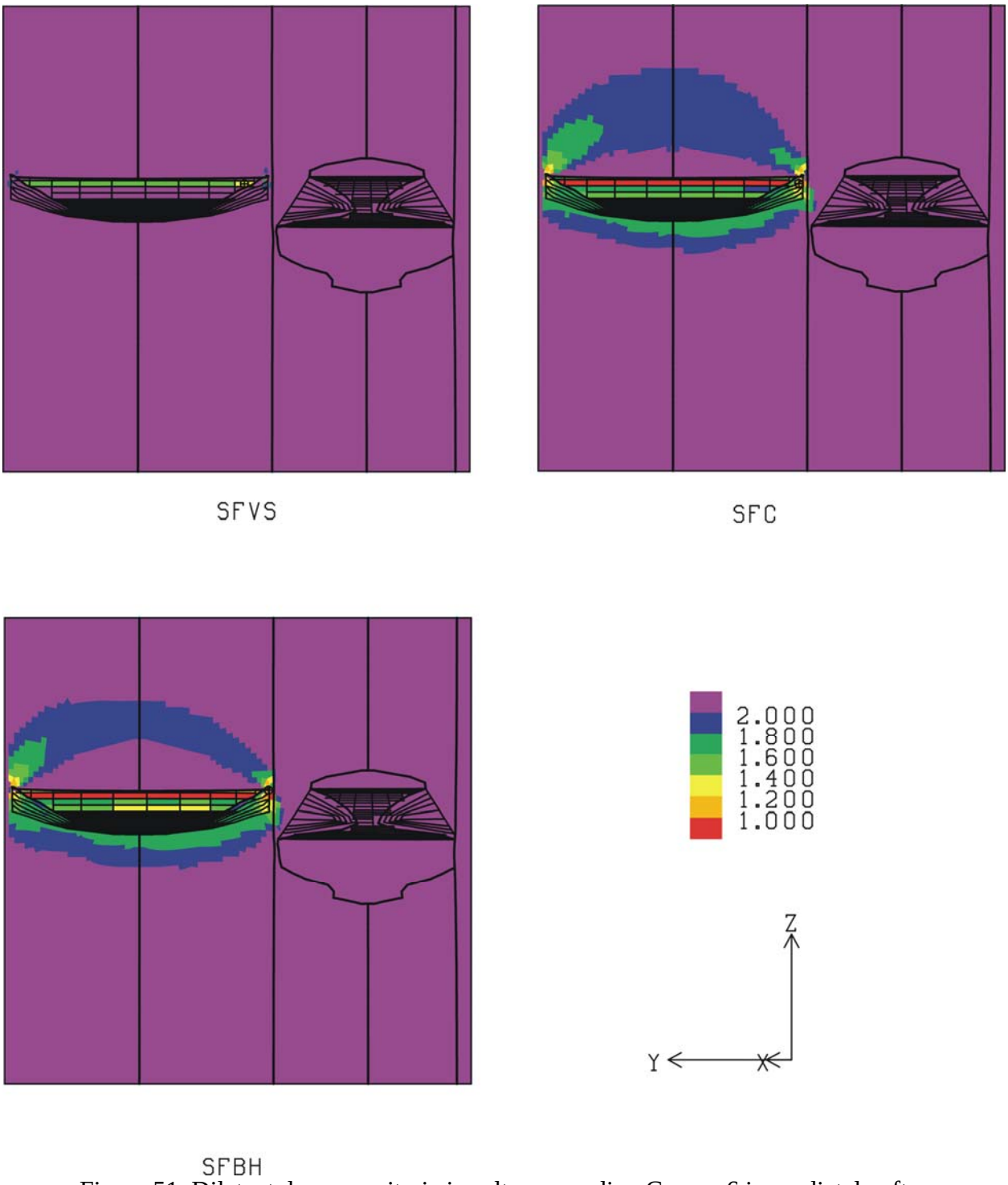

Figure 51. Dilatant damage criteria in salt surrounding Cavern 6 immediately after depressurization during workover (red values < 1.0, onset of dilatant damage).

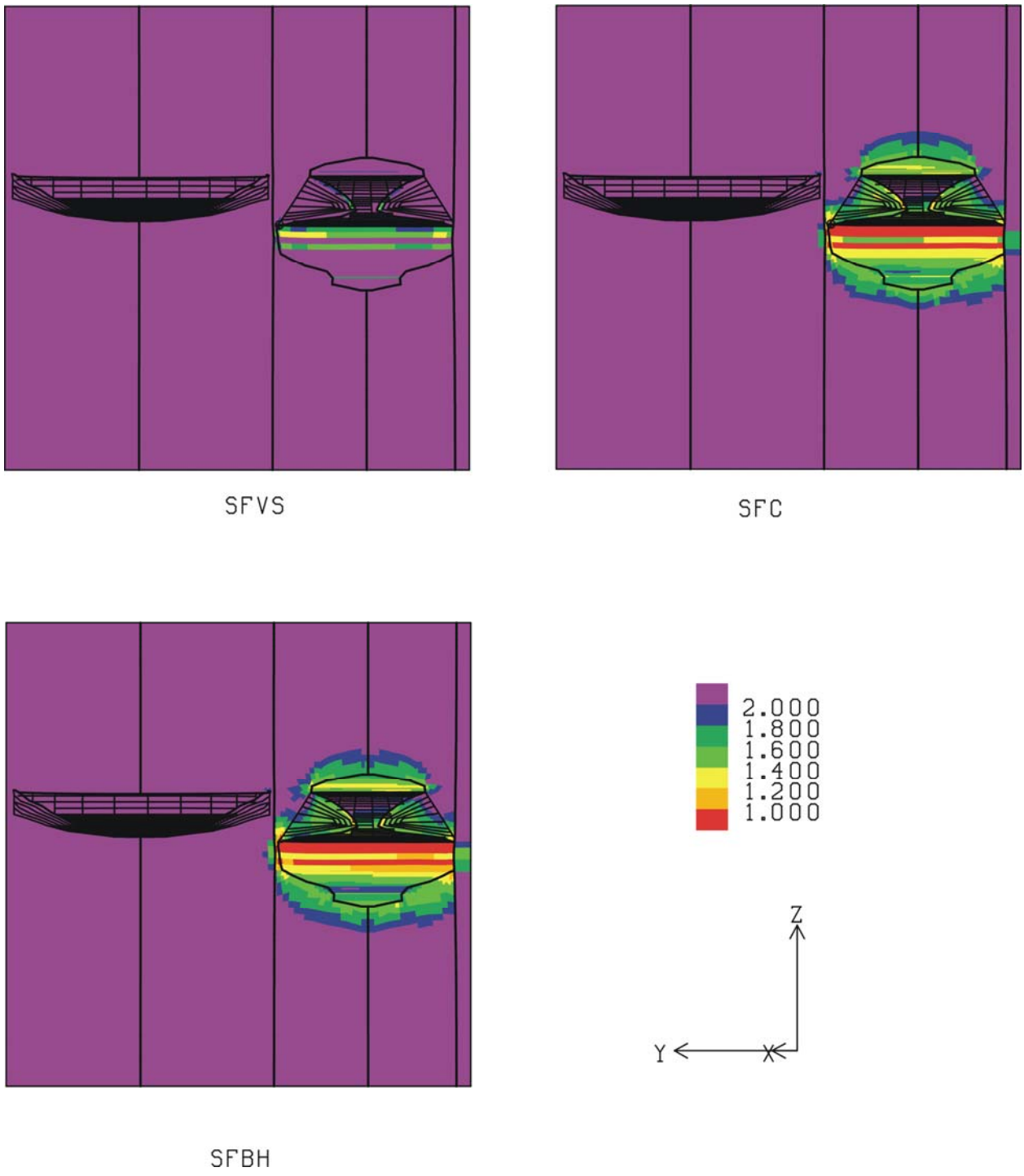

Figure 52. Dilatant damage criteria in salt surrounding Cavern 9 immediately after depressurization during workover (red values < 1.0, onset of dilatant damage).

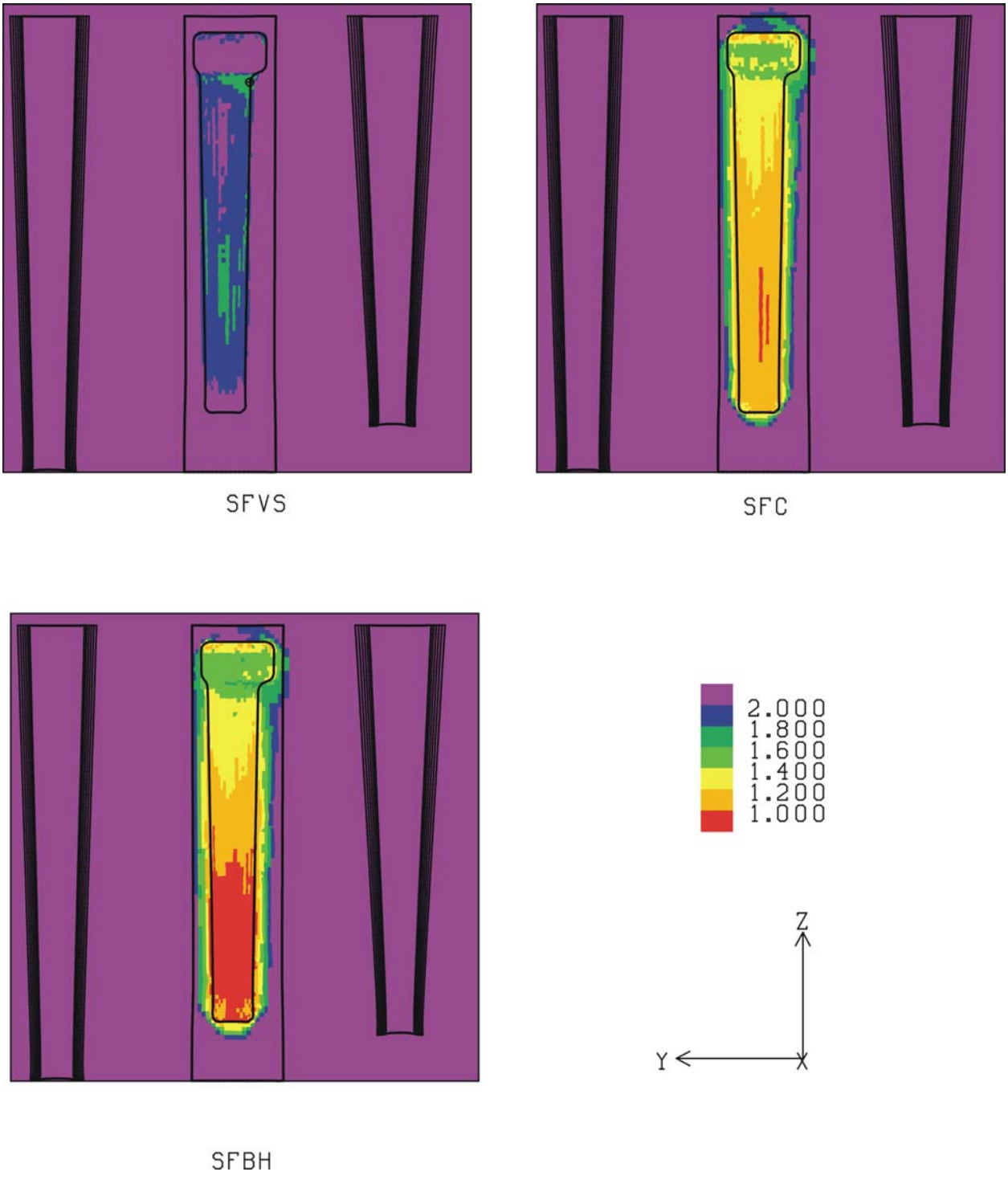

Figure 53. Dilatant damage criteria in salt surrounding Cavern 103 immediately after depressurization during workover (red values < 1.0, onset of dilatant damage).

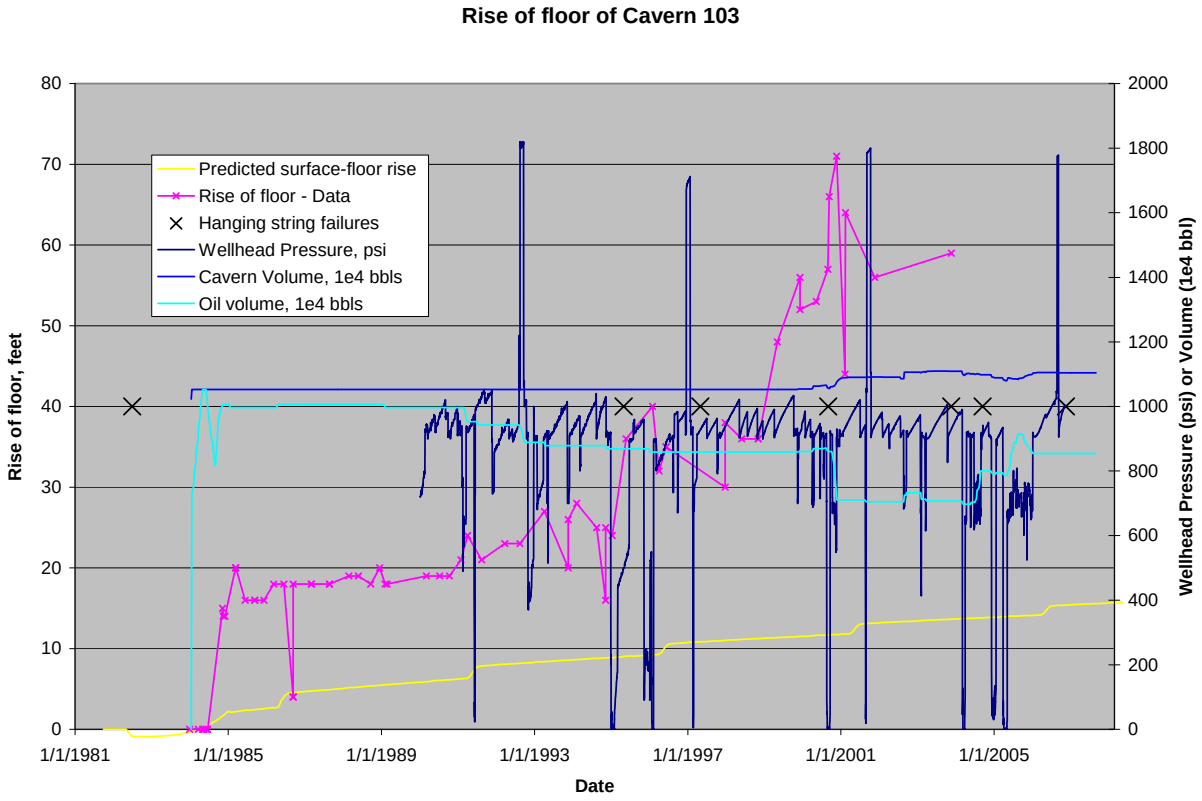

Figure 54. Floor rise, pressure, and volume data for Cavern 103 compared to predicted floor rise and documented hanging string failures.

Cavern 101 has no documented hanging string failure to date, but it has undergone two complete sonar scans in recent times, dated 1/16/2001 and 9/26/2006. Figure 55 shows the same comparison between the three damage factors, and again the bottom half of Cavern 101 is predicted to be in dilatant damage conditions using the RESPEC criterion based on Big Hill data. Figure 56 plots the predicted and measured elevation rise of the cavern floor, along with the wellhead pressure and cavern and oil volumes. Note again that large changes in the floor elevation often occur in conjunction with large pressure-changing activities. These changes are significantly larger than the rise in elevation predicted solely by creep. In particular, notice the period between November 2000 and August 2004, when the oil-brine interface was raised nearly 660 feet by the introduction of fresh water. Because of the presence of the fresh water, some salt is expected to be removed from the surrounding walls by dissolution. Figures 57 and 58 shows superimposed images of Cavern 101 from the two sets of sonar measurements. Figure 57 shows the entire cavern, and Figure 58 zooms in on the bottom 700 feet. The Caveman program (Ballard and Ehgartner, 2000) calculates the amount of salt dissolved between the sonar dates as 480,000 bbl. Assuming a 4.8 % insoluble content for the salt (Munson, 2006), results in 23,000 bbl of insoluble that could settle to the cavern floor. In addition to this insouble volume, creep is predicted to raise the floor level during this time by 37,000 bbl. Thus the floor volume is expected to decrease by 60,000 bbl. The difference in the sonar measurements shows a decrease of 430,000 bbl. This suggests that additional debris was accumulated on the floor of the cavern, perhaps from salt falls.

If the estimates here are reasonably correct, it is an indication that additional salt and/or sediment has been added to the bottom of the cavern by some process other than leaching. Whether this is a direct indication of salt falls occurring in Cavern 101 is not clear. However, this uncertainty in the actual condition of the cavern walls, particularly at the bottom of the deep caverns, leads to several conclusions:

- Additional series of laboratory tests of salt from West Hackberry and other SPR sites would be beneficial. In particular, a combination of triaxial compression and triaxial extension tests, where the salt samples are tested to dilatant failure, would greatly enhance the existing knowledge of the failure envelope of the salt at each site, and determine whether that failure is dependent on Lode angle.
- Log data, hanging string failure events, and sonar measurements can be used to monitor the status of the cavern at several points in time. However, these data points are sparse, so it is difficult to detect salt fall events unless an obvious failure (i.e., hanging string) occurs. Particularly because the caverns are between 20 and 60 years old, additional monitoring of the conditions of the cavern walls and well casings would be beneficial.
- If the new salt dilatancy criteria bears out through testing, the predicted dilatancy (and hence increased salt permeability) may explain the methane gas release mechanisms associated with gas intrusion into the caverns.

The other Phase 1 caverns (7, 8, and 11) did not experience the same drastic increase in damage potential as Caverns 101 and 103, primarily because they are not as deep as the newer caverns. The earlier conclusions that these three caverns should be eligible for enlargement (as produced during oil drawdowns) remain unchanged by this investigation.

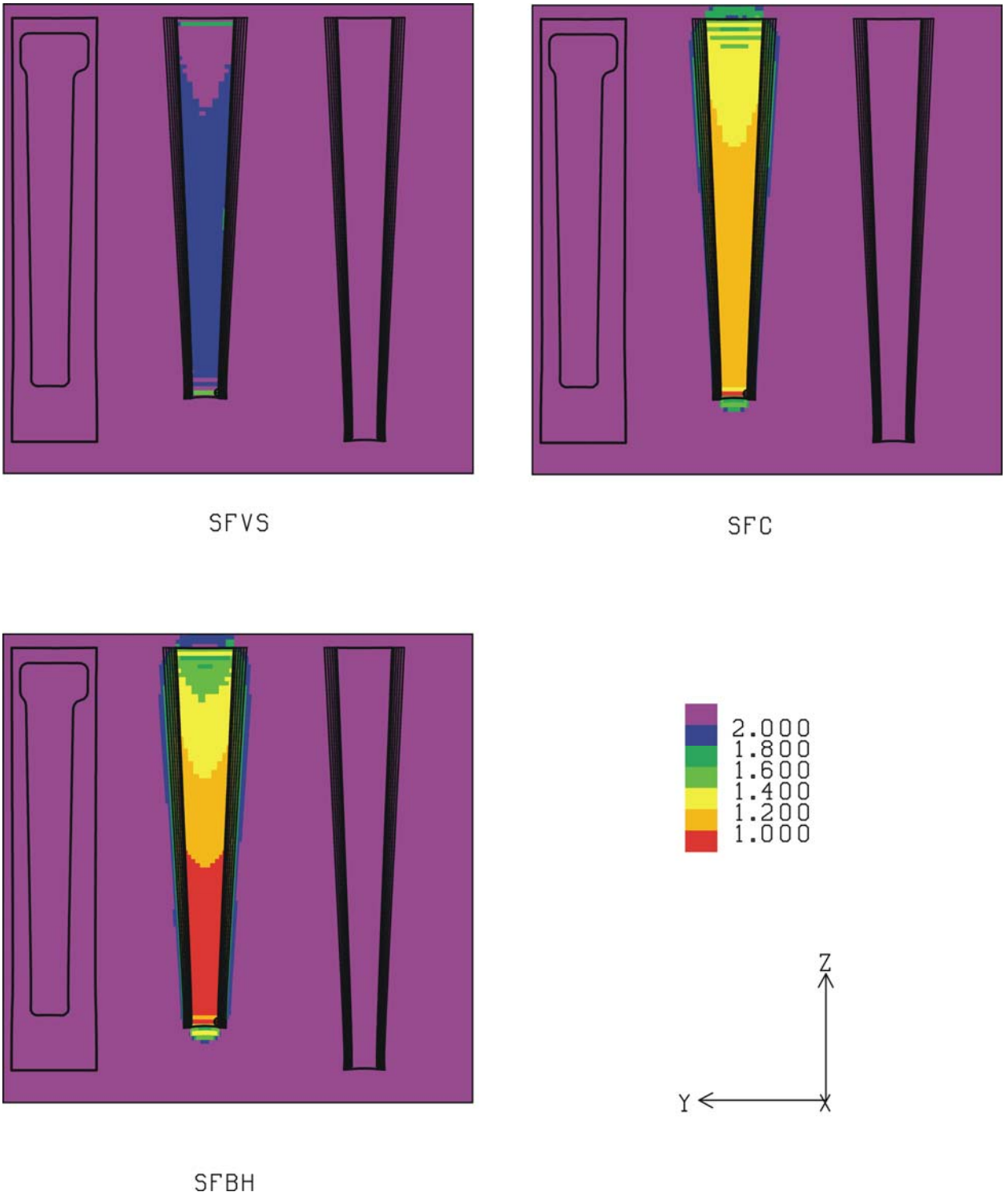

Figure 55. Dilatant damage criteria in salt surrounding Cavern 101 immediately after depressurization during workover (red values < 1.0, onset of dilatant damage).

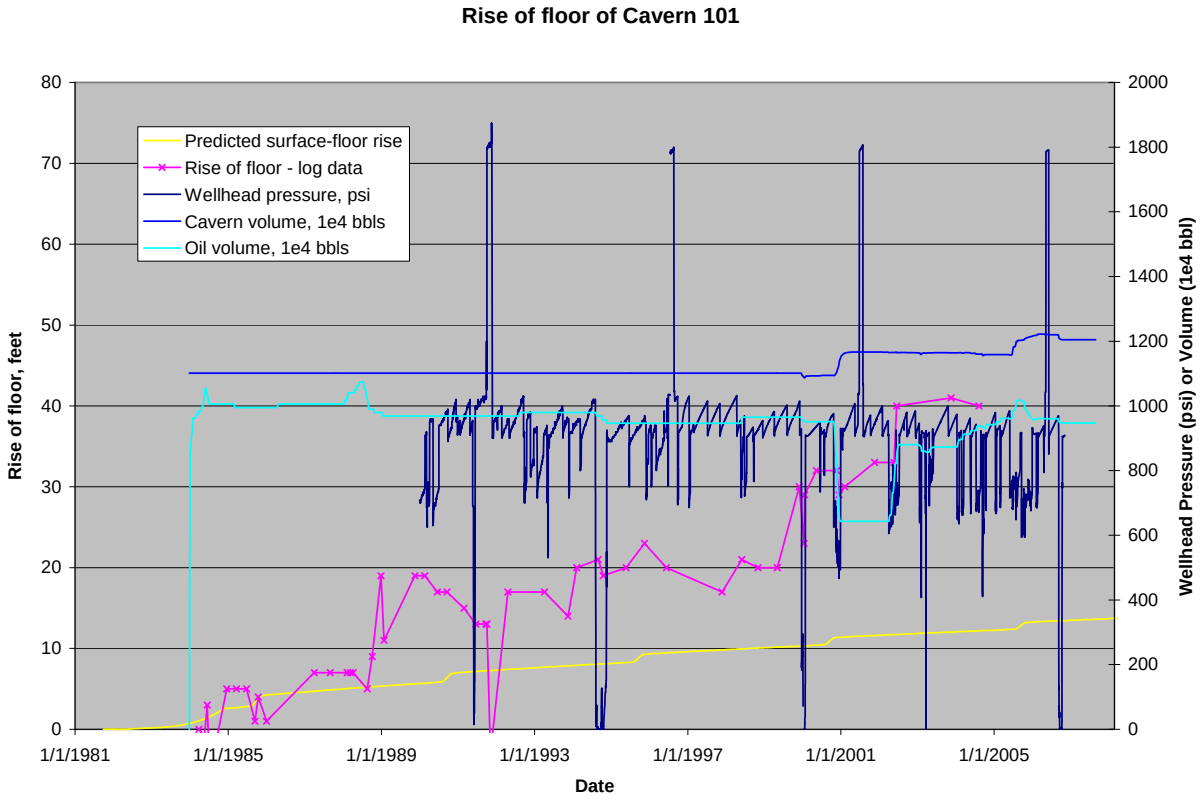

Figure 56. Floor rise, pressure, and volume data for Cavern 101 compared to predicted floor rise.

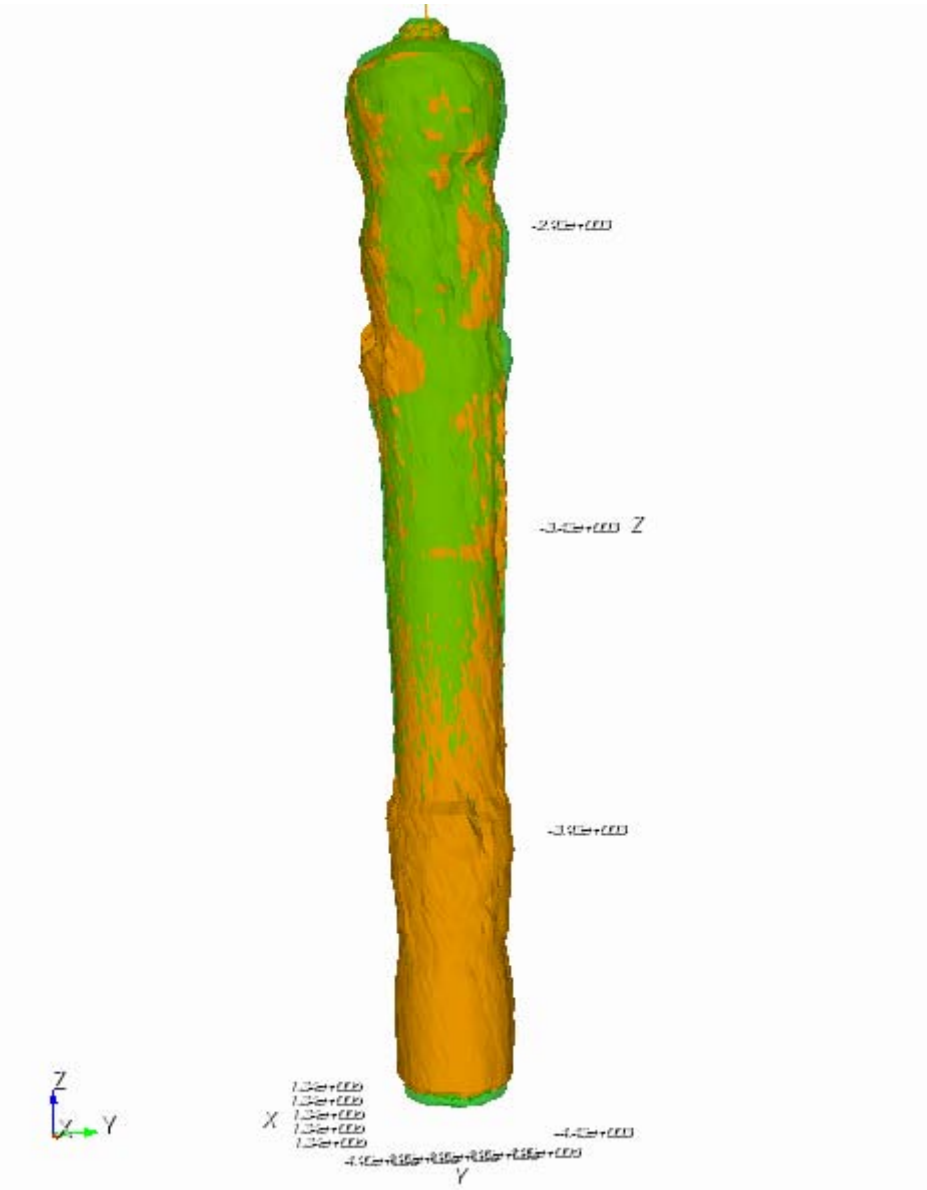

Figure 57. Superimposed sonar measurements of Cavern 101, from 1/16/2001 (green) and 9/26/2006 (yellow).

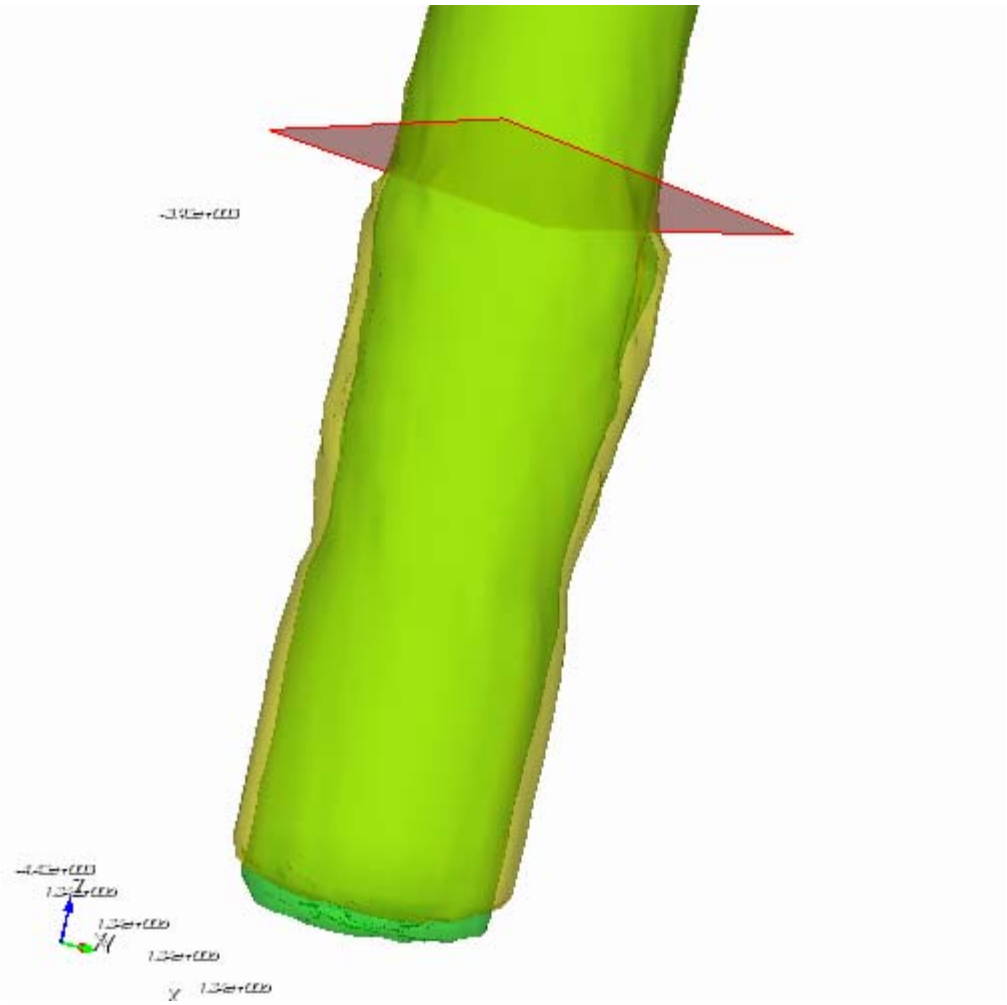

Figure 58. Superimposed sonar measurements of the bottom of Cavern 101, from 1/16/2001 (green) and 9/26/2006 (yellow).

5. ADDITIONAL DISCUSSION OF CAVERNS 6 AND 9

The results of the calculations presented in Section 4 illustrated some potential stability problems with the West Hackberry Cavern 6. Because of the dish-like shape of Cavern 6, the perimeter of the cavern is at risk of dilatant and tensile damage, particularly at the end of a workover operation. Because of this potential tensile cracking potential near Cavern 6, the close proximity of Cavern 9 (originally estimated to be 100 feet at their closest point) poses a risk of inter-cavern communications. Also an anomalous zone of salt may exist in the pillar between the two caverns. This may enhance the potential for a crack to propagate from Cavern 6 and intersect Cavern 9, causing cavern pressures to equilibrate. An operational scenario of having Cavern 9 in workover mode during the breach would pose a serious risk to operational safety and containment of oil. A breach when Cavern 6 is fully repressurized (the most likely condition) would result in approximately 55,000 bbl of oil entering into Cavern 9. With the wellhead removed during workover mode, the oil would eject onto the surface. This would pose a serious safety risk to the workover crew and potential environmental damage. The obvious reaction would be to operationally prohibit sequential workovers of Caverns 6 then 9, allowing for an adequate time between workovers to allow the tensile stress to relax to a compressive state (al least 3 months). However any induced fracture may not heal and Cavern 6 is predicted to damage during its workover, which increases the potential to connect the caverns during that time. To better evaluate the potential for damage to Caverns 6 and 9, some additional calculations have been performed.

The sonar data used to create the dish-like shape of Cavern 6 in the original calculations was based on some incomplete data sets. Deviations in the three wells in Cavern 6 and strapping data not originally included in the original sonar data sets provide a more accurate picture of the true geometry of Cavern 6 in 1982. Three wells enter into West Hackberry Cavern 6, and these wells were deviated. The coordinates at the surface and cavern ceiling are listed in Table 7, including nearby Cavern 9 wells which were also deviated. At cavern ceiling elevations, Well 6 deviates 105 ft to the NNE and Well 9 deviates 120 ft to the SW. This places the caverns a greater distance apart (220 ft) than surface coordinates would suggest. These ceiling coordinates were used in positioning cavern sonars relative to each other, other caverns, and the edge of dome.

Table 7. Deviations in the wells in Caverns 6 and 9

Well	Surface Coordinate		Ceiling Coordinate	
	East ft	North ft	East ft	North ft
WH6	4959	22434	4980	22537
WH6A	4959	22298	Does not enter cavern	
WH6B	5109	22343	5100	22666
WH6C	4806	22343	4793	22619
WH9	4820	21727	4756	21626
WH9A	4761	21583	4761	21584
WH9B	4695	21716	4765	21578

The most recent sonar of Cavern 6 (August 12, 1982) does not show any span larger than 850 feet. A note found on the front page of the sonar report by Dowell states that any radii larger

than 500 feet will not appear. Therefore the large 1200-ft ceiling spans noted in previous sonars are not represented in the 1982 sonar data.

Prior high resolution sonars performed on Cavern 6 are listed in Table 8 along with the average and maximum ceiling spans. Cavern 9 is also included as its location relative to Cavern 6 and is plotted in Figure 59. The sonars of Cavern 6, taken from the 3 different Cavern 6 wells, are in close agreement and show that the ceiling of Cavern 9 is located 230 feet from its edge. The closest point of approach is with the lower lobe of Cavern 9, at approximately 205 feet. Figure 60 shows Cavern 6 and 9 in their full volume and proximity.

Table 8. Measured spans of WH Cavern 6.

	Well	Avg. Ceiling Span, ft	Maximum Ceiling Span, ft
5/21/1980	6	1158	1243
5/21/1981	6	1145	1231
3/21/1980	6c	1124	1212
3/21/1980	6b	1129	1187

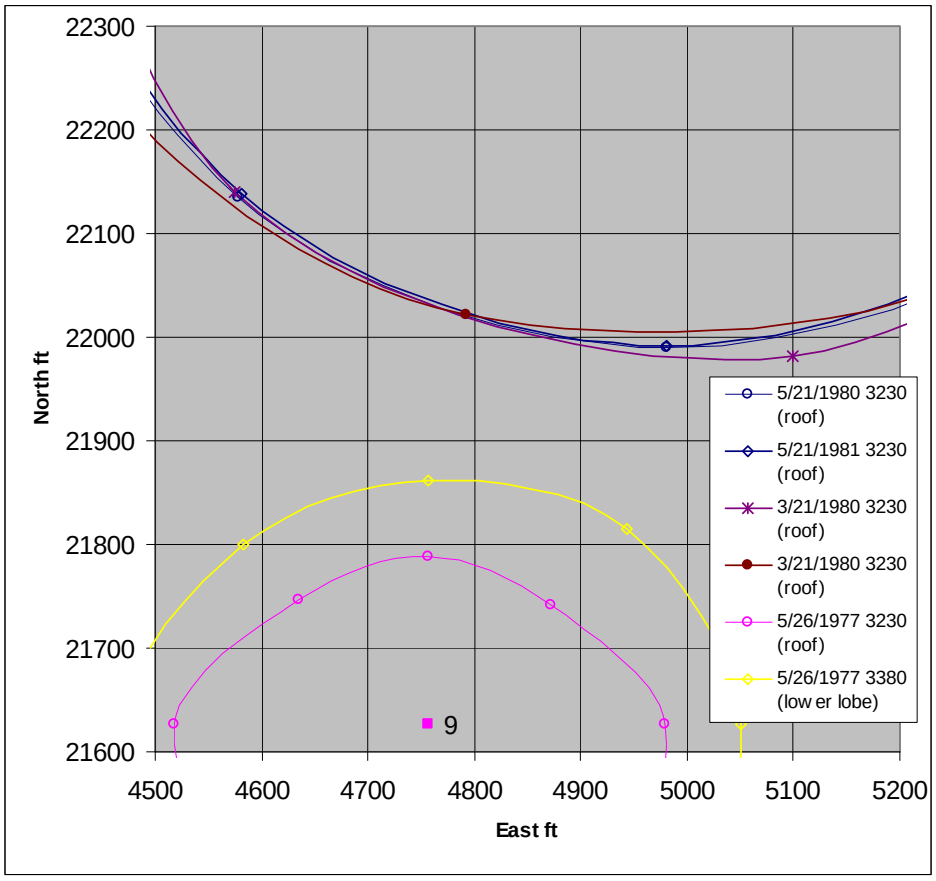

Figure 59. Proximity of Caverns 6 and 9.

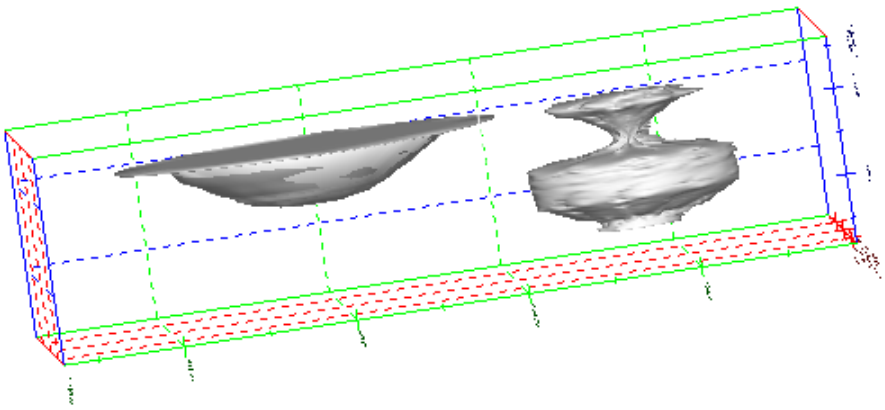

Figure 60. Caverns 6 and 9, from the most recent (1982) sonar and strapping data.

While the four 1980-1981 sonars of Cavern 6 agree with each other, they can also be checked with the available strapping data, particularly in the ceiling area where sonar may have some difficulty because of the range and wingtip geometry (Figure 61). Strapping data collected in Cavern 6 reflect the average cavern radius which is compared to the average of the sonar data (May 21, 1981) in Figure 62. The strapping data were collected during Cavern 6 drawdown to recertify it in 1980. Additional information is available following refill of Cavern 6 to 7,965,500 bbl. At that time (1984), the interface was measured at a depth of 3345 ft. The corresponding 1981 sonar volume at that depth is 7,934,875 bbl, or less than 1 percent difference. In contrast, the 1982 sonar data would place the interface below 3390 ft, the bottom of the cavern – an obvious error. The close agreements with the strapping data suggest that the 1980-1981 sonar data are correct, and Cavern 6 has a large 1200 ft ceiling span.

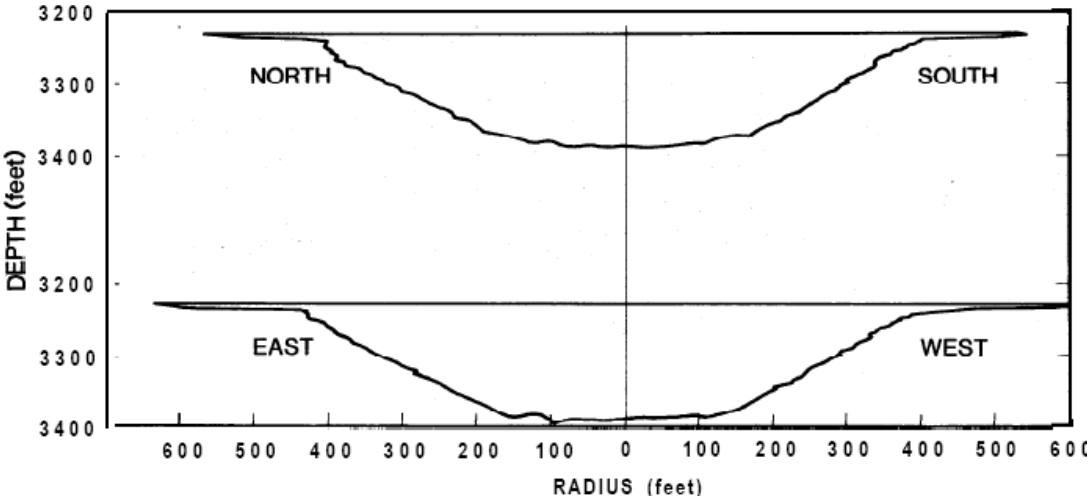

Figure 61. Profile of Cavern 6 based on 1980-1982 sonars.

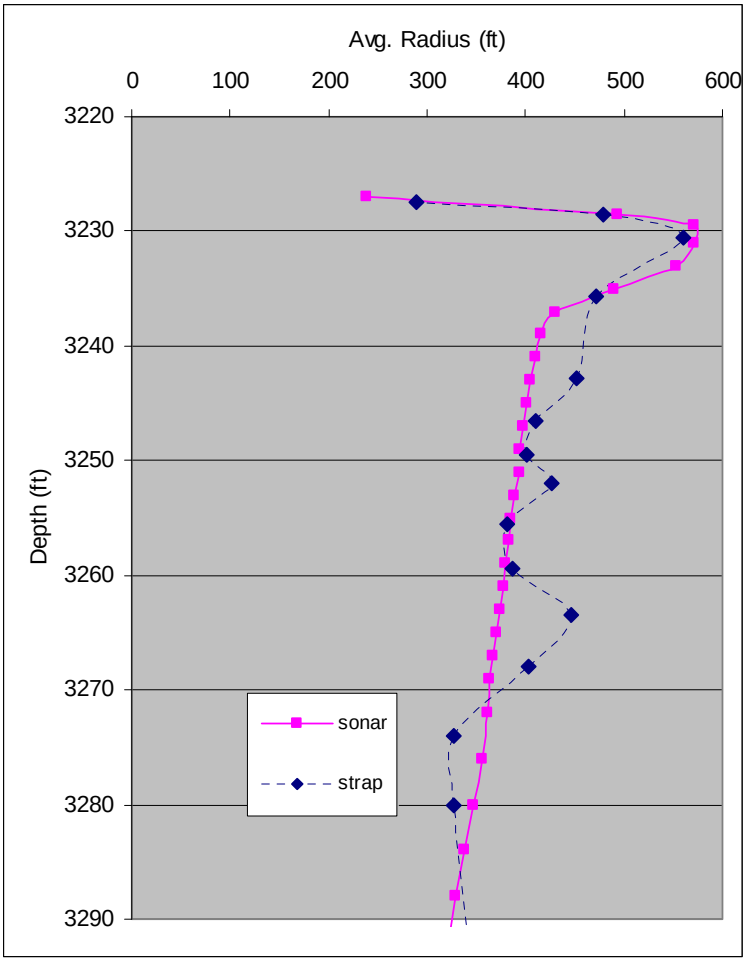

Figure 62. Radius of Cavern 6 measured from sonar and strapping data.

The sonar data indicate that the approximately 200-feet wide “rim” encircling Cavern 6 has been present since at least 1980, and was about 10 feet thick at the edge of the dish or bowl portion of the cavern. Unfortunately, the 1982 sonar measurements are the last data taken of the cavern

profile. The current condition of the rim of Cavern 6 is not known. This may be important for two reasons. One, the extension of the flat wide volume of the cavern may increase the already-high fracture potential around the perimeter, and consequently cause the cavern ceiling to subside more. Two, because of the geometry of the cavern, it is possible that the rim has been pinched off from the rest of the cavern, potentially trapping oil in the pinched section or in pockets near the rim that are at higher elevations than the access holes in the cavern ceiling. These possibilities were evaluated in the new calculations. Because of the uncertainty in the current shape of Cavern 6, results using the original estimated shape of Cavern 6 (no "rim") are still useful in evaluating the potential impacts of cavern operations to its stability.

The following is a summary of some of the results of the original calculations using the original estimated shape for Cavern 6 (no "rim") that are in Section 4. There are two ways in which the salt surrounding the caverns can be damaged: by stress-induced microfracturing causing dilatant damage and an increasing in permeability and the potential for crack propagation, and by tensile stresses which causes salt fracture and crack propagation. Figure 23 plots the Van Sambeek damage factor for a vertical cross-section of Caverns 6 and 9 on day 9730 from the original calculations; note how the top layer of Cavern 6 is red, indicating a damage factor less than 1 (means the onset of dilatant damage). Figure 24 is a close-up of the edge of Cavern 6, showing the location of the high deviatoric stress region around the perimeter. Because of the unusual shapes of these two caverns, the pressure changes during the drawdown to zero wellhead pressure, and the re-pressurization back to normal operating pressure causes transient deviatoric stresses in specific regions around the caverns. For Cavern 6, this region is always the perimeter of the dish-shaped cavern. At the start of the workover, the lower pressure in the cavern causes a temporarily larger compressive stress around the perimeter, creating the first low spike in the damage factor. The stresses improve with time during the workover, until the cavern pressure in Cavern 6 is increased again. Upon repressurization of the cavern to normal pressures, the same perimeter locations experience a temporary tensile loading, creating the potential for both tensile and dilatant fracturing.

Furthermore, there is evidence from the history plots of the minimum dilatant damage factor that significant pressure changes in Cavern 6 are reflected in smaller changes in Cavern 9 and vice versa. The influence of these two caverns on each other is an important design criterion for future operations. Cavern closure can be measured by the change in wellhead pressure over a period of time. The wellhead pressure naturally increases as a response to the decrease of volume from salt creep into the cavern; the wellhead pressure is then adjusted periodically at the surface facilities to maintain a reasonably uniform pressure over time. Wellhead pressure data are collected daily for all SPR wells. Pressure data from Caverns 6 and 9, plotted at times before and after the onset of workovers at the other cavern, show an increase in the pressure change rate; these pressure change rates correspond to changes in the cavern closure rate by factors of 2 to 4. Examples of pressure data for Cavern 6 at the onset of a workover in Cavern 9, and for Cavern 6 at the onset of a workover in Cavern 9, are shown in Figure 39. This measured change in closure rates verifies the analytical predictions that significant cavern interactions occur between Caverns 6 and 9 during workovers. This verification further strengthens the position that workover activities in Caverns 6 and 9 must be planned very carefully to prevent undesired communication between them.

The computational mesh for Cavern 6 was regenerated based on the more complete sonar information, and the calculations were originally resubmitted with no changes to the excavation and oil storage scenarios. This was found to be impractical; if the rim was created in 1946 along with the remainder of the original cavern, it was found to close well before the oil emplacement timeframe of 1979-1980. This result could indicate that the rim around Cavern 6 might have been created during the transition from brine to oil storage, when the pressures were increased substantially and the perimeter of the cavern experienced a high potential for fracturing. (There are no site data to either support or contradict this conjecture.) Therefore, the scenario was modified to create the rim of the cavern in 1980, when the cavern began its oil storage function. Figure 63 shows the plot of damage factor around Caverns 6 and 9 that is analogous to Figure 23. The region of high damage potential is concentrated at the edge of the rim of Cavern 6. Figure 64 shows a closer view of the rim when the cavern begins storage operations in about 1980 until when the rim is predicted to pinch closed sometime around 1989. Figure 65 continues these views, looking to the years 1994 and 2004. These plots indicate not only that the rim of Cavern 6 may have entrapped oil in it, but that the ceiling of the cavern may have sunk beneath the level of oil around the perimeter. The volume of this "lost" oil may be significant, as high as 1 MMB. Figure 66 compares the predicted drop in the ceiling elevation for both the original calculation and the calculations with the corrected Cavern 6 geometry. Note that the existence of the rim produces a significantly greater elevation drop in Cavern 6, which if true would substantiate the scenario shown in Figures 64 and 65.

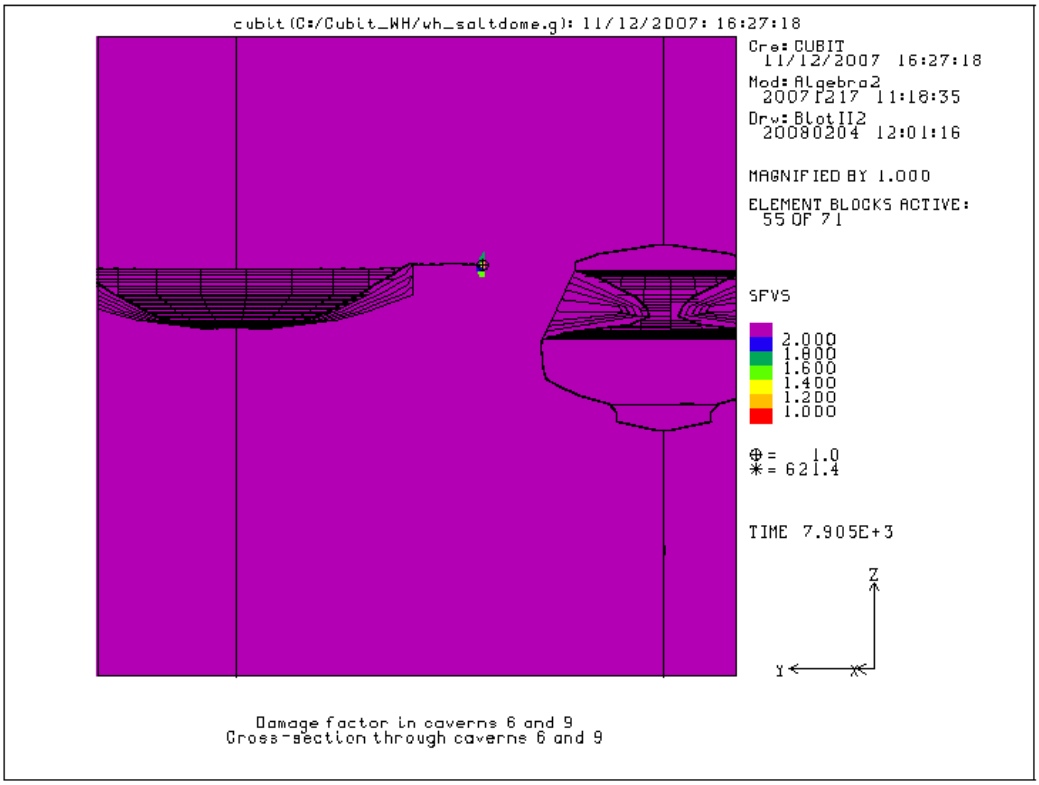

Figure 63. Damage near the rim of Cavern 6.

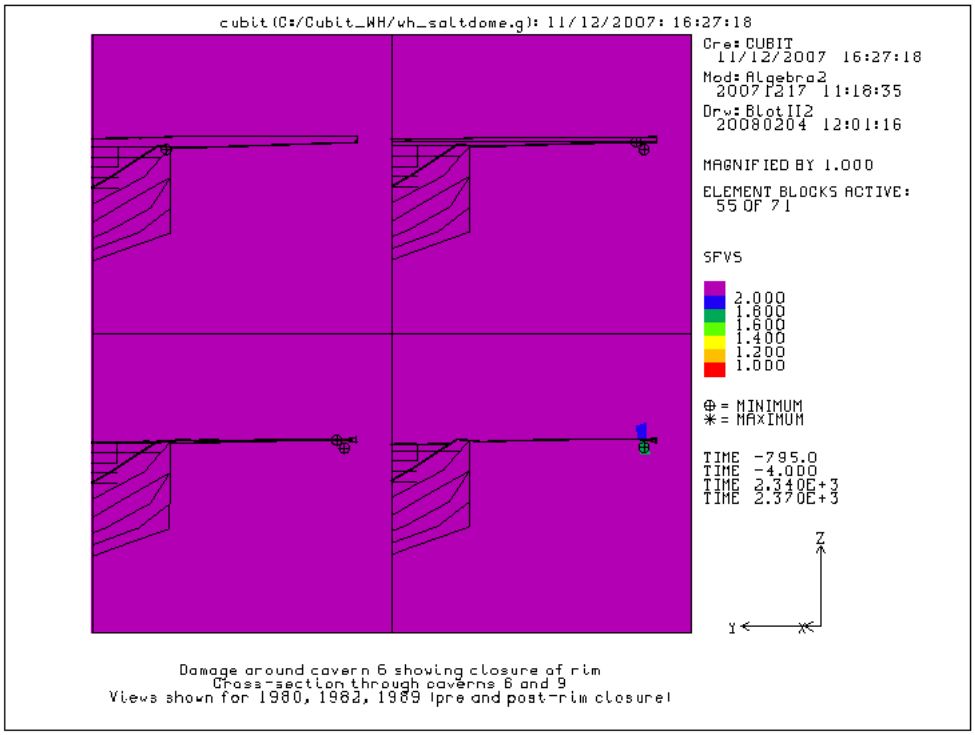

Figure 64. Closure of the rim of Cavern 6 around 1989.

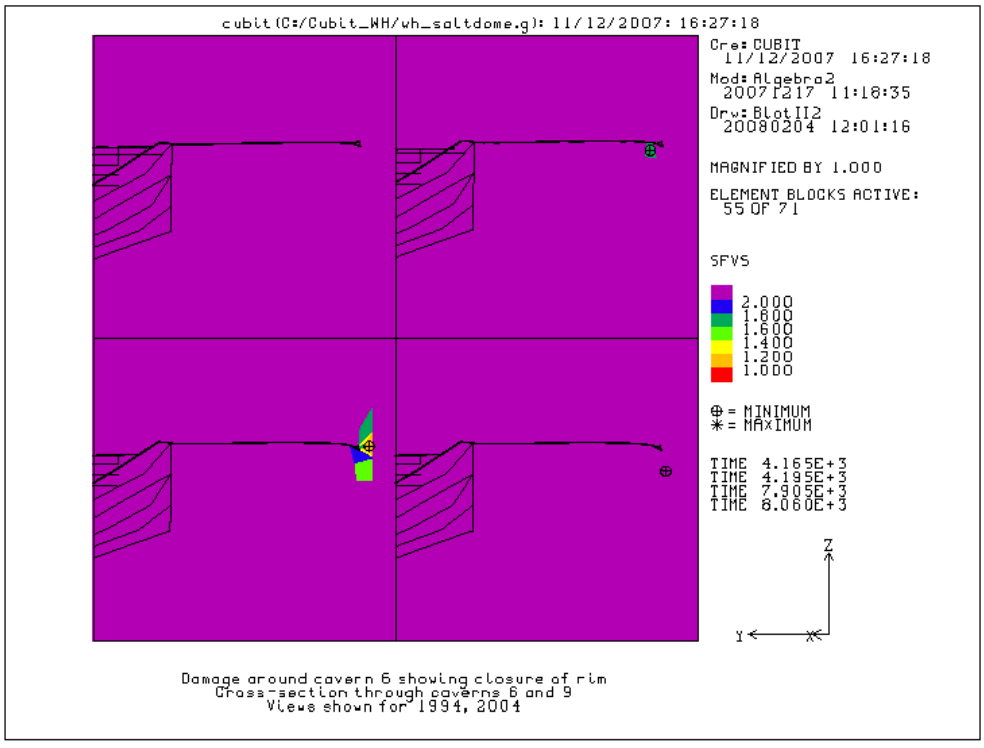

Figure 65. Continued subsidence of Cavern 6 after rim closure.

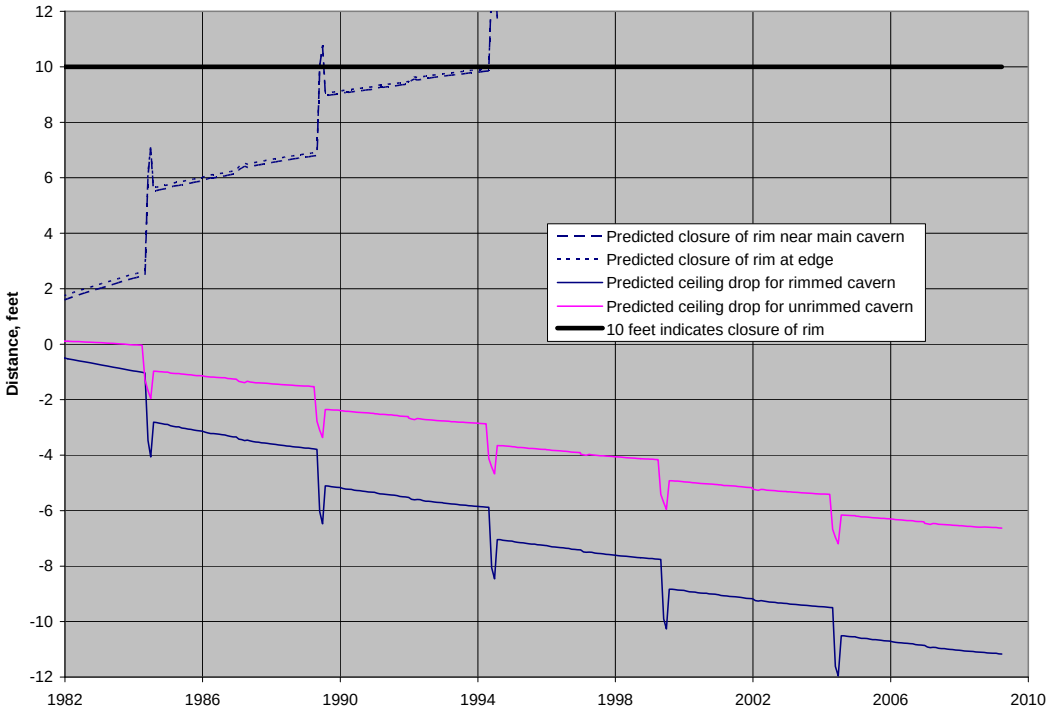

Figure 66. Predicted rim closure and ceiling drop for Cavern 6.

Data logs of Cavern 6 taken in the years 1983 to 1992 were used to determine if there is any site information which might confirm the scenario of "lost oil" described in Figures 64 and 65. Figure 67 shows the measured changes in oil volume and interface depth beginning in 1983. From Cavern 6 data logs, oil volume starts out constant then it reduces by 1MMB. During this volume reduction, caused by the inward deformation of the cavern by the creeping salt, one would expect the depth to the oil brine interface to start out constant and then move upward. In fact, the interface drops this entire time period between 10 and 20 feet. This phenomenon can be explained by the rim of cavern 6 which is predicted to close during this time period – on the order of 10 ft in agreement with the data. After 1992, the cavern exhibits expected or typical behavior – a continued decrease in oil volume (0.5 MMB) accompanied by a rising interface. Figure 68 shows the measured oil volume and the measured wellhead pressure for Cavern 6. Note that the operating wellhead pressure applied for Cavern 6 was about 600-700 psi in 1989, substantially less than the 900 psi pressures used in later years and in the calculations. Figure 69 overlays the predicted volume changes for Cavern 6 for the calculations with and without the rim. Note that the measure volume change lies between the two predicted values, adding to the likelihood of the scenario that the rim of Cavern 6 has closed, resulting in the period of the drop in elevation of the interface depth and the possible entrapment of oil in the pinched rim or in the cavern regions above the ceiling access points.

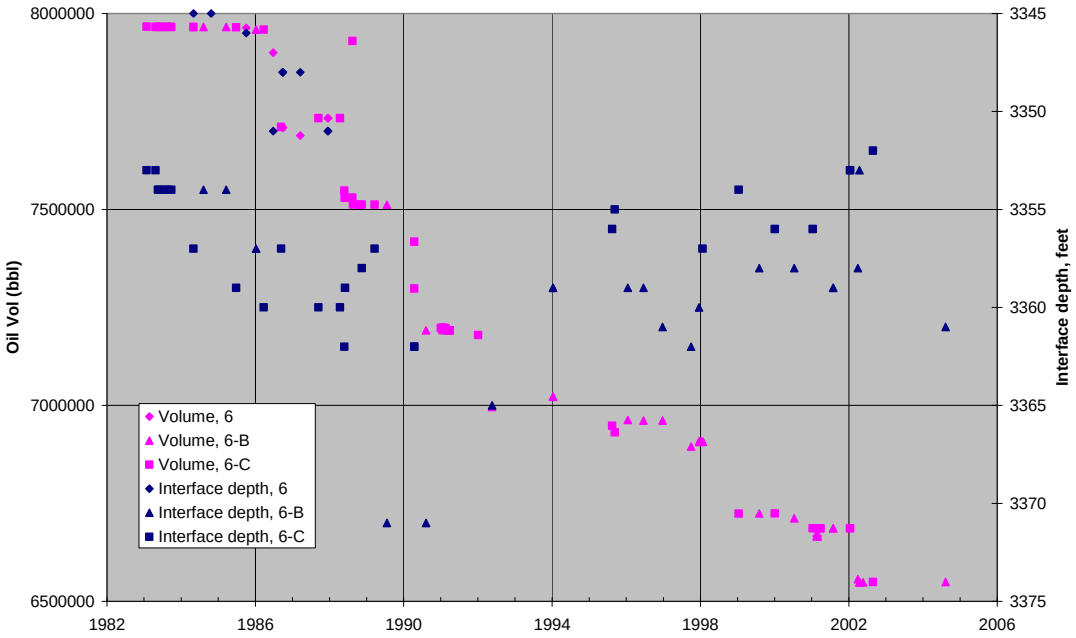

Figure 67. Measured oil volume and interface depth in Cavern 6.

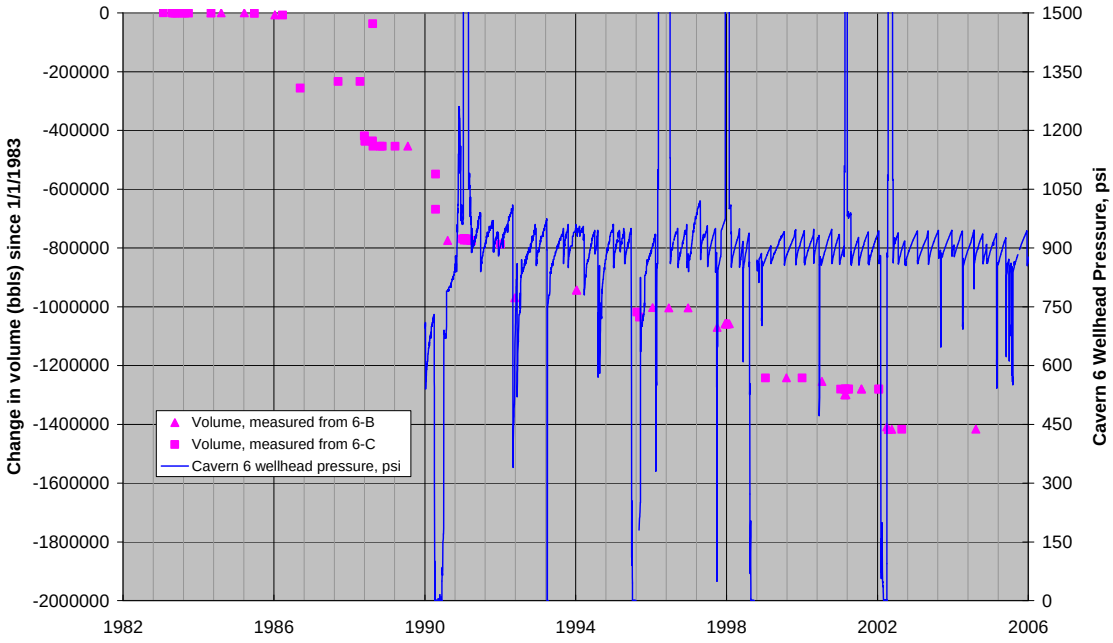

Figure 68. Measured oil volume and wellhead oil pressure in Cavern 6.

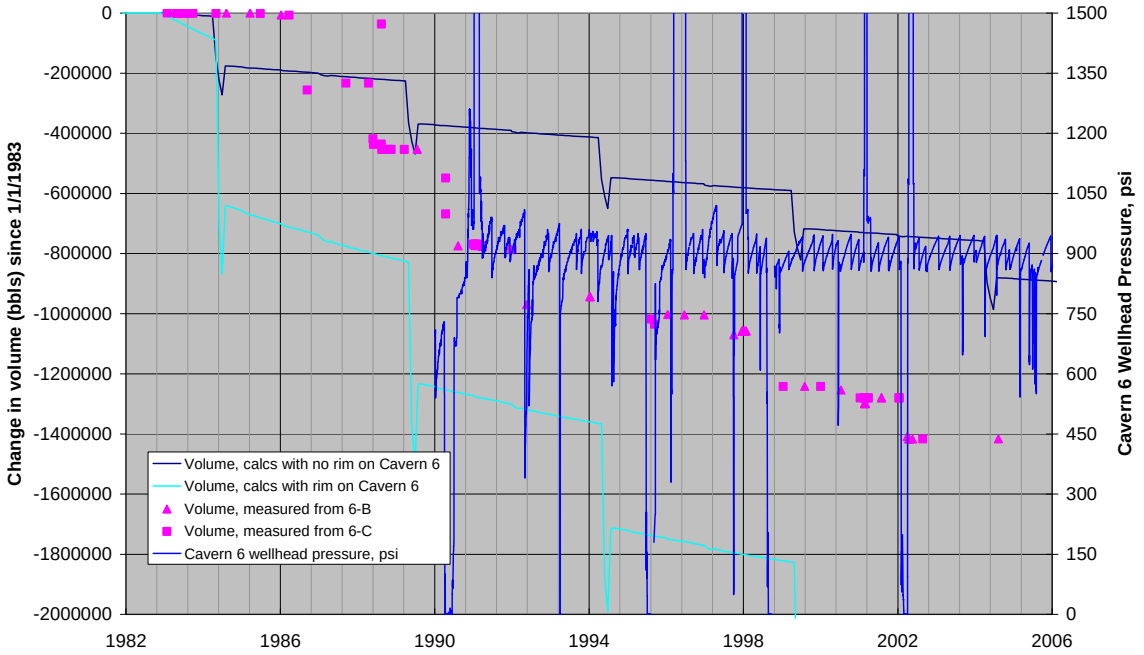

Figure 69. Measured vs. predicted volume changes in Cavern 6.

An additional simulation was run to determine the possibility of cavern stability issues resulting from near-coincidental workovers on both Caverns 6 and 9. In all previous calculations, the workovers in Caverns 6 and 9 had been equally spaced at every 2.5 years. In the new simulation, the wellhead pressures in Caverns 6 and 9 are dropped to zero simultaneously. When this happens, the 5-ft gap in the rim at that time immediately closes. In addition, the damage factor around the edge of the rim surpasses the failure threshold of 1.

The new calculations utilizing the 1982 version of Cavern 6 verify many of the conclusions drawn with the original calculations. Tensile stresses are predicted around the perimeter of Cavern 6 during and immediately following repressurization of the cavern and last for several months. Pressure applied to the large ceiling span apparently induces an elastic, tensile response at the edges of the ceiling. If a crack were to propagate and intersect Cavern 9, cavern pressures would equilibrate. The maximum equilibrated pressures are not problematic to the wellhead or production casings in either caverns, but an operational scenario of having Cavern 9 in workover mode during the breach would pose a serious risk to operational safety and containment of oil. A breach when Cavern 6 is fully repressurized could result in major safety and environmental problems in the operation of Cavern 9. It is imperative to allow for an adequate time between repressurization of Cavern 6 and the workover of Cavern 9. These analyses suggest a three-month period, but a reasonable safety factor must be applied given the analysis uncertainties and severe consequences. As such, the following conclusions have been determind regarding operation of Caverns 6 and 9:

- Repressurization in Cavern 6 after a workover will likely cause tensile stresses around the perimeter of the cavern.
- Pressure changes in Cavern 6 during a workover cause resulting pressure changes in Cavern 9, and vice versa. These coincident pressure changes indicate that there is already

some sort of communication between the caverns, most likely in the form of deviatoric stress changes, but there exists the possibility of the existence or future formation of salt fractures directly linking the two caverns.

- The rim around Cavern 6, as observed in the 1982 sonar and strapping data, has probably closed to an extent such that it is not available to store retrievable oil; however, the status of the rim is not certain. The status of the rim has implications on the coincident behavior of Caverns 6 and 9.

The following are recommended actions regarding caverns 6 and 9:

- New sonar and/or strapping data should be taken to learn the current geometry of Cavern 6. Such measurements would aid in determining if the rim is stil connected to the bowl of Cavern 6 and if there is retrievable oil there, as well as determining if there is oil in the upper corners of the bowl of Cavern 6 that cannot be removed using the standard water displacement techniques.
- Workovers performed on Caverns 9 should be performed no sooner than one year after the completion of a workover in Cavern 6. This period will allow the stressed salt around Cavern 6 enough time to heal and attain near-hydrostatic stress values, so to minimize the possibility of cracking the salt between Caverns 6 and 9. Performing the workovers in the opposite order (Cavern 9, then Cavern 6) does not appear to need such a stringent requirement, although it would probably be wise to keep the same delay.
- When performing a workover, CIT, or other pressure-changing procedure in Cavern 6 or 9, it is recommended that the pressure in both caverns be monitored and evaluated for evidence of unusual changes that might indicate a loss of product through a salt fracture.

6. CONCLUSIONS

These analyses evaluated the Phase 1 caverns at the West Hackberry SPR site for their current condition and for potential enlargement. The analyses also examined the overall performance of the West Hackberry site by evaluating surface subsidence, horizontal surface strains, and axial well strains. Finally, the analyses evaluated the possibility of nonlinear dilatancy behavior of the West Hackberry salt, and its possible ramifications on cavern performance. The following conclusions were obtained from the results of the analyses:

- Because of the dish-like shape of Cavern 6, the perimeter of the cavern is at risk of dilatant and tensile damage, particularly at the end of a workover operation. This potential will increase with the first and second leaching operations, but may be abated with the later expansions as the cavern takes on a more cylindrical shape.
- The times of highest potential of salt damage/salt falls are during large cavern pressure changes, such as depressurization or repressurization in workovers. Even at low cavern pressures, over time the stresses in the cavern walls will adjust to near isotropic conditions; there will be increased creep and cavern closure, but the potential for damage will dissipate as the cavern pressure remains constant.
- Because of expected tensile cracking potential near Cavern 6, the close proximity of Cavern 9 (200 feet at their closest point) poses a risk of inter-cavern communications. The potential exists for a crack to propagate from Cavern 6 and intersect Cavern 9, causing cavern pressures to equilibrate. An operational scenario of having Cavern 9 in workover mode during the breach would pose a serious risk to operational safety and containment of oil. A breach when Cavern 6 is fully repressurized (the most likely condition) could abruptly pressurize Cavern 9 and result in approximately 55,000 bbl of oil ejecting onto the surface in the absence of a wellhead or if the blowout prevent faulted. This would pose a serious safety risk to the workover crew and potential environmental damage.
- New sonar and/or strapping data should be taken to learn the current geometry of Cavern 6. Such measurements would aid in determining if the rim is in contact with the the bowl of Cavern 6. Should the ceiling contact the edge of the bowl, there may be oil isolated in the extremities of the rim or in the upper corners of the bowl that may not be removed using standard water displacement techniques.
- Workovers performed on Caverns 9 should be performed no sooner than one year after the completion of a workover in Cavern 6. This period will allow the stressed salt around Cavern 6 enough time to heal and attain near-hydrostatic stress values, so to minimize the possibility of cracking the salt between Caverns 6 and 9. Performing the workovers in the opposite order (Cavern 9, then Cavern 6) does not appear to need such a stringent requirement, although it may be prudent to keep the same delay.
- When performing a workover, CIT, or other pressure-changing procedure in Cavern 6 or 9, it is recommended that the pressure in both caverns be monitored and evaluated for evidence of unusual changes that might indicate a loss of product through a salt fracture.
- This report provides examples of cavern interactions observed between the caverns through historic pressure measurements. Additional and continuing work could be done to assess changes throughout time as more data are accumulated on the caverns.
- Cavern 9 has a middle section with a smaller radius, giving a cross-section of the cavern the look of a bell with a mid-cavern ledge. This ledge and the cavern wall underneath supporting the ledge are also locations with a significant potential for dilatant damage during workover

operations. This analysis designs a cavern enlargement process that gradually eliminates the ledge, resulting in a final bell shape with no enlargement in the radius over the majority of the cavern. This cavern enlargement procedure favorably eliminates the ledge, but in reality the leached shaped of the cavern may differ, and other leaching scenarios may result in interference with Cavern 6 or a heightened potential for dilatant damage.

- Additional analyses should be performed on the interactions of Caverns 6 and 9 that examine the influence of operating the caverns as a gallery, where pressures in both caverns are kept equal. If the results reduced the likelihood of a crack forming between the caverns, the modeled scenario could be implemented into practice.
- Caverns 7, 8, and 11 have no significant issues regarding dilatant damage in the surrounding salt, and may be enlarged with no adverse effect on cavern stability.
- The predictions indicate surface subsidence of an additional four feet between 2006 and 2034, to a total of 7 feet since 1991. If extended over a potential 100-year life of the facility, the potential displacement could reach a total of approximately 12 feet between 2006 and 2084 (15 feet since 1991). Because the surface structures at the wellhead are at elevations between 4 and 18 feet above sea level, the predicted subsidence may cause some of the wellheads to sink below sea level by the 2030's.
- Vertical strains in the locations of the original (c. 1946) and newer (c. 1981) wells providing access to the Phase 1 caverns in some cases have already exceeded established thresholds for cement failure (0.2 millistrains) and steel casing collapse (1.6 millistrains). In particular the greatest strain was predicted above Cavern 6 with yielding predicted in the 2000-2002 time-frame. This prediction was validated with the failure of Well 6B in 2001, requiring a liner in 2002. The vertical strain predictions presented here should be correlated with other known well casing problems or logging results to determine field-appropriate strain threshold values.
- Recent laboratory data from SPR (Lee et al. 2004) and non-SPR (DeVries et al., 2003) salts indicate that the onset of dilatant damage in salt is nonlinear between I_1 and $\sqrt{J_2}$, and that there may be an additional dependence on the Lode angle ψ, which relates to the relative compression or extension among the principal stresses. The utilization of dilatant damage criteria based on these studies indicate that significant portions of some caverns, including the walls beneath the ledge of Cavern 9, and the sections of Caverns 101 and 103 (and most of the post-1981 caverns) below 3600 feet of depth, may experience dilatant damage conditions during large pressure change events. Possible indications of salt fall (whether by large chunks or by "snowfall") may be induced from log data of cavern floor elevations and sonar measurements of the volume of the cavern.
- Additional series of laboratory tests of salt from West Hackberry and other SPR sites would be beneficial. In particular, a combination of triaxial compression and triaxial extension tests, where the salt samples are loaded to dilatant failure, would greatly enhance the existing knowledge of the failure envelope of the salt at each site, and determine whether that failure is dependent on Lode angle.
- Log data, hanging string failure events, and sonar measurements can be used to monitor the status of the cavern at several points in time. However, these data points are sparse, so it is difficult to detect salt fall events unless an obvious failure (i.e., hanging string) occurs. Particularly because the caverns are between 20 and 60 years old, additional monitoring of the conditions of the cavern walls and well casings would be beneficial, specifically cement bond and casing inspections logs.

7. REFERENCES

- Ballard, S. and B. L. Ehgartner, 2000. *CaveMan Version 3.0: A Software System for SPR Cavern Pressure Analysis*, SAND2000-1751, Sandia National Laboratories, Albuquerque, New Mexico.
- Blanford, M.L., M.W. Heinstein, and S.W. Key, 2001. *JAS3D. A Multi-Strategy Iterative Code for Solid Mechanics Analysis.* ***User's Instructions****, Release 2.0*. SEACAS Library, JAS3D Manuals, Computational Solid Mechanics / Structural Dynamics, Sandia National Laboratories, Albuquerque, New Mexico.
- DeVries, K.L., K.D. Mellegard, and G.D. Callahan, 2002. Proof-of-Concept Research on a Salt Damage Criterion for Cavern Design: a Project Status Report. Solution Mining Research Institute Spring Meeting, Banff, Alberta, Canada, April, 2002.
- DeVries, K.L., K.D. Mellegard, G.D. Callahan, and W.M. Goodman, 2005**.** *Cavern Roof Stability for Natural Gas Storage in Bedded Salt*, RSI-1829, prepared by RESPEC, Rapid City, South Dakota, for United States Department of Energy, National Energy Technology Laboratory, Pittsburgh, Pennsylvania.
- Ehgartner, B.L. and S.R. Sobolik, 2002. *3-D Cavern Enlargement Analyses*, SAND2002-0526, Sandia National Laboratories, Albuquerque, New Mexico.
- Ehgartner, B.L., 2004. Cavern Operating Pressure Risk Analysis. Letter Report to R.E. Myers, dated November 24, 2004.
- Ehgartner, B.L., 2006. Ullage Study Update. Letter Report to R.E. Myers dated November 21, 2006.
- Hoffman, E.L. and B.L. Ehgartner, 1993. *Evaluating the Effects of the Number of Caverns on the Performance of Underground Oil Storage Facilities*, Int. J. Rock Mech. Min. Sci. & Geomech. Abstr. Vol. 30, No. 7, pp. 1523-1526.
- Hugout, B., E. Chaudan, and M. Dussaud, 1988. *Influence of Creep on Shape of Salt Cavities of Natural Gas Storage*, Spring Meeting, Solution Mining Research Institute, Mobile, Alabama.
- Lama, R.D. and V.S. Vutukuri, 1978, *Handbook on Mechanical Properties of Rocks – Testing Techniques and Results* -, Series on Rock and Soil Mechanics, Vol. 3, No.2, Trans Tech Publications.
- Lee, M.Y., B.L. Ehgartner, B.Y. Park, and D.R. Bronowski, 2004. *Laboratory Evaluation of Damage Criteria and Permeability of Big Hill Salt*, SAND2004-6004, Sandia National Laboratories, Albuquerque, New Mexico.
- Magorian, T.R., J.T. Neal, S. Perkins, Q.J. Xiao, and K.O. Byrne. 1991. *Strategic Petroleum Reserve Additional Geologic Characterization Studies West Hackberry Salt Dome, Louisiana*, SAND90-0224, Sandia National Laboratories, Albuquerque, New Mexico.
- Morgan, H.S. and R.D. Krieg, 1990. *Investigation of an Empirical Creep Law for Rock Salt that Uses Reduced Elastic Moduli*, SAND89-2322C, presented at the 31st U.S. Symposium on Rock Mechanics held in the Colorado School of Mines in June 18-20, 1990, Sandia National Laboratories, Albuquerque, New Mexico.
- Munson, D.E., 1998. *Analysis of Multistage and Other Creep Data for Domal Salts*, SAND98-2276, Sandia National Laboratories, Albuquerque, New Mexico.

- Munson, D.E., 2006. *Features of West Hackberry Salt Caverns and Internal Structure of the Salt Dome*, SAND2006-5409, Sandia National Laboratories, Albuquerque, New Mexico.
- Park, B.Y., B.L. Ehgartner, M.Y. Lee, and S.R. Sobolik, 2005. *Three Dimensional Simulation for Big Hill Strategic Petroleum Reserve (SPR)*, SAND2005-3216, Sandia National Laboratories, Albuquerque, New Mexico.
- Peng, S.S., 1985. Coal Mine Ground Control. 2nd Ed., John Wiley and Sons, New York, New York.
- Preece, D.S. and J.T. Foley, 1984. *Long-Term Performance Predictions for Strategic Petroleum Reserve (SPR) Caverns*, SAND83-2343, Sandia National Laboratories, Albuquerque, New Mexico.
- Rautman, C.A., J.S. Stein, and A.C. Snider, 2004. *Conversion of the West Hackberry Geological Site Characterization Report to a Three-Dimensional Model*, SAND2004-3981, Sandia National Laboratories, Albuquerque, New Mexico
- Rautman, C.A. and A.C. Snider, 2007. *Sonar Atlas of Caverns Comprising the U.S. Strategic Petroleum Reserve Volume 4: West Hackberry Site, Louisiana*, SAND2007-6051, Sandia National Laboratories, Albuquerque, New Mexico
- Sattler, A.R. Milestone Requirement: Subtask 1.1.4, activity a2--Prepare plan for running casing inspection and cement bond logs. Letter report to Robert E. Myers, December 6, 2004.
- Thorton, C.H and I.P. Lew, 1983. *Concrete and Design Construction. Standard Handbook for Civil Engineers*, Chapter 8, 3rd ed., F.S. Merritt, editor, McGraw-Hill, New York, NY.
- Van Sambeek, L.L., J.L. Ratigan, and F.D. Hansen, 1993. *Dilatancy of Rock Salt in Laboratory Tests*, Int. J. Rock Mech. Min. Sci. & Geomech. Abstr. Vol. 30, No. 7, pp 735-738.
- Wawersik, W.R. and D.H. Zeuch, 1984. *Creep and Creep Modeling of Three Domal Salts – A Comprehensive Update*, SAND84-0568, Sandia National Laboratories, Albuquerque, New Mexico.
- Whiting, G. H., 1980. *Strategic Petroleum Reserve (SPR): Geological Site Characterization Report, West Hackberry Salt Dome*, SAND80-7131, Sandia National Laboratories Albuquerque, New Mexico.
- Woodrum, S., 2001. Cavern Integrity Report Pressure Data---Graphed. Letter Report to B.L. Ehgartner dated April 23, 2001.

DISTRIBUTION:

U.S. Department of Energy (electronic copy only)
Strategic Petroleum Reserve Project Management Office
900 Commerce Road East
New Orleans, LA 70123
Attn: W. Elias at Elias. Wayne@SPR.DOE.GOV
R. Myers at Robert.Myers@SPR.DOE.GOV

U.S. Department of Energy (3)
Strategic Petroleum Reserve Program Office
1000 Independence Avenue, SW
Washington, D.C. 20585
Attn: D. Johnson, FE-421

1	MS	0706	D.J. Borns, 6312
5	MS	0706	B.L. Ehgartner, 6312
1	MS	0706	A.R. Sattler, 6312
1	MS	0706	D.E. Munson, 6312
1	MS	0706	C.A. Rautman, 6312
1	MS	0751	TW. Pfeifle, 6315
5	MS	0751	S. R. Sobolik, 6315
1	MS	1395	B. Y. Park, 6821
1	MS	0701	J. A. Merson, 6310
1	MS	0376	J. G. Arguello, 1526
1	MS	0376	C. M. Stone, 1527
1	MS	0899	Technical Library, 9536 (electronic copy)

Electronic copy only to Wayne Elias at for distribution to DOE and DM


Sandia National Laboratories